



KATHOLIEKE UNIVERSITEIT  
**LEUVEN**

Arenberg Doctoraatsschool Wetenschap & Technologie  
Faculteit Ingenieurswetenschappen  
Departement Werktuigkunde

# Determining measurement uncertainties of feature measurements on CMMs

**Nick Van Gestel**

Proefschrift voorgedragen  
tot het behalen van de  
graad van Doctor in de  
Ingenieurswetenschappen

September 2011



# **Determining measurement uncertainties of feature measurements on CMMs**

**Nick Van Gestel**

Jury:

Prof. dr. Adhemar Bultheel, voorzitter  
Prof. dr. ir. Jean-Pierre Kruth, promotor  
Dr. ir. Philip Bleys, promotor  
Prof. dr. ir. Bert Lauwers  
Prof. dr. ir. Dominiek Reynaerts  
Prof. dr. ir. Wim Dewulf  
Dr. ir. Wolfgang Knapp  
(ETH Zürich)

Proefschrift voorgedragen  
tot het behalen van de  
graad van Doctor in de  
Ingenieurswetenschappen

September 2011

© Katholieke Universiteit Leuven – Faculteit Ingenieurswetenschappen  
Kasteelpark Arenberg 1 - bus 2200, B-3001 Heverlee

Alle rechten voorbehouden. Niets uit deze uitgave mag worden vermenigvuldigd en/of openbaar gemaakt worden door middel van druk, fotocopie, microfilm, elektronisch of op welke andere wijze ook zonder voorafgaande schriftelijke toestemming van de uitgever.

All rights reserved. No part of the publication may be reproduced in any form by print, photoprint, microfilm or any other means without written permission from the publisher.

D/2011/7515/115  
ISBN 978-94-6018-414-7

# Dankwoord

Mijn schrijfstrijd is nu gestreden! Aan iedereen, die op een of andere manier een rol speelde bij de totstandkoming van dit werk, BEDANKT.

In de eerste plaats ben ik mijn promotoren, prof. Jean-Pierre Kruth en Philip Bleys, veel dank verschuldigd. Jean-Pierre, bedankt om me in 2005 de kans te geven om in jouw onderzoeksteam te starten, en in het bijzonder voor het enorme vertrouwen dat ik sindsdien heb mogen genieten. Philip, bedankt om me bij de vele industriële projecten te betrekken, ik heb enorm veel van jou geleerd. Je technisch inzicht en oog voor detail hielpen me talloze keren vooruit bij mijn onderzoek.

Tevens dank aan prof. Bert Lauwers, prof. Dominiek Reynaerts en prof. Wim Dewulf voor het nalezen van de tekst en hun constructieve opmerkingen. I would especially like to thank Wolfgang Knapp for his in-depth reading of this text. Your comments and suggestions certainly improved the quality of this work.

Plezier scheppen in je werk wordt bevorderd door fijne collega's. Deze waren er op PMA in overvloed, te veel om op te noemen. De middagpauzes en SET-activiteiten waren momenten om naar uit te kijken en nooit meer te vergeten. Mijn speciale dank aan al degenen die zich voor de sociale activiteiten inzetten.

Aan het 'selecte groepje' van de gele trap: bedankt. Ik heb me daarboven geen enkel moment verveeld. Aan mijn collega's van de onderzoeksgroep metrologie: Philip, Joachim, Pieter-Jan, Steven, Frank, Kim, Haibin en Bart, bedankt voor de fijne samenwerking. Bart, je bemerkingen op de tekst hebben me goed geholpen. Joachim, bedankt voor je assistentie bij de vele metingen.

Ook het aanstekelijke enthousiasme van mijn collega Wim, van campus De Nayer, zal ik niet licht vergeten. De samenwerking met jou gedurende die eerste jaren was een waar genoegen. Ik denk nog vaak met trots terug aan de mooie projectresultaten die we samen behaalden.

Tevens mijn dank aan allen die vaak tot 's avonds laat het metrologielokaal bevolkten, op een aangename werksfeer kon ik steevast rekenen. Als er één iemand onlosmakelijk verbonden is met 'de metrologie' is het wel prof. Paul Vanherck. Paul,

jouw enthousiasme voor metrologie zal me altijd bijblijven en inspireren. Bedankt ook aan alle collega's van het vaste personeel. Karin, Lieve, jullie ondersteuning is goud waard. Dirk, Eddy, Franske, bedankt voor de steeds perfect afgewerkte werkstukken.

*Student zijn: dat verleert men niet, dat is men, of men is het niet.* Kerels uit het Kempenland, mijn studententijd is voor altijd onlosmakelijk verbonden met onze club 'Moeder Geelse'. Van de vele andere mensen die mijn studentenjaren tot een onvergetelijke tijd hebben gemaakt zou ik enkelen expliciet willen bedanken: Didier, Ward, Kristof, Koen, bedankt voor de hulp, de fijne samenwerking en het plezier gedurende die vijf studentenjaren.

Aan de vrienden thuis, die het haperende plaatje 'geen tijd' ondertussen wel beu zijn gehoord. Onze jarenlange vriendschap en ontspannende cafémomenten zorgden ervoor dat het schrijfwerk me nooit te zwaar is gevallen.

Gedurende mijn doctoraat heb ik steeds op de steun en hulp van familie en schoonfamilie kunnen rekenen. Bedankt allemaal, en in het bijzonder mijn ouders, voor de onvoorwaardelijke steun en alle kansen die ik kreeg.

Liefste Catheline, mijn laatste, maar dan ook grootste troef. Jij spoorde me aan om nog 'even' in Leuven te blijven. Zonder jou was mijn doctoraat wellicht een ijle droom, en de afwerking ervan een loodzware opgave. Jij gaf me echter de luxe om de laatste maanden bijna volledig aan mijn teksten te wijden. Catheline en Diederik, dankzij jullie liefde zou ik veel kunnen missen en blij kunnen zijn met maar heel weinig.

En daarmee kom ik tot het besluit dat je een doctoraat, zoals zoveel in het leven, niet op je eentje verwezenlijkt ...

Nick Van Gestel,  
Retie, september 2011.

# Samenvatting

De afmetingen van technische producten zijn vaak van enorm groot belang om hun correcte werking te garanderen. Maattoleranties geven aan hoe sterk de werkelijke afmetingen mogen afwijken van de vooropgestelde afmetingen. Dimensionele kwaliteitscontrole verzekert dat de afmetingen van het product voldoen aan deze toleranties. Voor enkelvoudige en niet-complexe producten volstaan eenvoudige meetinstrumenten zoals schuifmaten en schroefmicrometers, terwijl voor meer complexe producten en seriemetingen vaak coördinatenmeetmachines (CMM's) worden gebruikt.

Omdat meetinstrumenten ook meetfouten vertonen zal een meetresultaat nooit volledig correct zijn. Dit betekent dat er altijd een meetonzekerheid is die mee in rekening moet gebracht worden bij het controleren van een product ten opzichte van zijn toleranties. Als de meetonzekerheid wordt verwaarloosd kan dit leiden tot het onterecht goed- of afkeuren van producten, met soms ernstige gevolgen. Betrouwbare meetonzekerheden zijn absoluut noodzakelijk voor het eenduidig keuren van toleranties.

Het bepalen van meetonzekerheden voor coördinatenmeetmachines is moeilijk vanwege het grote aantal invloedsfactoren op de meetonzekerheid (zoals CMM-hardwarefouten, temperatuur, meetstrategie etc.). Daarom kunnen conventionele onzekerheidsberekeningsmethodes, gebaseerd op analytische voortplanting van standaard onzekerheden, niet worden toegepast. Onzekerheidsberekeningsmethodes gebaseerd op Monte-Carlosimulaties zijn een goed alternatief voor de conventionele methodes. Deze methodes kunnen veel beter omgaan met de complexiteit van CMM-metingen.

Dit proefschrift beschrijft vier bijdragen tot het bepalen van meetonzekerheden met Monte-Carlomethodes bij het meten van vormelementen met CMM's:

- Bij het bepalen van meetonzekerheden van vormelementen gemeten met CMM's wordt de invloed van vormfouten vaak verwaarloosd omdat de vormfouten op voorhand niet gekend zijn en daarom moeilijk in rekening te brengen zijn. Vormfouten van vormelementen, zoals bv. cirkels, lijnen,

vlakken en cilinders, kunnen nochtans een belangrijke invloed hebben op de meetonzekerheid, zeker wanneer deze vormelementen met een beperkt aantal meetpunten worden gemeten. Het verwaarlozen van de invloed van vormfouten resulteert in minder betrouwbare, mogelijks foute waarden voor de meetonzekerheid, wat kan leiden tot het onterecht goed- of afkeuren van producten. Dit proefschrift ontwikkelt **een methode om de invloed van vormfouten op de meetonzekerheid te bepalen**.

- De meetonzekerheid van een CMM varieert over het meetvolume. Dit is vooral te wijten aan de bewegingsfouten van de CMM in combinatie met de Abbe-afstanden tot de meetschalen. Dit proefschrift beschrijft **een methode om de bewegingsfouten van de CMM te modelleren**. De methode is gebaseerd op het kinematische model van de CMM en gesimuleerde bewegingsfouten voor de verschillende assen. In tegenstelling tot andere methodes is bij deze benadering geen kalibratie van het model noodzakelijk. De enige noodzakelijke input voor deze methode zijn de posities van de meetschalen en een geldige ISO 10360-2 specificatie van de CMM.
- Dit proefschrift presenteert ook **een onzekerheidsberekeningsmethode die de invloed van vormfouten en hardwarefouten van de CMM combineert voor de bepaling van meetonzekerheden bij het meten van vormelementen**. Deze methode is gebaseerd op een Monte-Carlomethode bestaande uit twee stappen: een eerste stap om de onzekerheid op de gemeten vormfout te bepalen, een tweede stap om de onzekerheid op de andere parameters van het vormelement te bepalen.
- Gemeten vormelementen worden vaak gebruikt om werkstukassenstelsels te bepalen of andere vormelementen te construeren (bv. een geconstrueerd punt als intersectie van twee gemeten lijnen). Dit betekent dat er ook onzekerheden zijn voor de werkstukassenstelsels en de geconstrueerde vormelementen. Ook gemeten waarden voor vorm- en plaatstoleranties (loodrecht, evenwijdigheid, coaxialiteit etc.) zullen een geassocieerde meetonzekerheid hebben. Onzekerheidsberekeningssoftware voor CMM's moet deze afgeleide onzekerheden mee in rekening brengen. Dit proefschrift implementeert **een onzekerheidsberekeningssoftware die de invloed van vormfouten en CMM hardwarefouten op de meetonzekerheid van vormelementen en afgeleide parameters in rekening brengt**.



# Abstract

The dimensions of technical products are often of major importance for their proper functioning. Dimensional tolerances define how much the true dimensions may deviate from the aimed dimensions. Dimensional quality control ensures that the dimensional properties of the product comply with the tolerances. For single and non-complex products instruments like vernier calipers and micrometer screw gauges can be used, while for more complex inspection tasks and series measurements usually coordinate measuring machines (CMMs) are used.

Because measurement devices also show measurement errors, a measurement result will never be exact. This means there will always be a measurement uncertainty that should be taken into account while evaluating conformance of products to tolerances. If measurement uncertainty is neglected, this can result in false rejection or false acceptance of products, with possibly far-reaching consequences. Reliable measurement uncertainties are indispensable for unambiguous evaluation of tolerances.

Measurement uncertainty determination for coordinate measuring machines is difficult because of the many uncertainty contributors (CMM hardware errors, temperature, measurement strategy etc.) that are involved. Therefore conventional uncertainty calculation methods, based on analytical propagation of standard uncertainties, can not be applied. Measurement uncertainty determination based on Monte Carlo simulations is a valuable alternative to conventional uncertainty calculation methods. These methods can cope much better with the complexity of CMM measurements.

This thesis describes four contributions to the determination of measurement uncertainties for feature measurements on CMMs by means of Monte Carlo methods:

- When considering measurement uncertainties for feature measurements on CMMs, the influence of feature form deviations is often neglected because feature form deviations are not known in advance and hence difficult to model or to account for. Form deviations of features, like e.g. circles, lines, planes and cylinders, can have an important influence on the measurement uncertainty,

particularly if only a limited set of points is sampled. Neglecting the influence of form deviations results in less reliable or wrong uncertainty statements, that may lead biased acceptance or rejection of parts. This thesis describes **a method to determine the influence of feature form deviations on the measurement uncertainty.**

- The measurement accuracy of a CMM varies over the measurement volume. This is mainly related to the geometric errors of the CMM in combination with the Abbe-offsets to the scales. This thesis presents **a method to model the geometric errors of a CMM.** It is based on the kinematic model of the CMM and simulated motion errors of the different axes. In contrast to other approaches the proposed method does not need an error mapping of the CMM. The only input needed for this method are the scale positions and a valid ISO 10360-2 specification of a CMM.
- This thesis also elaborates **an uncertainty determination method to combine the influence of feature form deviations and CMM hardware errors on the measurement uncertainty for feature measurements.** This method relies on a two-step Monte Carlo method: a first step to determine the form deviation uncertainty, a second step to determine the uncertainties of the other feature parameters.
- Measured features are often used to construct part coordinate systems or other features (e.g. a constructed point as intersection of two measured lines). This means there will also be uncertainties associated with part coordinate systems and constructed features. Similarly there will also be uncertainties related to measured geometrical tolerance values (perpendicularity, parallelism, coaxiality etc.). Uncertainty evaluation software for CMMs should take into account these derived uncertainties. This thesis describes the implementation of **an uncertainty evaluation software that takes into account the influence of feature form deviations and CMM hardware errors on measurement uncertainties of features and derived parameters.**

# Nomenclature

## Abbreviations, acronyms

ASME	American Society of Mechanical Engineers
BMS	Bounding Measurements Set
CAD	Computer Aided Design
CAQ	Computer Aided Quality control
CMM	Coordinate Measuring Machine
CMS	Coordinate Measuring System
CT	Computed Tomography
CTE	Coefficient of Thermal Expansion
CVE	Computer-aided Verification and Evaluation
UES	Uncertainty Evaluating Software
DMIS	Dimensional Measuring Interface Standard
EDM	Electrical Discharge Machining
FFT	Fast Fourier Transform
FPS	Full Parametric Simulation
GUM	Guide to the Expression of Uncertainty in Measurement
ISO	International Organization for Standardization
LCL	Lower Confidence Limit
LSL	Lower Specification Limit
LSQ	Least Squares
MC	Minimum Circumscribed
MCM	Monte Carlo Method
MCS	Machine Coordinate System
MI	Maximum Inscribed
MPE	Maximum Permissible Error
MZ	Minimum Zone
NIST	National Institute of Standards and Technology
NMI	National Metrology Institute
NPL	National Physical Laboratory

OVCMM	Offline Virtual CMM
OOP	Object Oriented Programming
PCS	Part Coordinate System
PDF	Probability Density Function
PMA	Production engineering, Machine design and Automation
PTB	Physikalisch-Technische Bundesanstalt
SBC	Simulation By Constraints
SI	International System of units ( <i>Fr.: Système International d'unités</i> )
UCL	Upper Confidence Limit
UES	Uncertainty Evaluation Software
UPR	Undulations Per Revolution
UPL	Undulations Per Length
USL	Upper Specification Limit
VDI	Association of German Engineers ( <i>Ger.: Verein Deutscher Ingenieure</i> )
VIM	International Vocabulary of Metrology ( <i>Fr.: Vocabulaire International de Métrologie</i> )
VCMM	Virtual CMM

## Symbols

### General symbols

$p$	Position of a feature
$o$	Orientation of a feature
$s$	Size (diameter) of a feature
$f$	Form deviation value of a feature
$M$	Number of Monte Carlo runs
$n$	Number of points used to construct a virtual feature
$N, m$	Number of sampling points
$l$	Array containing the probing point locations
$meas\chi, true\chi, err\chi$	Measured, true and error value of parameter $\chi$
$u, u_c$	Standard uncertainty, combined standard uncertainty
$U$	Expanded uncertainty
$k$	Coverage factor
$Y$	Measurand
$y$	Measurement result, estimate of the measurand
$y'$	Measurement result, with expanded uncertainty, $U$
$X_i$	Input quantity
$x_i$	Estimate for input quantity $X_i$
$x_{i,k}$	$k^{th}$ observation of input quantity $X_i$

$\lambda_s, \lambda_c, \lambda_f$	Cutoff wavelengths
$f_c$	Cutoff frequency
$p$	Level of confidence

## Modelling form deviations

$d()$	Function describing feature form deviation
$\mathbf{d}$	Array containing form deviation profile of a feature
$T_i$	$i^{th}$ Chebyshev polynomial
$s$	Parameter determining the slope of a linear form deviation
$c$	Parameter determining the curving of a linear form deviation
$a_i$	Amplitude of the $i^{th}$ harmonic component of a Fourier series
$N$	Maximum harmonic order of the Fourier series
$w()$	Weighting function
$\mathbf{w}$	Weighting array
$\delta$	Interpolation error
$C_i$	$i^{th}$ point of the circular profile
$N_i$	$i^{th}$ point of the nominal circular profile
$D_i$	$i^{th}$ scaled deviation vector

## Modelling CMM hardware errors

$\{i\}$	Frame (or coordinate system) $i$
${}^bT_a$	Homogeneous Transformation matrix between frame $\{b\}$ and $\{a\}$
${}_a\mathbf{p}^{i,f}$	Coordinates of the $i$ th point of feature $f$ with respect to frame $\{a\}$
${}_a p_x^{i,f}$	$x$ -coordinate of the $i$ th point of feature $f$ with respect to frame $\{a\}$
$exz$	Straightness error motion of $z$ in $x$ direction
$eyz$	Straightness error motion of $z$ in $y$ direction
$ezz$	Positioning error of $z$
$eaz$	Tilt error motion of $z$ around $x$ (pitch)
$ebz$	Tilt error motion of $z$ around $y$ (yaw)
$ecz$	Roll error motion of $z$
${}_2x0z$	$x$ -origin of the $z$ -scale, expressed in frame $\{2\}$
${}_2y0z$	$y$ -origin of the $z$ -scale, expressed in frame $\{2\}$
${}_2z0z$	$z$ -origin of the $z$ -scale, expressed in frame $\{2\}$
$z_{enc}$	Position value read from the $z$ -scale
$e()$	Function describing geometric error of an axis
$\mathbf{e}$	Array containing geometric error of an axis
$s$	Parameter determining the slope of a modelled geometric error
$c$	Parameter determining the curving of a modelled geometric error
$a_i$	Amplitude of the $i^{th}$ harmonic component of a Fourier series

$N$	Maximum harmonic order of the Fourier series
$e_{tot}$	Largest value of the geometric error over the range of the axis
$e_{max}$	Maximum possible value for the geometric error per travel length
$t$	Total travel of the axis
$v$	Performance indicator for a virtual CMM
$^{mpe}l$	Maximum permissible error for a given length
$^{err}l$	Measured error on a given length
${}^0\mathbf{p}^{0,m}$	Position of the probe head mounting point in frame $\{0\}$ (MCS)
${}^0\mathbf{p}^{0,p}$	Position of the probe tip in frame $\{0\}$ (MCS)

## Specific terminology

<i>Actual measured value</i>	Value measured in <i>real life</i> .
<i>Actual true value</i>	True value of the measurand in <i>real life</i> , which is usually unknown.
<i>Simulated measured value</i>	Value measured in <i>simulation</i> .
<i>Simulated true value</i>	True value of measurand in <i>simulation</i> , which is known.
<i>Profile points</i>	Set of points representing the profile / contour of a feature.
<i>Buffer points</i>	Sampled (measured) points of a feature that are stored for later usage.
<i>Actual CMM</i>	CMM used in <i>real life</i> .
<i>Virtual CMM</i>	CMM used in <i>simulation</i> .

# Contents

<b>Dankwoord</b>	<b>i</b>
<b>Samenvatting</b>	<b>iii</b>
<b>Abstract</b>	<b>v</b>
<b>Nomenclature</b>	<b>vii</b>
<b>Contents</b>	<b>xi</b>
<b>1 Introduction</b>	<b>1</b>
1.1 Dimensional quality control . . . . .	1
1.2 Coordinate measuring systems . . . . .	2
1.3 Measurement uncertainty . . . . .	6
1.4 Accept or reject (ISO 14253-1) . . . . .	8
1.5 Metrological traceability . . . . .	11
1.6 GUM method . . . . .	13
1.7 Measurement uncertainty for CMM measurements . . . . .	15
1.8 Goals and scope of the research . . . . .	20
1.9 Means at researcher's disposal . . . . .	21
1.10 Conclusion . . . . .	22

<b>2</b>	<b>Evaluation of CMM measurement uncertainty</b>	<b>23</b>
2.1	Pitfalls of the GUM . . . . .	23
2.2	Performance evaluation tests . . . . .	26
2.3	Methods for uncertainty evaluation of CMM measurements . . . . .	30
2.4	Monte Carlo methods for measurement uncertainty determination . . . . .	31
2.5	Improving current uncertainty evaluation software . . . . .	37
2.6	Conclusion . . . . .	38
<b>3</b>	<b>Integrating feature form deviations in uncertainty modelling</b>	<b>39</b>
3.1	Case study . . . . .	39
3.2	Form deviation, waviness and roughness . . . . .	43
3.3	Former research on the influence of form deviations . . . . .	46
3.4	Error simulation method . . . . .	47
3.5	Profile simulator . . . . .	48
3.6	Sampling module . . . . .	66
3.7	Feature fitting module . . . . .	68
3.8	Error calculation module . . . . .	68
3.9	The number of Monte Carlo iterations, $M$ . . . . .	69
3.10	Results of the error simulation method . . . . .	71
3.11	Conclusions . . . . .	73
<b>4</b>	<b>Modelling CMM hardware errors</b>	<b>75</b>
4.1	Hardware uncertainty contributors . . . . .	75
4.2	Measuring geometric errors . . . . .	77
4.3	Modelling geometric errors . . . . .	80
4.4	Modelling probing system errors . . . . .	97
4.5	Conclusions . . . . .	100
<b>5</b>	<b>Determining task-specific measurement uncertainties</b>	<b>103</b>



- 5.1 Error calculation method extended with hardware uncertainties . . . 103
- 5.2 Uncertainty calculation method . . . . . 104
- 5.3 Conclusions . . . . . 111
- 6 Derived uncertainties, software layout and implementation 113**
- 6.1 Uncertainty on part coordinate systems . . . . . 113
- 6.2 Constructed feature uncertainty . . . . . 117
- 6.3 Uncertainty on measurement of geometrical tolerances . . . . . 118
- 6.4 Software layout . . . . . 120
- 6.5 Algorithm libraries . . . . . 120
- 6.6 Interface to the CMM measurement software . . . . . 122
- 6.7 Conclusions . . . . . 123
- 7 Verification of results 125**
- 7.1 Test 1: Set of gauge blocks . . . . . 125
- 7.2 Test 2: Circle with form deviation . . . . . 128
- 7.3 Test 3: Plate with holes . . . . . 133
- 7.4 Conclusions . . . . . 137
- 8 General conclusions 139**
- 8.1 Context of the research . . . . . 139
- 8.2 Main contributions . . . . . 140
- 8.3 Suggestions for future research . . . . . 143
- A Errors expressed relatively to the measured form deviation 147**
- B Measured geometric errors of Coord3 MC 16 151**
- C Class descriptions 157**
- Bibliography 161**

<b>Curriculum vitae</b>	<b>169</b>
<b>List of publications</b>	<b>171</b>

# Chapter 1

## Introduction

This chapter situates the topic of the thesis within a larger framework. It describes the most important goals of the work with the prerequisite limiting constraints, the means at the researcher's disposal and it defines the scope of the research.

### 1.1 Dimensional quality control

Dimensional quality control is an important part of the production process in manufacturing industry. It is indispensable for the accuracy assertion of the products. Parts are designed and produced to fulfil a certain function. In order to be sure that the part will eventually be able to fulfil this function, the designer assigns tolerances to the part. Tolerances indicate how much a property may deviate from its nominal value. They are necessary because it is impossible to make a part that matches exactly the nominal specifications. The tolerances need to be sufficiently narrow to guarantee a proper functioning of the part, nevertheless they need to be sufficiently broad to allow a cost-effective production. The narrower the tolerances, the more expensive the product.

Dimensions of a part are often of major importance. Dimensional quality control ensures that the dimensional properties of the product comply with the tolerances. In addition to dimensional quality control, products often undergo other tests to check for a.o. surface and material properties. Frequently only a sample of a complete production batch is inspected; sometimes every part needs to be checked.

## 1.2 Coordinate measuring systems

For single inspection tasks of non-complex products, commonly used (1D) inspection instruments, like e.g. vernier calipers, screw micrometers and height measuring devices, are often most suited. For more complex inspection tasks, like e.g. positional tolerances or repetitive measurements, conventional *coordinate measuring machines (CMMs)* are very useful. During the last decades CMMs have become indispensable in the production environment. Besides conventional coordinate measuring machines there are many other *coordinate measuring systems (CMSs)* which are more and more used for coordinate metrology.

### 1.2.1 Conventional coordinate measuring machines

A conventional CMM has, just like many manufacturing machines, a Cartesian X-Y-Z-configuration. At the end of the Z-axis a probing system is mounted. The probing system, which can be moved in 3D-space, detects points on the surface of the workpiece. These points are used to reconstruct features like e.g. circles, lines, planes, cylinders, . . . The parameters of the features and the relationships between the features allow to evaluate the tolerances. Figure 1.1 illustrates the different CMM components, the CMM structure and the probing system are discussed in the next paragraphs.

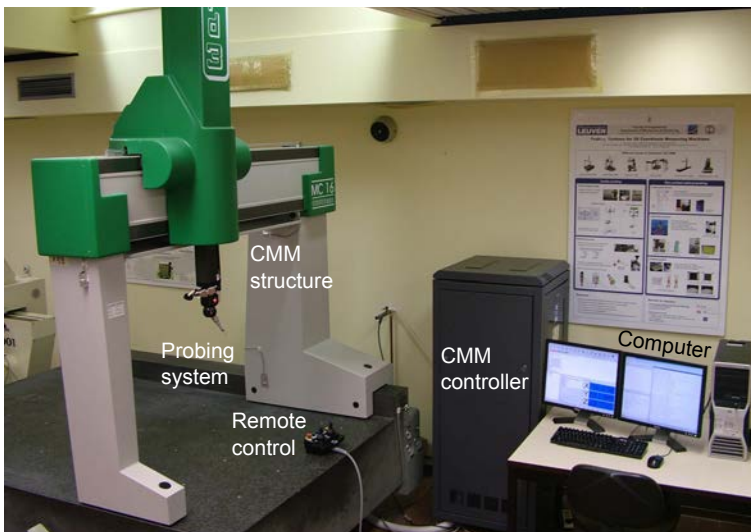


Figure 1.1: A conventional coordinate measuring machine (Coord3 MC 16 CMM at the Department of Mechanical Engineering of K.U.Leuven) and its components.

## CMM structure

There is a wide variety in measuring ranges and axes configurations for conventional CMMs. Figure 1.2 shows the most common CMM configurations. Every configuration has specific advantages and disadvantages regarding accuracy, accessibility and cost. The hardware of conventional CMMs is discussed in more details in Chapter 4.

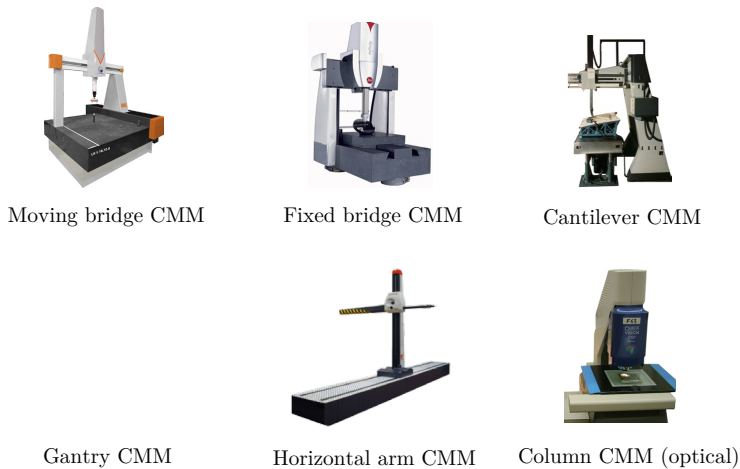


Figure 1.2: Common CMM configurations. Adapted from [1].

## Probing system

There are a large number of different probing systems for CMMs. Probing systems can be classified in two large groups: *contact probing systems* and *non-contact probing systems*. Contact probing systems are often called *tactile probing systems* and since most non-contact probing systems use optical methods for point detection, they are often referred to as *optical probing systems*. Non-contact probing systems do not have to make (mechanical) contact with the workpiece in order to probe points. As a result they measure much faster, furthermore they will not deform a flexible workpiece while probing. Contact probing systems have mostly the advantage of being more accurate and reliable. Figure 1.3 shows a further classification of these two groups of probing systems.

The most popular contact probing system for CMMs is definitely the *touch-trigger probe*. When the probe approaches the workpiece surface, the probe tip touches the surface and the stylus will deflect. This is detected by the probe sensor which

triggers the machine to read out the position of the axes. Taking into account the diameter of the probing tip, the position of the point on the surface can be determined. Many ways have been developed to detect the deflection of the probe [2]. Most commercial touch-trigger probing systems make use of an electrical switch or strain gauges.

Some probing systems do not only detect deflection (i.e. contact) of the stylus but also measure the amount of deflection of the probe tip. These *measuring probes* are usually more accurate than touch-trigger probes. Since the deflection of the probe tip is known, this information can be used as a feedback for the CMM. This makes it possible to scan a path while the probe tip is continuously in contact with the workpiece. Probes used in *scanning mode* can be less accurate due to accelerations and stick-slip, but will be able to measure a larger number of points in a shorter time [3, 4]. During the last decade several contact micro-probes, used for measuring very small features and dimensions, have been developed [2, 5].

When looking at the non-contact probing systems, 2D probing systems are of most interest. Vision probes are mostly used on special dedicated CMMs (see Figure 1.2). Also laser line scanners have become very popular in recent years. Because they can measure more than ten thousand points a second they can easily digitise the complete surface of a workpiece. This makes them very suited for measuring free form surfaces like e.g. car bodies and mould products. The accuracy of laser line scanners is not yet competitive with contact probing systems [6].

## 1.2.2 Other types of coordinate measuring systems

Although this section is outside the direct scope of this thesis, it is important to realise that a lot of other types of coordinate measuring systems exist. In industry these systems are more and more used as an alternative for a conventional CMM. Most of these systems are portable and are therefore often called *portable or mobile CMMs*. Figure 1.4 gives an overview of the most important non-conventional CMMs [7]. They are divided into two categories: systems for discrete point measurements and systems for scanning point measurements. The latter are suited for surface digitisation.

The only CMS, besides the conventional CMM, based on *serial kinematics* is the measuring arm. Several systems for discrete point measurements are based on *two angular measurements and one optical length measurement*. A third category can be considered as systems relying on *multiple optical angular measurements*.

Coordinate measuring systems for scanning measurements can be divided into four categories: (1D) *point scanning*, (2D) *laser line scanning*, (3D) *fringe projection* systems and (3D+) *computed tomography*. Many CMSs for discrete point measurements can be equipped with a laser line scanner to perform scanning

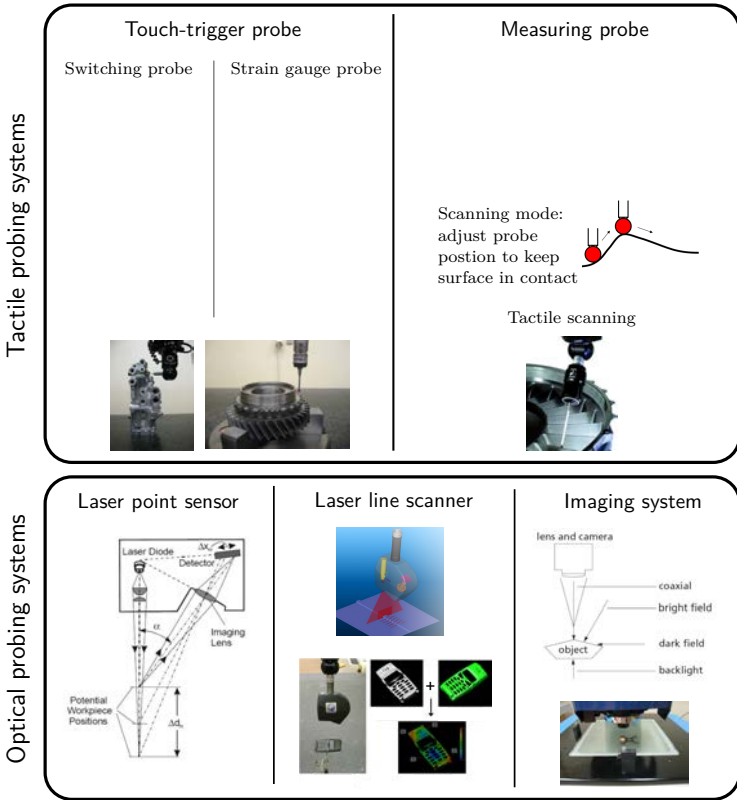


Figure 1.3: A classification of probing systems for CMMs. Adapted from [1].

measurements. Fringe projection systems can be used as a stand-alone CMS for surface digitisation but their limited measuring range can also be extended by combining them with photogrammetry [9]. Computed tomography (CT) is an emerging but very promising technology for coordinate metrology [10]. CT can be used to measure features *inside* parts, which can not be reached with conventional probing systems.

Because of their working principles, non-conventional CMMs often have very *non-uniform measurement uncertainties*. E.g. laser trackers will have low uncertainties in radial direction, due to the laser interferometer measurement. Perpendicular to this direction the uncertainty will be much higher due to the limited resolution of the angular encoders. This is important to keep in mind while measuring.

In recent years several of these CMSs have become very popular. However it is very unlikely that they will replace conventional CMMs. The growth of this type of CMSs

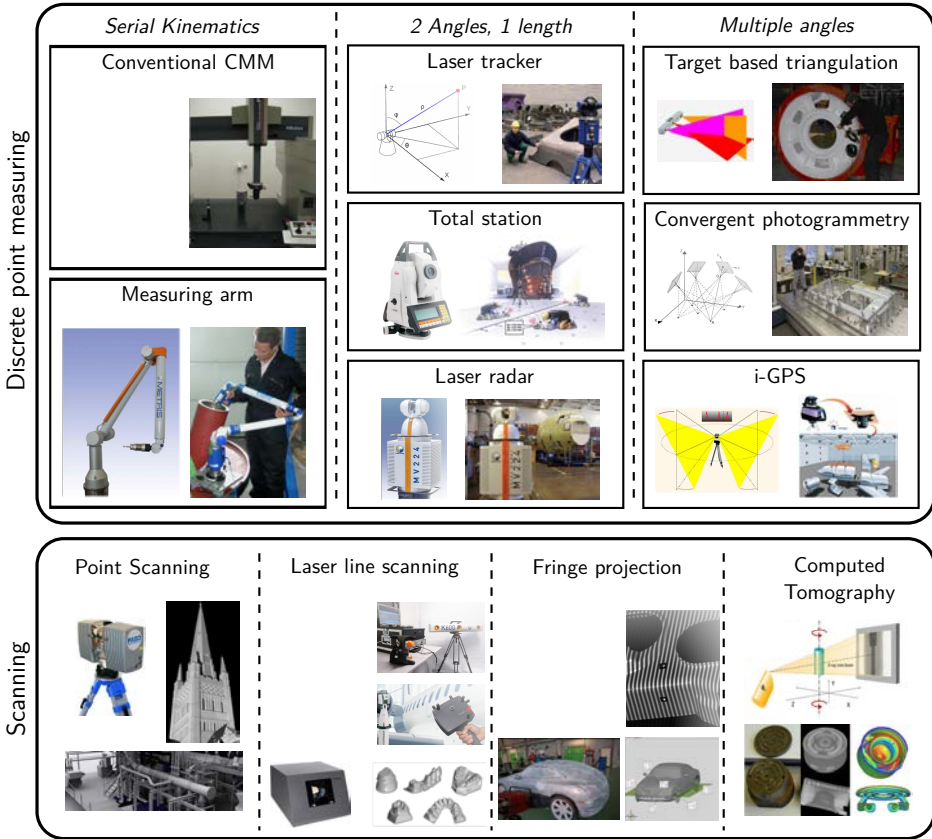


Figure 1.4: A classification of common coordinate measuring systems. Adapted from [8].

rather opened a new application domain for coordinate metrology. Measurements that were impossible or difficult some years ago are now possible as a result of these upcoming technologies. This can also be concluded from the results of recent projects performed by K.U.Leuven, Groep T and De Nayer Instituut [7, 11].

### 1.3 Measurement uncertainty

When performing a measurement of any kind, one can be sure of one fact: the measurement result will never be exact. Even with the best measuring equipment,



used under the best circumstances, there will always be a measurement error. The measurement error can be defined as follows:

**Definition 1.1** *Measurement ERROR =*  
*MEASURED quantity value - TRUE quantity value*

This definition is very suited for theoretic purposes and for reasoning about measurement errors but poses problems when trying to quantify the measurement error. Since the true value of the measurand (= quantity intended to be measured) is never known it is impossible to define the measurement error. To overcome this issue, ISO-VIM uses a twofold definition [12]:

**Definition 1.2** *Measurement ERROR =*  
*MEASURED quantity value - REFERENCE quantity value*

*The reference quantity value can be:*

- *the true quantity value. In this case the measurement error can not be known, as the true value is never and will never be identifiable.*
- *a reference standard with a measured quantity value having a negligible measurement uncertainty, or a conventional quantity value. In this case the measurement error is known, although its value will not be completely correct.*

This means that the measurement error is only known when performing calibration measurements. Generally the measurement error is unknown. This does not mean that no quantitative indication of the quality of the measurement result can be given. Although the measurement error is unknown, it is often possible to specify the measurement uncertainty. The following two definitions give an understandable definition for measurement uncertainty [13]:

**Definition 1.3** *The MEASUREMENT UNCERTAINTY is an estimate characterising the range of values within which the true value of a measurand lies. (VIM:1984)*

**Definition 1.4** *The MEASUREMENT UNCERTAINTY is a measure of the possible error in the estimated value of the measurand as provided by the result of a measurement.*

Again both definitions are very useful for reasoning about measurement uncertainty but they focus also on unknowable quantities like ‘error’ and ‘true value’. Therefore ISO-VIM currently adopts following definition [12]:

**Definition 1.5** *The MEASUREMENT UNCERTAINTY is a non-negative parameter characterising the dispersion of the quantity values being attributed to a measurand, based on the information used.*

Avoiding the use of unknowable quantities resulted in a very vague definition. Definitions 1.3 and 1.4 of measurement uncertainty are more comprehensible and furthermore also consistent with the current VIM definition. Therefore it is the author's opinion that using definition 1.5 is superfluous in most circumstances.

It is absolutely necessary to specify the measurement uncertainty of a measurement in order to have a quantitative indication of the quality of the measurement. In ISO-GUM (paragraph 0.1) this is stated very clearly [13]:

“When reporting the result of a measurement of a physical quantity, it is obligatory that some quantitative indication of the quality of the result be given so that those who use it can assess its reliability. Without such an indication, measurement results cannot be compared, either among themselves or with reference values given in a specification or standard.”

Also the ISO 9000 standards family imposes to specify the measurement uncertainty. Before getting into more detail about methods to determine measurement uncertainties, two important metrological concepts that require the determination of measurement uncertainties are discussed in the following sections:

- The concept of ‘accept or reject’ decisions (ISO 14253-1).
- The concept of traceability.

## 1.4 Accept or reject (ISO 14253-1)

Workpiece specifications are usually given as an upper (USL) and lower (LSL) specification limit. These limits should not be exceeded by the true value of the measurand. When neglecting the influence of measurement uncertainty, proving conformance or non-conformance with specification is very straightforward. When the measured value lies within the specification (or tolerance) limits there is conformance with specification. When the measured value lies outside the specification limits there is non-conformance with specification. The range of possible measurement results is divided in a conformance and non-conformance zone.

In practice however, there will always be a measurement uncertainty that needs to be taken into account. As a consequence the sharp edge between conformance and

non-conformance zone will disappear and a zone of uncertainty will appear. This is illustrated in Figure 1.5.

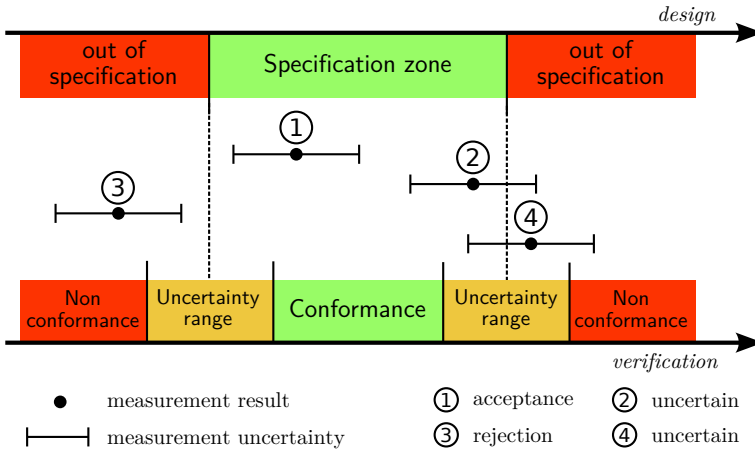


Figure 1.5: Proving (non-)conformance with specification, ISO 14253-1.

The complete statement of the result of measurement can be expressed as follows (see Section 1.6):

$$y' = y \pm U \quad (1.1)$$

Where  $y$  represents the measurement result,  $U$  the expanded uncertainty and  $y'$  the result of measurement as complete statement<sup>1</sup>.

Conformance with specification is proved when the result of measurement, complete statement,  $y'$ , falls completely within the specification [14]:

$$LSL < y - U \quad \text{and} \quad y + U < USL$$

Non-conformance with specification is proved when the result of measurement, complete statement,  $y'$ , falls completely outside the specification zone:

$$y + U < LSL \quad \text{or} \quad USL < y - U$$

Neither conformance nor non-conformance with specification can be proved when the result of measurement, complete statement,  $y'$ , includes one of the specification

<sup>1</sup>In Eq. 1.1 and Figure 1.5 it is supposed that the uncertainty range is symmetric to the measured value, i.e. the measured value lies in the middle of the uncertainty range. This is not a prerequisite, equations represented in this section are, mutatis mutandis, also valid for asymmetric uncertainty ranges.

limits:

$$y - U < LSL < y + U \quad \text{or} \quad y - U < USL < y + U$$

This situation occurs when  $y$  falls within one of the uncertainty ranges:

$$LSL - U < y < LSL + U \quad \text{or} \quad USL - U < y < USL + U$$

It is clear that the width of this uncertainty zone depends on the magnitude of the measurement uncertainty. This means that it is *impossible to accept or reject without specification of the measurement uncertainty*. The conformance zone reduces with increasing measurement uncertainty. This is illustrated in Figure 1.6. Under certain circumstances (very narrow specification zones in combination with high measurement uncertainties) it is possible that the conformance zone completely disappears. Under these circumstances it is impossible to prove conformance according to ISO 14253-1<sup>2</sup>.

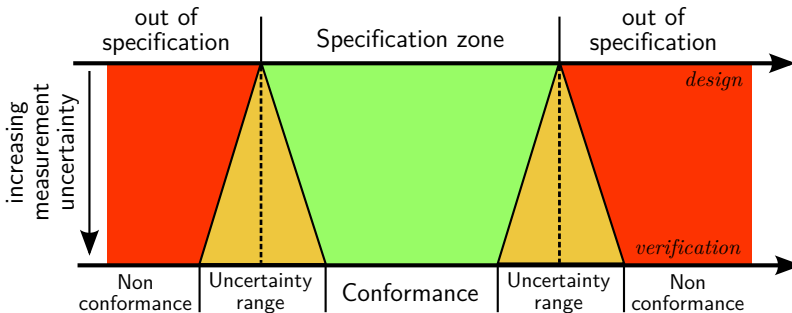


Figure 1.6: Influence of increasing measurement uncertainty on (non-)conformance zone, ISO 14253-1.

The measurement uncertainty always works against the party that wants to proof conformance or non-conformance. A lower measurement uncertainty will benefit the party that is trying to provide the proof.

**Remark 1.1** *To avoid the problems related to the uncertainty zone, where neither conformance or non-conformance decisions can be taken, the ‘1/10 rule of thumb’ is often used. This rule states that the measurement uncertainty should not exceed one tenth of the width of the specification zone. If this is the case, the measurement uncertainty can be neglected. This rule however suffers from several shortcomings:*

- *Most important, it allows both false rejection and false acceptance.*

<sup>2</sup>Customer and supplier may agree on other rules to prove conformance.

- *It makes it impossible to measure narrow tolerances, because these measurements will not comply with the ‘1/10 rule’. Therefore this rule is often weakened to the ‘1/5 rule’, allowing even more false rejection and false acceptance.*
- *When the measurement uncertainty is large compared to the width of the specification zone, it is more difficult to prove conformance according to ISO 14253. Sometimes it is even impossible to prove conformance because the conformance zone completely disappeared. However, it will always be possible to prove non-conformance when the product is sufficiently far out of specification (this unfortunately occurs often in practice when the specification zone is very narrow). According to ISO 14253 it is possible to prove non-conformance even when the measurement uncertainty is larger than the width of the specification zone. According to the ‘1/10 rule’ it is impossible to make decisions once the measurement uncertainty exceeds one tenth of the width of the specification zone.*

*It is the author’s opinion that the use of this ‘1/10 rule of thumb’ should be strongly discouraged in favour of the ISO 14253 approach.*

**Remark 1.2** *ISO 14253 intentionally uses the term specification limit instead of tolerance limit. This is because ISO 14253 applies for checking specifications of workpieces (defined by tolerance limits) as well as for checking specifications of measuring equipment itself (often defined by maximum permissible errors, MPE).*

*Although this approach is very logic, it often poses problems when it is applied to measuring equipment. Often the wrong uncertainty is taken into account. When a vernier calliper is used to check the specification of a workpiece, the most important uncertainty contributor to take into account is the one of the vernier calliper (e.g.  $U_v = 0.07$  mm), together with influences of temperature, workpiece, handling etc. However, when evaluating the specification (MPE) of the vernier calliper, by measuring e.g. a gauge block, the situation is different. In this case the gauge block is testing the vernier calliper, so the uncertainty of the gauge block (e.g.  $U_e = 0.0003$  mm) should be taken into account (together with temperature, handling etc.) and not the one of the vernier calliper.*

## 1.5 Metrological traceability

Another important metrology concept, that also relies on measurement uncertainty, is *metrological traceability*<sup>3</sup>. According to ISO-VIM, traceability is defined as

<sup>3</sup>Instead of ‘metrological traceability’ often the abbreviated term ‘traceability’ is used. To avoid confusion with other uses of the term ‘traceability’, the word ‘metrological’ should not be omitted. [12]

follows [12]:

**Definition 1.6** *The METROLOGICAL TRACEABILITY is the property of a measurement result whereby the result can be related to a reference through a documented unbroken chain of calibrations, each contributing to the measurement uncertainty.*

This unbroken chain of calibrations is the *metrological calibration chain*. To establish this metrological calibration chain a *calibration hierarchy* is needed:

**Definition 1.7** *The CALIBRATION HIERARCHY is a sequence of calibrations from a reference to the final measuring system, where the outcome of each calibration depends on the outcome of the previous calibration.*

An illustration of metrological traceability through a calibration hierarchy for dimensional measurements is given in Figure 1.7. The *measuring equipment* (e.g. screw micrometer) is the first step in the traceability chain. Measuring equipment is often calibrated with *working standards* by the user. Working standards are calibrated with *secondary standards* by accredited calibration laboratories. These secondary standards are calibrated with *primary standards* by national metrology institutes (NMI). Primary standards are directly linked to *SI-units*. Since each calibration depends on the outcome of another calibration, measurement/calibration uncertainty will only rise when going down in the calibration hierarchy.

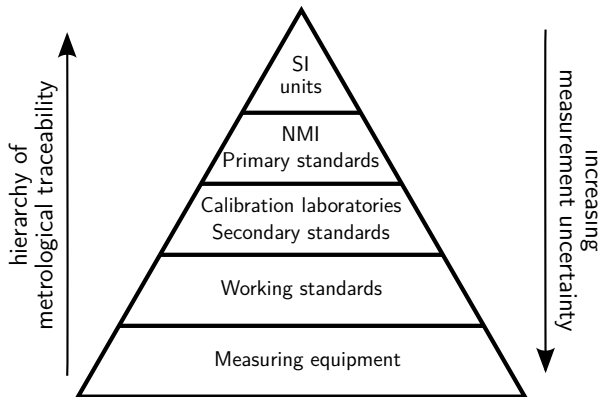


Figure 1.7: Illustration of metrological traceability through a calibration hierarchy.

**Remark 1.3** *It is a common misconception that traceable measurements are also accurate. This is false, a measurement with a very high measurement uncertainty can be perfectly traceable.*

## 1.6 GUM method

The two previous sections illustrated the importance of measurement uncertainty. This section will describe how measurement uncertainty is usually determined according to the ‘Guide to the expression of uncertainty in measurement’, referred to as ISO-GUM [13].

### 1.6.1 Measurement function

In many cases, the *measurand*  $Y$  is not measured directly, but is determined from *input quantities*  $X_i$  by a *measurement function*:

$$Y = f(X_1, X_2, \dots, X_N) \quad (1.2)$$

An estimate of the measurand  $Y$ , denoted by  $y$ , can be obtained from Eq. 1.2 by using input estimates  $x_i$  for input quantities  $X_i$ . So the result of the measurement is given by:

$$y = f(x_1, x_2, \dots, x_N) \quad (1.3)$$

### 1.6.2 Combined standard uncertainty

The combined standard uncertainty  $u_c(y)$  is the estimated standard deviation associated with measurement result  $y$ . This standard deviation can be derived from the estimated standard deviations associated with the input estimates  $x_i$ , termed standard uncertainties and denoted by  $u(x_i)$ :

$$u_c^2(y) = \sum_{i=1}^N \sum_{j=1}^N \frac{\partial f}{\partial x_i} \frac{\partial f}{\partial x_j} u(x_i, x_j) \quad (1.4)$$

$$= \sum_{i=1}^N \left( \frac{\partial f}{\partial x_i} \right)^2 u^2(x_i) + 2 \sum_{i=1}^{N-1} \sum_{j=i+1}^N \frac{\partial f}{\partial x_i} u(x_i, x_j) \quad (1.5)$$

Eq. 1.5 is based on the first-order Taylor series approximation of Eq. 1.3 and is also called the ‘rule of propagation of uncertainty’<sup>4</sup>. The partial derivatives  $\partial f / \partial x_i$  are equal to  $\partial f / \partial X_i$  evaluated for  $X_i = x_i$ . These partial derivatives are also called *sensitivity coefficients*.  $u(x_i, x_j)$  denotes the estimated covariance associated with

<sup>4</sup>This rule is often referred to as ‘general law of error propagation’. Since the inputs are uncertainties it is more appropriate to call it ‘law of propagation of uncertainty’.

$x_i$  and  $x_j$ , so  $u(x_i, x_i)$  equals  $u^2(x_i)$ . When all input quantities are independent, Eq. 1.5 simplifies to:

$$u_c^2(y) = \sum_{i=1}^N \left( \frac{\partial f}{\partial x_i} \right)^2 u^2(x_i) \quad (1.6)$$

### 1.6.3 Type A and B evaluation of standard uncertainty

In order to calculate the combined standard uncertainty from Eq. 1.5 or 1.6 the standard uncertainties of all input estimates  $x_i$  need to be known. ISO-GUM defines two types of standard uncertainty evaluation:

- Type A: evaluated from a series of repeated observations.
- Type B: evaluated from available knowledge.

#### Type A evaluation of standard uncertainty

If an input quantity  $X_i$  is estimated from  $n$  independent repeated observations, the arithmetic mean  $\bar{X}_i$  is used as an estimate for  $x_i$ . The associated standard uncertainty is calculated as the experimental standard deviation of the mean:

$$u(x_i) = s(\bar{X}_i) = \frac{\sqrt{\frac{1}{n-1} \sum_{k=1}^n (x_{i,k} - \bar{x}_i)^2}}{\sqrt{n}}$$

#### Type B evaluation of standard uncertainty

It is not always possible to have a set of independent observations for each input quantity. In this case, the standard uncertainties  $u(x_i)$  are determined by scientific judgement based on all available information on the possible variability of input quantity  $X_i$ . This information includes previous measurement data, manufacturer's specifications, calibration data, experience, . . .

**Remark 1.4** *Type A evaluation of uncertainties is often linked to random errors and type B to systematic errors. This is an important misconception. Uncertainties due to random errors can be evaluated as type B and uncertainties due to systematic errors can be evaluated as type A.*

*Notice also that the terms random and systematic error are very dependent on the field of view as well as temporal and spatial constraints. This is the reason why usage of the terms 'random' and 'systematic' errors is discouraged by ISO-GUM. According to GUM known systematic errors should be compensated.*



**Remark 1.5** *Type B evaluation can have the same or even better reliability than type A evaluation, certainly when the number of observations for type A evaluation is low.*

## Expanded uncertainty

The expanded uncertainty is used when one wants to define an *interval* that covers a large fraction of the distribution of the values that could be reasonably attributed to the measurand. The expanded uncertainty is defined as the standard uncertainty multiplied by a coverage factor  $k$ :

$$U = k \cdot u_c(y)$$

The result of a measurement is then expressed as  $Y = y \pm U$ . When the probability distribution characterised by  $y$  and  $u_c(y)$  is approximately normal and the number of degrees of freedom is sufficiently large, one can assume that taking  $k = 2$  corresponds to an interval with a level of confidence  $p$  of about 95 %, and that taking  $k = 3$  corresponds to an interval with a level of confidence of about 99,7 %.

## 1.7 Measurement uncertainty for CMM measurements

### 1.7.1 Uncertainty contributors for CMM measurements

To evaluate the measurement uncertainty of CMM measurements, a lot of uncertainty contributors need to be taken into account. There are several ways to classify all uncertainty contributors. One possible classification is given in Figure 1.8.

Following five classes can be identified:

**Hardware** This category contains the errors related to the hardware components of the CMM like probe errors, CMM geometric errors including scale errors.

**Environment** Environmental conditions will have an important influence on the measurement uncertainty. Temperature is here of extreme importance. Not only temperature deviations (from 20 °C) but also temperature gradients, in time and space, will influence the measurement uncertainty [15]. Other environmental influences like vibrations, non-constant air supply (in case of air bearings) and lighting conditions (in case of optical probing systems [16, 17]) can also influence the measurement uncertainty.

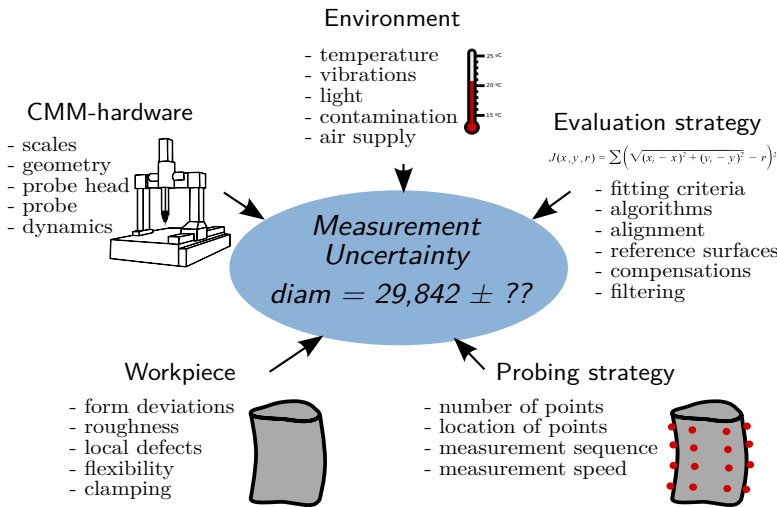


Figure 1.8: Uncertainty contributors for CMM measurements.

**Workpiece** The workpiece itself also has an important influence on the measurement uncertainty. A common source of measurement uncertainty are form deviations, but also surface imperfections like roughness and local defects (e.g. burrs and scratches) can be important. Sometimes also deformations due to probing forces or clamping play a role.

**Probing strategy** The probing strategy determines the number of measurement points and their location. Furthermore, the measuring sequence and settings like measurement velocity can be important. The more complex the probing system that is used, the more parameters will influence the measurement uncertainty.

**Evaluation Strategy** The evaluation strategy covers: the type of fitting criteria (least squares, minimum zone, ...), the algorithm accuracy, the possible filters used, the alignment strategy, the selected reference surfaces, the used compensations etc.

## 1.7.2 Task-specific measurement uncertainties

The multiplicity of uncertainty contributors and their strong interaction make that measurement uncertainties will depend a lot on the specific measurement task. That is why uncertainties that take all (or most of) the uncertainty contributors and their interactions into account, are often called *task-specific uncertainties*.

Chapter 2 illustrates that it is very difficult to apply the conventional GUM approach to calculate task-specific measurement uncertainties. It also discusses the current state-of-the-art alternatives to calculate task-specific measurement uncertainties. The following examples will show the importance of task-specific measurement uncertainties for CMMs.

### Interaction of form deviations and sampling strategy: circular features

The best known example of form deviations interacting with sampling strategy is the measurement of a 3-lobed circular form deviation with six equally distributed points. If the measurement points are taken in the tops and valleys of the 3-lobed contour, the complete out-of-roundness of the circle can be identified from the measurement, however if the start point is rotated with  $30^\circ$  none of the out-of-roundness of the circle will appear in the measurement (Figure 1.9(a)).

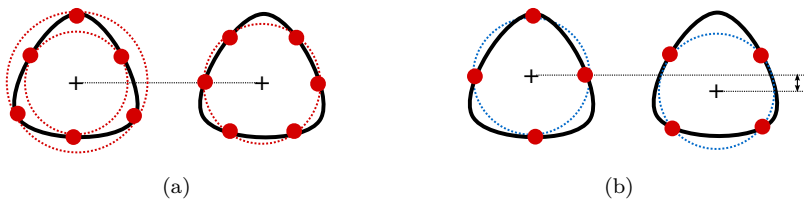


Figure 1.9: Measuring a circle with 3-lobed form deviation.

Contrary to popular belief, this is not only of importance for the roundness and diameter uncertainty but also for position uncertainty. This is illustrated in Figure 1.9(b) for a four points measurement of a 3-lobed circle (i.e. circle with a 3-lobed form deviation).

### Interaction of form deviations, sampling strategy and evaluation strategy

Measurement point distribution in combination with feature form deviations can have an important influence on the measurement uncertainty. Figure 1.10 represents a cut plate with a large opening that is somewhat curved (exaggerated in the figure). Suppose this plate is measured twice: once with only 6 points (Figure 1.10(a)) and once scanned (e.g. with a laser scanner) resulting in a very large set of measurement points (Figure 1.10(b)).

When the orientation of the least squares planes is considered, there will be a large difference in orientation for the two measuring methods (the difference in orientation is somewhat exaggerated in Figure 1.10(b)). Since there are more points on the left side of the plane, the orientation of the least squares plane will be

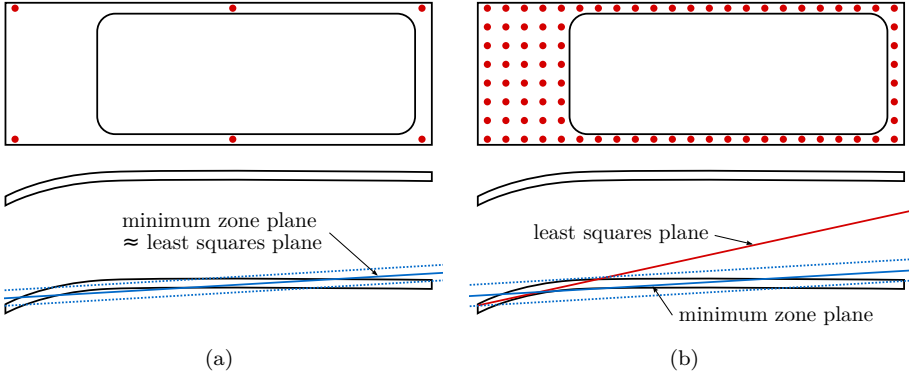


Figure 1.10: Measuring a curved plate.

determined mainly by the orientation of this part of the plane. If the minimum zone fitting criterion is used instead of least squares, the difference in orientation of the associated planes will be much smaller. This illustrates how also the evaluation strategy can influence the measurement uncertainty.

**Interaction of temperature with sampling strategy and clamping**

Although most accurate CMM measurements are done in a temperature controlled room, temperature will still have an influence on the measurement uncertainty. Consider the workpiece of Figure 1.11. The most narrow tolerance applies to the distance between the first and last step of the shaft (450 mm). This should be kept in mind when measuring the part. Instead of measuring all steps sequentially one should measure the first and last step immediately after each other. This will reduce the influence of thermal effects (of machine and workpiece) significantly.

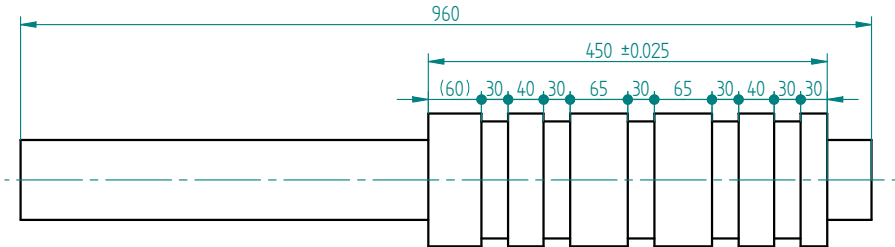


Figure 1.11: Measuring a stepped axis.

For measurements that take quite some time it can be important where the workpiece is clamped. The error due to thermal expansion (or shrinkage) of the workpiece can be reduced by 50% just by clamping the workpiece of Figure 1.11 in the middle instead of at the side.

**Measurements that are ill conditioned: measuring a circle segment**

A well known example of ill conditioned measurements is the measurement of a circle segment [18]. The measurement of a small circle segment will always result in very high measurement uncertainties on both diameter and position. A small measurement error will have a large influence on the measurement results. This is illustrated in Figure 1.12 where both circles seem to fit to the measured points quite well.

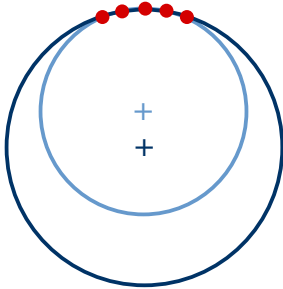


Figure 1.12: Measuring a circle segment.

**Measurements that are ill conditioned: measuring coaxiality**

Figure 1.13(a) shows another example of an ill conditioned measurement. The coaxiality tolerance is given with respect to datum A, which is a very short cylinder. This means that a small measurement error can result in a large error on orientation of the datum axis. It is very likely that the measured coaxiality value is dominated by the measurement error on the datum axis. This kind of measurements will result in high measurement uncertainties.

Figure 1.13(b) shows the same part but now the datum feature and the tolerated feature are interchanged. Since the datum feature is much larger in this case, the errors on the orientation of the datum axis will be much smaller. As a consequence the measurement uncertainty on the coaxiality value will also be much smaller.

Some people argue that Figure 1.13(a) is rather an example of a badly designed part than it is an example of a part that will result in high measurement uncertainties.

It is true that the represented part also suffers from an ill conditioned design, but this does not necessarily mean that it is a bad design. It regularly occurs that these types of tolerances are inevitable. The designs in Figure 1.13(a) and 1.13(b) are completely different, and should thus also fulfil another function.

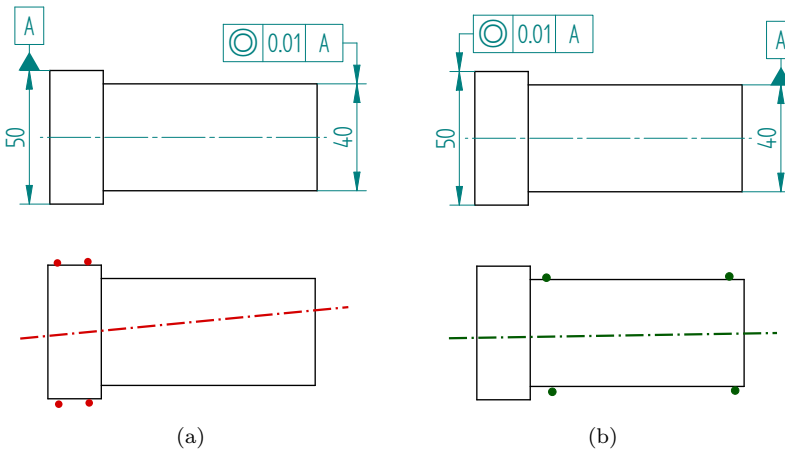


Figure 1.13: Measuring a coaxiality tolerance.

### 1.7.3 Influence of form deviations on measurement uncertainty

Feature form deviations (shortly form deviations) are deviations from the perfect form of the feature. A circle will never be perfectly round, a line never perfectly straight and a plane never perfectly flat, whatever manufacturing process is used. The type of form deviation is usually related to the manufacturing process that is used, therefore it is also called the *manufacturing signature*. Chapter 3 discusses typical form deviations for several types of features. That chapter also illustrates that form deviations are often the most important source of measurement uncertainty.

People who tried to determine task-specific measurement uncertainties for CMMs focussed until now almost only on CMM hardware uncertainties (see Chapter 2). To obtain reliable uncertainty statements, all uncertainty contributors should be incorporated, including feature form deviations.

## 1.8 Goals and scope of the research

The goal of this research can be formulated as follows:

*Determine for each CMM measurement result a measurement uncertainty in order to make unambiguous evaluation of tolerances possible and dimensional quality control more reliable.*

Some additional requirements will be taken into account:

- The research should focus on the *integration of the influence of feature form deviations* in the uncertainty statement. This has not been addressed before and is very important for reliable uncertainty statements.
- The uncertainty determination should be possible in an *automated* way with as little user input as possible.
- The developed method should be implemented as a software package for a *conventional CMM* but needs to be extendable to other types of CMMs (e.g. measuring arm, laser tracker, ...).

## 1.9 Means at researcher's disposal

The dimensional metrology room of the department of mechanical engineering at K.U.Leuven houses two conventional computer controlled coordinate measuring machines:

- a **Mitutoyo FN-905** moving bridge CMM (see Figure 1.14) with a specification of  $U_1 = 4.2 + 5 \cdot L/1000 \mu\text{m}$ . The CMM is equipped with an articulating probe head.
- a **Coord3 MC 16** moving bridge CMM (see Figure 1.1), retrofitted with a Metris-LK controller. It has an ISO 10360-2 specification of  $MPE_E = \pm (5 + 5 \cdot L/1000 \mu\text{m})$ . The CMM is equipped with an articulating probe head. It uses the Metris Camio software with DMIS (Dimensional Measuring Interface Standard) as its native programming language [19]. The software has also extensive capabilities to communicate with third party software. This makes this software very suited for research.

Both machines have been used during the research, but the implementation of the software is done with the Coord3 machine.

Most computer analyses during the research are done with Matlab®. The uncertainty evaluation software is also developed with Matlab® but could be easily translated to other programming languages because of the object oriented implementation.



Figure 1.14: Mitutoyo FN-905 CMM at the Department of Mechanical Engineering of K.U.Leuven.

## 1.10 Conclusion

This introductory chapter clarifies the importance of knowing the uncertainties of measurement results in order to make unambiguous evaluations of specifications possible. The conventional GUM recipe, based on analytical error propagation, is the best known method for uncertainty evaluations. However, because of some drawbacks of this basic GUM method and the complexity of CMM measurements, this method is not really suited for uncertainty evaluations of CMM measurements. This will be explained in the next chapter.

The large number of uncertainty contributors for CMM measurements implies that uncertainty statements for CMMs are very task-specific. Almost every CMM measurement will have another measurement uncertainty. In order to obtain reliable measurement uncertainties every uncertainty contributor should be taken into account. The influence of feature form deviations is often neglected but has nevertheless an important influence on the measurement uncertainty.

The final aim of this research is to determine a measurement uncertainty for each CMM measurement in order to make unambiguous evaluation of tolerances possible and dimensional quality control more reliable.



## Chapter 2

# Evaluation of CMM measurement uncertainty

The multiplicity of uncertainty contributors and their strong interactions make uncertainty evaluations for CMM measurements very complicated. This chapter illustrates that the conventional GUM approach for the calculation of uncertainty is not suited for CMM measurement. In addition, the advantages and drawbacks of the state-of-the-art alternatives for measurement uncertainty evaluation are discussed. Finally this chapter tries to indicate how current uncertainty evaluation software could be improved to obtain complete and reliable uncertainty statements for CMM measurements.

### 2.1 Pitfalls of the GUM

As already mentioned in Chapter 1, the standard recipe for determination of measurement uncertainties is described in the *Guide to the expression of uncertainty in measurement* or shortly *GUM*. This document is meant as a guideline for uncertainty evaluation of all kinds of measurements. Notwithstanding its general validity there are not many people using the GUM for uncertainty evaluation of their measurement results. Many people are not even using any kind of uncertainty evaluation at all.

The use of the conventional GUM procedure should be promoted more. It uses a very straightforward approach that gives reliable uncertainties for most kinds of measurements. However, there are some important pitfalls related to the use of the

conventional GUM procedure that should be avoided. These issues should be kept in mind when using the GUM:

1. *Assumption of independence:* In order to avoid the complex covariance terms of Eq. 1.5 it is often assumed that all uncertainty contributors are independent. This is done because it simplifies the calculation but also because it is often impossible to obtain the covariances of all input quantities. In order to take into account all covariances, the complete covariance matrix should be known. Sometimes it is justified to make these simplifications but it can also lead to large underestimations (in case of positive correlations) or overestimations (in case of negative correlations) of the measurement uncertainty. Important covariances should not be neglected.
2. *Propagation of standard deviations:* The conventional GUM uses standard deviations as a measure for uncertainty. The uncertainties of all input quantities are expressed as standard deviations, the uncertainty of the output quantity is also a standard deviation. One could use the expanded uncertainty with coverage factor  $k$  to obtain an uncertainty interval. Usually one would like to choose a value of  $k$  that corresponds to a certain level of confidence  $p$  (e.g. 95 % or 99 %). This is only possible under very specific circumstances because this requires information about the output distribution. People often wrongly assume that a coverage factor of  $k = 2$  will correspond to a 95 % level of confidence. This will only be true if the measurement result has a normal distribution. Assuming a normal distribution when the true distribution has a high skewness or curtosis can lead to completely wrong coverage intervals. If the measurement result follows a Poisson distribution (non-negative and heavily skewed for small values of  $\lambda$ ), which occurs in many engineering problems, calculating the expanded uncertainty will often lead to infeasible intervals with a negative LCL. On the other side, the UCL will be highly underestimated.
3. *First order Taylor approximation:* The conventional GUM-method is based on the first order Taylor approximation of the measurement function. As long as this linear approximation is acceptable in the interval of interest (interval around the measurement result) this leads to correct uncertainty statements. If the linear approximation is insufficient, the calculated measurement uncertainty will be incorrect. The following measurement function will always lead to (almost) zero uncertainty if the estimate  $x$  is (almost) zero, independent of the value of  $a$  and the input uncertainty  $u(x)$ :

$$y = f(x) = ax^2 \quad \Rightarrow \quad u(y) = 2ax \cdot u(x)$$

Although it is possible to use higher order Taylor approximations, this is seldom done in practice.

4. *Analytical relationship*: The conventional GUM-method assumes that the measurand can be written as an analytical function of a set of input quantities with associated uncertainties. If this analytical relationship is not available, the sensitivity coefficients can not be determined. As an alternative, sensitivity coefficients could be determined experimentally but this is a time consuming process and only possible for a limited set of problems.

The complexity of the measurement process of CMMs, with all the different uncertainty contributors, makes it impossible to define an analytical relationship between all uncertainty contributors and the measurand. Besides that, most CMM measurement results are obtained by using iterative fitting algorithms that do not provide an analytical relationship.

5. *Systematic errors*: The GUM-method also assumes that all known systematic effects are identified and compensated. The uncertainties due to imperfect compensation of known systematic effects are taken into account as an additional uncertainty contributor. This is a very good way to deal with systematic effects. However, in practice it is often very hard to compensate for all known systematic effects. Temperature deviations (from 20 °C) of the part have an important systematic effect on the measurement uncertainty<sup>1</sup>. However during most CMM measurements there is no compensation for temperature deviations of the part.

Despite the issues mentioned above, the conventional GUM-method will provide correct uncertainty statements for many measurements in practice. The simplifications made by using the conventional GUM are of minor importance and will not affect the calculated uncertainties. But in some situations it is inappropriate (e.g. first order approximation not valid) or impossible (e.g. no analytical relationship) to use the conventional GUM-method.

The lack of an analytical relationship between the input quantities and the measurement result is the most important reason why the conventional GUM-method can not be applied to CMM measurements. A valuable alternative to the conventional GUM-method is the use of Monte Carlo simulations to determine measurement uncertainties. Recently a supplement that is dealing with Monte Carlo simulations for measurement uncertainty evaluation, has been added to the GUM standard [21]. Section 2.4 explains these Monte Carlo methods and also discusses state of the art CMM uncertainty evaluation methods, that also use Monte Carlo simulations.

---

<sup>1</sup>ISO/TR 16015 prescribes how to deal with systematic errors and uncertainty of length measurements due to thermal influences [20]. Under certain circumstances measured lengths can be reported without compensating for systematic errors due to thermal influences; in these situations the correction value should nevertheless be provided together with the measured length.

## 2.2 Performance evaluation tests

Although uncertainties are almost never specified for CMM measurements, it is still possible to make statements about the accuracy of a CMM. This can be done by *performance evaluation tests*. These tests make use of a *calibrated test-artefact* that is measured according to a *specified measurement strategy* and *specified environmental conditions*. The measured deviations from the calibrated values can be used as a performance indicator of the CMM, although it can not be considered as a measurement uncertainty. Performance evaluation tests can be specified by the user or they can be taken from international standards.

### 2.2.1 ISO 10360: Acceptance and reverification tests for coordinate measuring machines (CMM)

The ISO 10360 standard describes several performance evaluation tests for conventional CMMs. The most frequently used part of this standard is ISO 10360-2:2001<sup>2</sup> [22]. This standard describes two performance tests, one to evaluate probing performance and one to evaluate size measuring performance:

**Probing test** A calibrated sphere is measured with 25 points according to a given sampling pattern. Orientation of the stylus can be chosen by the user. A Gaussian associated sphere is fitted through all 25 points. For each of the 25 points the radial distance  $R$  is calculated. The range of these distances defines the probing error  $P$ :

$$P = R_{\max} - R_{\min}$$

**Size test** A set of five material standards of size (step gauge or gauge blocks) is measured under seven different orientations on the CMM. Each measurement is repeated three times. The shortest material of size should be smaller than 30 mm, the longest should be longer than 66% of the largest spatial diagonal of the measuring volume of the CMM. For each of the 105 measurements, the error on size  $E$  is calculated. All errors are plotted on a graph as a function of the measured length.

The probing error,  $P$ , and the error on size,  $E$ , should not exceed a given maximum permissible error (MPE).  $MPE_P$  is specified as a single value, while  $MPE_E$  is usually expressed in the following way:

$$MPE_E = \pm(A + L/K)$$

---

<sup>2</sup>Recently ISO 10360-2 has been updated. The probing test has been moved to an updated version of ISO 10360-5. This means that ISO 10360-2:2009 now only contains the size test.

with

- $A$  a positive constant expressed in  $\mu\text{m}$ ;
- $K$  a dimensionless constant;
- $L$  the measured size in mm.

In case of *acceptance tests*, these values are stated by the manufacturer of the CMM. In case of *reverification tests*, they are defined by the user. The latter could be useful when the CMM is installed in a non-conditioned environment and a lower accuracy is allowed. The result of a ISO 10360-2 test is *fail* or *pass*, it should never be the purpose of this test to define the MPE values.

Table 2.1 gives an overview of all current standards in the ISO 10360 series, part 8 till part 11 are not yet published.

ISO 10360-1:2000	Vocabulary
ISO 10360-2:2009	CMMs used for measuring linear dimensions
ISO 10360-3:2000	CMMs with the axis of a rotary table as the fourth axis
ISO 10360-4:2000	CMMs used in scanning measuring mode
ISO 10360-5:2010	CMMs using single and multiple stylus contacting probing systems
ISO 10360-6:2001	Estimation of errors in computing Gaussian associated features
ISO 10360-7:2011	CMMs with imaging probing systems
ISO/DIS 10360-8	CMMs with optical distance sensors
ISO/DIS 10360-9	CMMs with multiple probing systems
ISO/CD 10360-10	Laser trackers for measuring point-to-point distances
ISO/WD 10360-11	Computed tomography

Table 2.1: Overview of ISO 10360 (August 2011).

## 2.2.2 Acceptance and reverification tests for other coordinate measuring systems

The use of ISO 10360, as a standardized way for describing and checking CMM performance, is widely adopted by industry. This makes it a lot easier to compare CMMs of different manufacturers. Unfortunately the use of ISO 10360 is currently restricted to conventional (Cartesian) CMMs.

Many problems arise when one tries to apply an unmodified version of ISO 10360-2 to other types of coordinate measuring systems. Many non-Cartesian CMSs have measurement uncertainties that are very dependent on the measurement direction and the location in the measurement volume. Furthermore, establishing reference lengths longer than 66 % of the measurement range is impossible for most non-Cartesian CMSs. E.g. a laser tracker has a low measurement uncertainty in the radial direction but the measurement uncertainties in directions perpendicular

to the radial direction can be very high, due to the limited resolution of the angular encoders. Laser trackers have ranges of 100 m and more. It is very hard to establish a reference length of this size. Part 10 of ISO 10360, that is currently under development, describes acceptance and reverification tests for laser trackers. Part 11, also under development, covers computed tomography.

Until now only finalised national standards for performance evaluation of other coordinate measuring systems exist. The most important national standards for CMSs, other than Cartesian CMMs, are summarised in Table 2.2.

Type of CMS	Standard	Title
Articulated arms	VDI 2617-9	Accuracy of coordinate measuring machines - Characteristics and their reverification - Acceptance and reverification tests for articulated arm coordinate measuring machines
	ASME B89.4.22	Methods for performance evaluation of articulated arm coordinate measuring machines
Laser trackers	VDI 2617-10	Accuracy of coordinate measuring machines - Characteristics and their checking - Acceptance and reverification tests of lasertrackers
	ASME B89.4.19	Performance evaluation of laser-based spherical coordinate measurement systems
Computed tomography	VDI 2617-13	Accuracy of coordinate measuring machines - Characteristics and their testing; Guideline for the application of DIN EN ISO 10360 for coordinate measuring machines with CT-sensors
Fringe projection systems	VDI 2634	Optical 3D measuring systems

Table 2.2: National standards on performance evaluation tests for other coordinate measuring systems, apart from conventional CMMs.

Recently the ISO 10360 series has been extended with some standards on probing systems for CMMs, different from conventional tactile probing systems. As can be seen in Table 2.1, ISO 10360 now also covers imaging probing systems (part 7) and optical distance sensors (part 8). Part 9 discusses performance tests for CMMs with multiple probing systems.

Unfortunately laser line scanners, that are becoming more and more popular for conventional and non-conventional CMMs, are currently not covered by ISO 10360. Part 8 focusses on 1D optical distance sensors (like e.g. laser focussing sensors). The test described in Part 8 could, *mutatis mutandis*, be adapted to serve as a performance test for laser line scanners. Unfortunately all optical probing systems are influenced by a lot of uncertainty contributors and many of them will not be revealed by the current performance tests described in ISO 10360. Recently quite

some research has been done on performance tests for optical probing systems on CMMs at K.U.Leuven and other labs [6, 23, 24].

Creating standards describing performance tests for all types of CMSs is a great challenge for the coming years. When these new standards can get widely adopted, it will enable the user to verify the stated performance of a CMS and compare performances of different CMSs. One should however always be careful when comparing performance statements, even when these statements are according to international standards. Measurement conditions (like e.g. temperature range of the room, measuring speed, ...) are seldom imposed by the standard, so they can be determined by the manufacturer or the user. When determined by the manufacturer, they are regularly too strict for the normal working environment of the CMS.

### 2.2.3 Difference with measurement uncertainty

Performance evaluation tests are very important and useful. However, unlike what many people think, they give absolutely no uncertainty statement for a CMM measurement. One could argue that a performance specification of a CMS can be considered as a task-specific measurement uncertainty for workpieces that are similar to the test artefact used during the performance test. In this perspective, the ISO 10360-2 statement about error on size can be considered as an uncertainty statement for a similar length measurement if the probe configuration, the environmental conditions, measurement strategy, the surface quality, etc. are all (approximately) the same as during the performance test. These conditions are seldom fulfilled in practice. It will for example be impossible to use the  $MPE_E$  value, provided by the ISO 10360-2 specification, to calculate the uncertainty when measuring the characteristics of a circle. It will also be impossible to use it to calculate the uncertainty on an angle measurement.

A CMM expert can get a rough idea about the measurement uncertainty for several measurement tasks. For many other measurement tasks this will be far more difficult or even impossible (cf. Section 1.7.2). Obtaining *reliable* uncertainty statements, based on only performance specifications and expert knowledge is very hard, due to the task specificness of the measurement uncertainty for CMMs. Every measurement task will have a different measurement uncertainty. Performance specifications are defined for one specific measurement task under very specific circumstances and the results can not just be “extrapolated” to other measurement tasks. Performance evaluation tests should be used for *benchmarking*, not for uncertainty statements.

## 2.3 Methods for uncertainty evaluation of CMM measurements

Since the conventional GUM approach is not suited for CMM measurements and results of performance tests can not be used as uncertainty statements, other methods should be used to determine measurement uncertainties for CMMs. Regularly used methods are:

- *Use of multiple measurements strategies without calibrated workpieces or standards (ISO/TS 15530-2 - deleted)*: In case of multiple measurement strategies, the measurement under consideration is performed multiple times. This allows to determine the repeatability/reproducibility of the measurement. The repeatability and reproducibility of a measurement are lower limits for the measurement uncertainty. Measurement repeatability is determined under constant measurement conditions while measurement reproducibility is determined under changing measurement conditions<sup>3</sup>. The repeatability and reproducibility are independent of the true value, which is an advantage of this method since the true value will not be known. At the same time it is a disadvantage because systematic errors with respect to the true value are not taken into consideration and hence no upper limit for the measurement uncertainty is provided. This method allows to determine a lower limit for the measurement uncertainty but does not provide an upper limit. Since measurement repeatability and reproducibility do not account for systematic errors, it will be difficult to prove full traceability by this type of methods. This is probably also one of the reasons why this standardisation project is deleted. This method is nevertheless useful when no other ways to determine measurement uncertainties are available.
- *Use of multiple measurements strategies with calibrated workpieces or standards (ISO/TS 15530-3 [25])*: A similar experimental approach as described above is used. The measurement is also performed multiple times, but in this case a *calibrated* workpiece or standard is used as test object. The calibrated workpiece used during the uncertainty evaluation should be very similar to the workpiece used during the actual measurement. The errors measured during the uncertainty evaluation with the calibrated workpiece are used to determine measurement uncertainties for actual measurements. The variations in measurement conditions during the uncertainty evaluation should be similar to the variation in measurement conditions during the actual measurement. Since this method makes use of calibrated workpieces it also accounts for systematic measurement errors, which makes it also easy to prove traceability. This is a very reliable method to determine measurement uncertainty, but it is usually very expensive and time consuming [26].

---

<sup>3</sup>For complete definitions of repeatability / reproducibility / accuracy, see ISO-VIM [12].



- *Use of computer simulation (ISO/TS 15530-4 [27]):* When computer simulation is applied, the actual measurement will be simulated multiple times. The simulation is based on a mathematical model of the measurement process and takes into account all important influence quantities. During simulation, these influence quantities are varied within their assumed ranges. This will result in variations on the simulated measurement results. The spread on the simulated measurement results is used to determine the measurement uncertainty. Since this is a non-experimental approach, it is much faster and cheaper. The main difficulty is to find a mathematical model that incorporates all influence quantities. It is important to know which influences are incorporated during the simulations. This method is discussed in more details in the next section. Software to calculate measurement uncertainties is called *uncertainty evaluation software (UES)*.
- *Use of expert judgement:* Use of expert judgement is probably the most popular method to determine measurement uncertainties. Measurement uncertainties are calculated based on the knowledge and experience of a CMM expert. Regarding the complexity of CMM measurements, expert judgement will not always be reliable and is only recommended when no other methods are applicable.

## 2.4 Monte Carlo methods for measurement uncertainty determination

### 2.4.1 Monte Carlo methods as alternative to the conventional GUM approach

The use of computer simulation for determination of measurement uncertainties is becoming a valuable alternative for the conventional GUM framework. Recently a supplement to the GUM has been published. This supplement describes the propagation of probability distributions through a mathematical model of measurement as a basis for evaluating measurement uncertainty, and its implementation by a Monte Carlo method [21]. It is said that this alternative approach is of particular value when:

- The linearisation of the model provides an inadequate representation
- The probability function of the output quantity departs appreciably from a Gaussian distribution or a scaled and shifted  $t$ -distribution, e.g. due to marked asymmetry (skewness) or kurtosis.

If the approach described in this document is applied correctly, it can get around all pitfalls described in Section 2.1. In case the method is applied for measurements that also allow a valid application of the conventional GUM uncertainty framework, the calculated standard uncertainties will be the same.

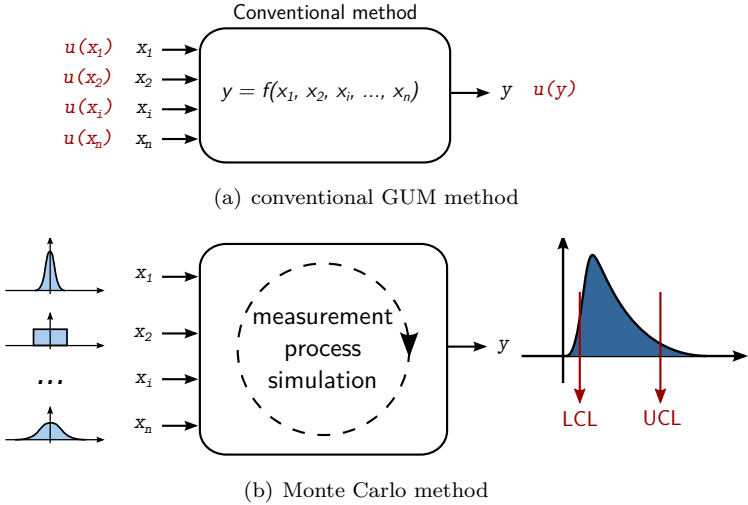


Figure 2.1: Determination of measurement uncertainties through propagation of standard uncertainties  $u(x)$  (a) and propagation of distributions (b).

Figure 2.1 illustrates schematically the difference between the conventional GUM uncertainty framework (a) and the use of Monte Carlo methods to calculate measurement uncertainties (b). In the conventional GUM framework the measurement uncertainty is calculated through propagation of standard uncertainties. The result is also a standard uncertainty. When using propagation of probability density functions the resulting probability functions can seldom be calculated analytically. Instead Monte Carlo methods can be used. Monte Carlo methods propagate distributions by performing random sampling from probability distributions of input quantities. The resulting output distribution can be used to determine standard uncertainties as well as lower (LCL) and upper confidence limits (UCL).

It is also possible to combine the use of Monte Carlo methods with the conventional GUM approach. The conventional GUM method will often be used to determine the standard uncertainties for the input distributions.

## 2.4.2 State of the art

Monte Carlo methods have already been successfully applied to determine uncertainties for machine tool error mappings and for calibration measurements on CMMs [28, 29, 30]. They are also popular for tolerance analysis. Several authors have also used Monte Carlo methods to build UES for CMM measurements. The most important contributions are summarized below.

### Virtual CMM

The idea of using Monte Carlo simulations to determine CMM measurement uncertainties was first introduced by researchers from PTB in Germany [31]. They called their concept *Virtual CMM (VCCM)* and described it as follows: “The virtual CMM performs a point by point simulation of measurements, emulating the measurement strategy and the physical behavior of the CMM with the dominating uncertainty contributions disturbing the measurement”.

As illustrated in Figure 2.2, the VCMM can be considered as an extension to the normal CMM measurement process. The thick black line represents the regular measurement process, the gray line the VCMM extension. For every single probed point, the VCMM generates multiple ( $n$ ) simulated probed points. Through every set of simulated points a feature is fitted, using the same algorithms as for the real probed points. The probability density functions (PDFs) of the simulated feature parameters can be used to determine the measurement uncertainty.

In order to simulate realistic CMM behaviour, all uncertainty contributors need to be measured or estimated. Probe errors can be determined by measuring a reference sphere. When multiple probes are used, this is done for all of them. Geometric errors are determined by measuring a calibrated ball plate. The ball plate measurement can be used to determine all 21 parametric errors components (see Chapter 4) and to compensate for the errors through software correction. Remaining geometric uncertainties (due to ball plate calibration uncertainty, drift, limitations of the method, . . .) can be used as input for the VCMM. Some other uncertainty contributors that are difficult to measure, like e.g. temperature influence, are either estimated or neglected [32].

Instead of using ball plate measurements also other techniques (a.o. laser interferometer measurements) could be used to determine the geometric errors of the CMM and related uncertainties. Because CMM uncertainties (of the current CMM state) can be modelled very accurately in this way, this approach leads to very accurate uncertainty estimates since it has the ability to model the ‘sweet and bad spots’ [*sic*] of the actual CMM [33]. Nevertheless this approach has also some important disadvantages. These methods are usually very time consuming

and will fail when the error state of the CMM changes (due to thermal influences or temporal drift) which makes them less robust.

CMM manufacturer Zeiss offers an optional module to their Calypso CMM software, called OVCMM (Offline Virtual Coordinate Measuring Machine) to calculate measurement uncertainties. This module is based on the VCMM engine of PTB.

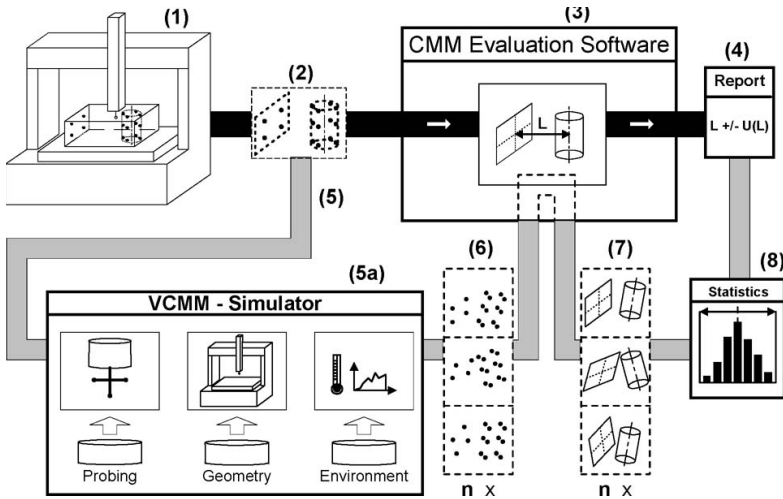


Figure 2.2: The Virtual CMM (VCMM) concept [34]: the actual CMM (1), actual measured points (2), CMM software calculating associated features (3), measurement report (4), probing point locations as input for the UES (5), CMM simulator (5a), simulated measured points (6), simulated associated features (7), PDFs of feature parameters (8).

### Simulation by constraints

Phillips et al. called the methods that use complete parametric error specification of the CMM (like Virtual CMM) *full parametric simulation (FPS)* [33]. The authors suggested a generalization of FPS in order to make it easier to implement and more robust. They call their approach, developed at NIST, *simulation by constraints (SBC)* [33].

When using SBC, one starts with building a very large set of virtual CMMs, each having a different (random) error state. Every virtual CMM is characterized by 21 parametric errors. In theory this set could be infinite. In practice one will not simulate positioning errors larger than 1 mm if the actual CMM shows no errors larger than 10  $\mu\text{m}$ . This very large set of virtual CMMs, that covers the complete

*state space* of the CMM, is afterwards bounded by a bounding measurements set (BMS). The BMS contains a set of actual measurements of a reference length (e.g. a step gage). Every measurement of the bounding measurements set is also measured by all virtual CMMs. Every CMM state that shows the same errors as the complete BMS (taking into account the repeatability and the uncertainty of the reference length) is retained, all other CMM states are rejected. The success ratio will, of course, be very low (between  $10^{-4}$  and  $10^{-7}$ ). In order to be more time efficient they implemented gradient search techniques to find good virtual states more quickly. The BMS defines a bounded region in state space that contains all 'good CMM states'. Each of the states could be the true state because each of the virtual states shows the same errors as the true state of the CMM.

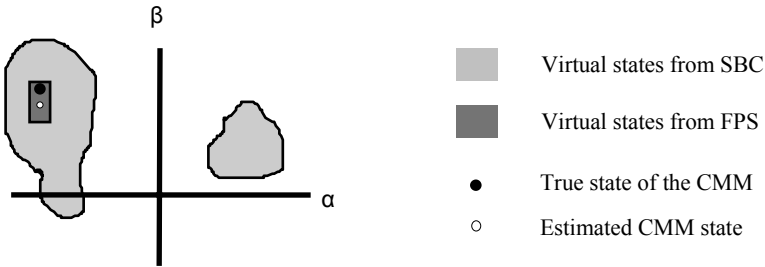


Figure 2.3: Schematic illustration of the simulation by constraints concept [33].

Figure 2.3 illustrates this visually for a 2 dimensional state space. The figure shows that the bounded region by the BMS contains the true state of the CMM but also contains the possible states of the CMM that would result from FPS. Moreover, if a very extended BMS is used, the obtained region will be the same as the one with FPS. That is why the authors call their method a generalization of FPS. To determine measurement uncertainties, the resulting subset of virtual CMMs can be used in a similar way as described above for Virtual CMM.

**Expert CMM**

In the Expert CMM project another UES, similar to VCMM, was developed [35]. Balsamo et al. focussed with their implementation mainly on modularity and generality. They also proposed a two-step implementation: (1) Calculating the uncertainty of the point coordinates due to hardware, environment, ... (2) propagating the point uncertainty through the part program, which defines the measurement strategy, to get the final uncertainty of the feature parameters. It also seems that the results of this project where integrated in a patent [36]. The patent is assigned to CMM manufacturer Brown & Sharp DEA.

### PUNDITCMM

PUNDITCMM is a commercial UES for CMM measurements. The hardware uncertainty contribution is based on the SBC approach of NIST [26]. A demo version of the software is available at the Department of Mechanical Engineering at K.U.Leuven. The software is meant for offline utilisation and is not connected to any type of conventional CMM software. It has the ability to import the CAD-file of a workpiece and has a build-in database of common CMMs. The measurement uncertainty is also determined by means of Monte Carlo simulation. An interesting feature of this software is the ability to add form deviations to the nominal feature (Figure 2.4). This allows the user to investigate the influence of form deviation on the measurement uncertainty for a given measurement strategy. The uncertainties are calculated based on the distribution of the simulated measurement results.

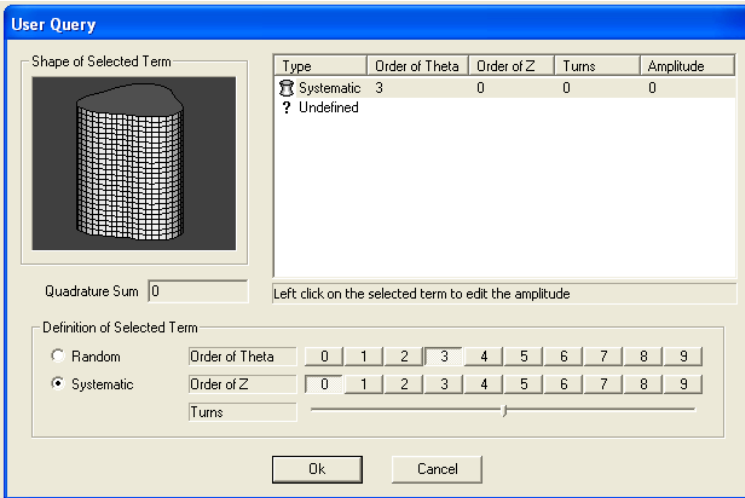


Figure 2.4: Ability to model form deviations in the PUNDITCMM software.

The PUNDITCMM software allows to investigate the influence of feature form deviations in combination with CMM hardware errors and the sampling strategy on the measurement result. However, the software does not really integrate the influence of feature form deviations because it is based on “what if” scenarios: e.g. “What will be the uncertainties if a circle with a diameter of 50 mm and a 3-lobed roundness deviation of 0.075 mm is measured with 4 equidistant sampling points?” The user can model a feature with a specific, user defined, form deviation (Figure 2.4). Thereafter the measurement uncertainty is determined for a given sampling strategy applied to the modelled feature. This is a very useful tool, but it does not allow to transfer the uncertainties to real CMM measurements, since the true value of the form deviation and its true shape (elliptic, 3-lobed, etc) are

assumed to be known (given), while they generally are unknown. This is the most important obstruction for modelling the influence of feature form deviation on CMM measurement uncertainties: other uncertainty contributors, like e.g. uncertainties due to CMM hardware, can be assessed in advance, but the influence of feature form deviations will depend on the unknown magnitude and shape of the true form deviation of the feature to be measured.

## 2.5 Improving current uncertainty evaluation software

The examples in the previous section showed that using Monte Carlo simulations for CMM measurement uncertainty evaluation has already been investigated since more than 10 years. Although some research results are incorporated in commercial software (Pundit CMM and OVCMM extension for ZEISS Calypso software) those software are not yet broadly adopted in industry<sup>4</sup>. According to the author, the most important reasons for this are:

1. *Missing uncertainty contributors*: It is impossible to incorporate all uncertainty contributors. Therefore it is important to document which uncertainty contributors are included and which are not. This is also emphasized by ISO 15530-4 [27]. Current implementations of UES focus mainly on hardware uncertainties. Two important uncertainty contributors for discrete tactile measurements, that are missing in current UES, are *feature form deviations* and *temperature influences*. Until now, the influence of feature form deviations was never fully integrated in UES for CMMs.
2. *No online determination of uncertainties*: Both commercial UES (OVCMM and PUNDITCMM) are offline software packages. This means that uncertainties are calculated before or after the actual CMM measurement. This means extra workload and is unwanted for most users. Offline software has the advantage of being independent from conventional CMM software. Furthermore there will be no risk that an error or crash of the UES will influence the conventional CMM software. Monte Carlo simulations can also take a lot of time, which poses problems for online operation. The latter issue has become less important with increasing computer power.

Although good reasons can be found for offline operation of UES, not many users are willing to spend much extra time for uncertainty evaluation. If an uncertainty estimate needs to be provided for every measurement result, the most seamless solution is to perform the uncertainty determination online.

---

<sup>4</sup>An inquiry by the author (end 2009) showed that Rolls-Royce was the only European company that used the Pundit software. According to people from PTB the OVCMM module from Zeiss was only installed at some NMIs.

3. *Lack of interest from manufacturers and industry:* Almost everyone is convinced that providing measurement uncertainty is of great importance, but almost no one is willing to spend effort on it. People should get convinced that they can earn money by taking measurement uncertainties serious.

CMM manufacturers will not be eager to provide software that informs the user about measurement uncertainty. Calculated measurement uncertainties will be often higher than the ISO 10360 specification of the CMM. However, most CMM users will not like a third possibility besides *fail* and *pass*. Having parts where no decision can be made seems to make quality control more complicated.

## 2.6 Conclusion

This chapter started with a discussion about the pitfalls of the conventional GUM approach. This showed that the conventional GUM framework is not suited for evaluation of CMM measurement uncertainties. Results of acceptance and reverification tests can be used for verification and benchmarking but not for uncertainty evaluations, contrary to many people's opinion. Valid methods for uncertainty evaluations of CMM measurements include *multiple measurement strategies*, the use of *calibrated workpieces*, *expert judgement* and *computer simulation*.

The use of computer simulation has a good potential and is already investigated by several authors. There even exists commercially available uncertainty evaluation software, but this software is not yet adopted by industry. Current software neglects some important uncertainty contributors, like the influence of feature form deviations, and can not be used online. This thesis proposes an uncertainty evaluation software, based on Monte Carlo simulations, that incorporates uncertainty contributors due to feature form deviations and that can run online during CMM measurement.



# Chapter 3

## Integrating feature form deviations in uncertainty modelling

In Chapter 1 and Chapter 2 it has already been indicated that form deviations have an important influence on the measurement uncertainty for CMMs, and that current uncertainty evaluation software (UES) is not able to take this uncertainty contributor into account. This chapter starts with a case study to illustrate that feature form deviations of the workpiece are often the most important uncertainty contributor, more important than hardware uncertainties of the measuring equipment. Afterwards it is clarified which surface irregularities are categorized as form deviations. After discussing previous work on this topic this chapter elaborates a method to quantify the influence of form deviations on the measurement uncertainty. At first hardware uncertainties are neglected. The next chapter shows how this method can be extended to incorporate hardware uncertainties. Finally some results will illustrate how this method can be useful in practice.

### 3.1 Case study

Some examples in Section 1.7.2 already showed that feature form deviations can have an important influence on the measurement uncertainty. This case study is meant to illustrate that form deviation can (often) be the most important uncertainty

contributor. In these situations the current UES will highly underestimate the measurement uncertainty.

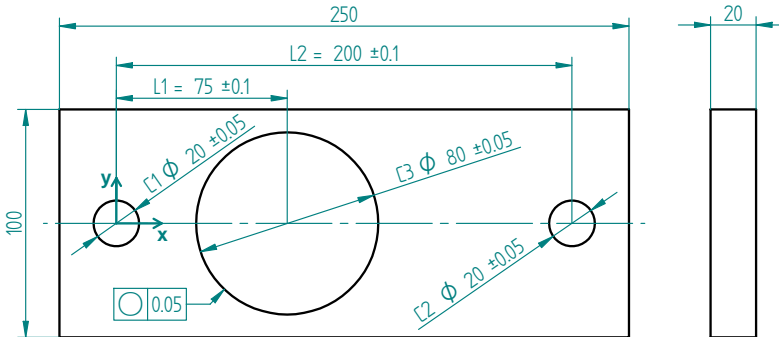


Figure 3.1: Test part for case study.

Figure 3.1 shows the drawing of the test part of this case study. The part is manufactured in aluminium on a Maho MH5000W three axes milling machine. Due to clamping on the machine, the central hole C3 of the part shows a 2-lobed form deviation of about 0.1 mm (this means that the roundness is out of specification according to the drawing of Figure 3.1). The form deviations of the 2 outer holes are much smaller.

After machining, the position, diameter and roundness of the central hole are measured several times on the Coord3 MC16 CMM (cf. Section 1.9). The least squares fitting criterion was used to determine the associated features. Each time the part is relocated to a different position and orientation on the CMM, to incorporate the influence of scale and geometric errors of the CMM. At each position the circle is measured twice with  $N$  equidistant sampling points: once with a fixed starting point at starting angle  $\theta_s = 45^\circ$  to the x-axis of the part coordinate system and once with a random starting point. The alignment procedure is the same in both situations. Table 3.1 gives the results of these measurements for  $N = 4$ , at three different positions on the CMM. It can be seen that the variation of the measured feature parameters is much larger when the starting angle  $\theta_s$  is random. This is due to the interaction of feature form deviations and sampling strategy.

When more points are measured, the influence of form deviations diminishes. To illustrate: Figure 3.2 plots the measurement results obtained at 35 different positions on the CMM for  $N = 4$  to  $N = 15$  equidistant measuring points. The dispersion of the measurement results for fixed starting angle is mainly due to hardware influences of the measuring equipment (no influence of measuring strategy, minimal temperature deviation). The dispersion of the measurements with varying starting angle also incorporates the influence of the form deviation of the measured circle and is significantly larger. These dispersions are an indication

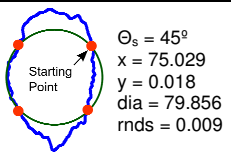
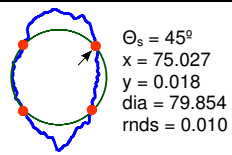
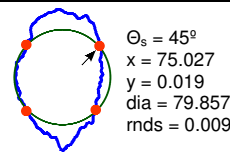
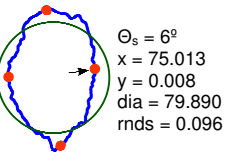
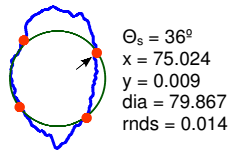
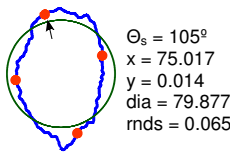
	CMM position 1	CMM position 2	CMM position 3	max. $\Delta$
$\Theta_s$ fixed	 $\Theta_s = 45^\circ$ $x = 75.029$ $y = 0.018$ $\text{dia} = 79.856$ $\text{rnds} = 0.009$	 $\Theta_s = 45^\circ$ $x = 75.027$ $y = 0.018$ $\text{dia} = 79.854$ $\text{rnds} = 0.010$	 $\Theta_s = 45^\circ$ $x = 75.027$ $y = 0.019$ $\text{dia} = 79.857$ $\text{rnds} = 0.009$	$\Delta x = 0.002$ $\Delta y = 0.001$ $\Delta \text{dia} = 0.003$ $\Delta \text{rnds} = 0.001$
$\Theta_s$ random	 $\Theta_s = 6^\circ$ $x = 75.013$ $y = 0.008$ $\text{dia} = 79.890$ $\text{rnds} = 0.096$	 $\Theta_s = 36^\circ$ $x = 75.024$ $y = 0.009$ $\text{dia} = 79.867$ $\text{rnds} = 0.014$	 $\Theta_s = 105^\circ$ $x = 75.017$ $y = 0.014$ $\text{dia} = 79.877$ $\text{rnds} = 0.065$	$\Delta x = 0.011$ $\Delta y = 0.006$ $\Delta \text{dia} = 0.023$ $\Delta \text{rnds} = 0.082$

Table 3.1: Influence of the starting angle ( $\theta_s$ ) on the measured circle parameters in case of equidistant sampling with  $N = 4$ : roundness plot (blue), sampled points (red), fitted least squares circle (green), dimensions in mm, dia = diameter, rnds = roundness.

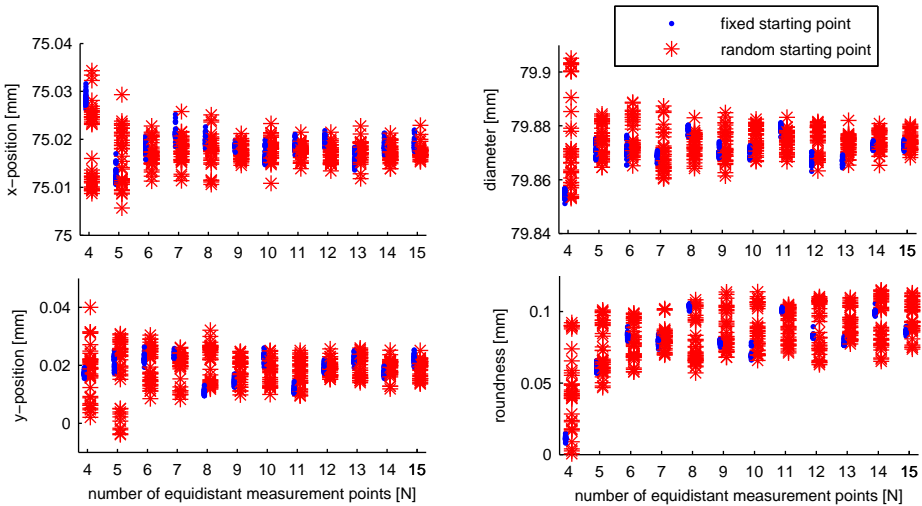


Figure 3.2: Influence of the number of sampling points  $N$  (abscissae) and the sampling point location (fixed starting point vs. random starting point) on the dispersion of the measured circle parameters:  $x$ -position,  $y$ -position, diameter and roundness (ordinates).

for the measurement uncertainties. It can be seen that the form deviation does not only influence roundness and diameter uncertainty, but also has an important influence on position uncertainty. Even for  $N = 10$  the dispersion of the results is about twice as large when the starting angle is random.

Many CMMs may have much lower hardware uncertainties than the one used in this case study<sup>1</sup>. With a more accurate CMM the dispersion of the fixed angle measurements can be even smaller. In these cases the relative influence of the form deviation will be even more important. If the true form deviation is smaller, the uncertainty due to the form deviation will also be lower. In case of a ‘perfectly’ round circle (e.g. ring gauge) there would be no difference in dispersion between both sampling strategies<sup>2</sup>. Unfortunately most workpieces do have form deviations, the influence of which can not be neglected.

If the measurement uncertainty would be determined with currently available (correctly calibrated) UES the calculated measurement uncertainty would approximately cover the dispersion range of the measurements with fixed starting angle (blue dots in Figure 3.2). The calculated measurement uncertainty will not cover the errors from the measurements with varying starting angle since the UES does not incorporate the influence of form deviation. For the same reason the calculated uncertainty interval of the x-position for a 4-points measurement at  $45^\circ$  will not overlap with the uncertainty interval of the x-position for a 5-points measurement (although they should overlap) and none of both uncertainty ranges will cover the true value ( $x = 75.018$ ). This *true value* was determined by the average of multiple measurement, at multiple locations, with many points ( $> 100$ ) and by using the least squares fitting criterion.

It is clear that the influence of the feature form deviations needs to be taken into account in order to obtain reliable evaluations of the measurement uncertainty. Measurement uncertainty strongly depends on the magnitude of the true form deviation, yet this is completely unknown before the measurement. Therefore, integrating this influence is quite difficult with conventional uncertainty evaluation methods.

---

<sup>1</sup>Measured geometric errors of the used CMM are given in Appendix B.

<sup>2</sup>The effect of probe pre-travel variation will still remain. Because of this and some other minor influences the dispersion for sampling with random starting angle will always be somewhat larger than the dispersion for a fixed starting angle, even in case of a ring gauge measurement.

## 3.2 Form deviation, waviness and roughness

### 3.2.1 Definition and classification

Before discussing the influence of form deviations on measurement uncertainty, it should first be clearly defined what is meant by form deviation. Most workpieces are composed of geometrical features like planes, cylinders, circles and lines. These actual geometrical features will differ from the nominal geometrical features due to imperfections during machining. Geometrical deviations consist of [37]:

- Size deviation
- Locational deviations
- Orientational deviations
- Form deviations
- Waviness
- Roughness
- Surface discontinuities
- Edge deviations

Form deviation, waviness, roughness and surface discontinuities all represent deviations from the perfect profile or perfect surface of the feature. Surface discontinuities, like e.g. cracks or pores, are usually not taken into account when assessing deviations of size, location, orientation, form, waviness and roughness [37].

Current standards do not define very clear boundaries between form deviation, waviness and roughness. Surface irregularities are usually classified based on the origin of the deviation. According to ISO 4287 the regions of form deviation, waviness and roughness are defined by the cutoff wavelengths  $\lambda_s$ ,  $\lambda_c$  and  $\lambda_f$  (see Table 3.2) [38], but the values of these wavelengths are not defined by ‘hard and fast’ mathematical rules [39].  $\lambda_s$  and  $\lambda_c$  can be chosen based on ISO standards [40, 41], but the selection of  $\lambda_f$  is not standardised. This makes it hard to define a clear boundary between form and waviness. The VDI/VDE 2601 standard mentions a more stringent classification based on the ratio between width and depth of the deviations [42]. Although this definition is more clear, there is still an overlap between waviness and roughness (see Table 3.2). Sometimes the terms micro and macro deviations are used instead of form deviation, waviness and roughness. Macro deviations can be measured with measuring devices that are also used for size, orientation and location, over the entire feature length. Micro deviations are measured on a representative part of the surface with special equipment like roughness measuring devices. This is a very interesting classification, but also in this case the boundaries are never very clear because they will depend on the kind of measuring equipment that is used.

Geometrical deviation	ISO 4287	VDI/VDE 2601	Micro Macro
Form	wavelengths $> \lambda_f$	ratio width:depth of deviation $> 1000:1$	Macro deviations
Waviness	$\lambda_c < \text{wavelengths} < \lambda_f$	ratio width:depth of deviation between 1000:1 and 100:1	↓
Roughness	$\lambda_s < \text{wavelengths} < \lambda_c$	ratio width:depth of deviation between 150:1 and 5:1	Micro deviations

Table 3.2: Classification of form, waviness and roughness according to ISO 4287 (with cutoff wavelengths  $\lambda_s$ ,  $\lambda_c$  and  $\lambda_f$ ) and VDI/VDE 2601.

### 3.2.2 Dominating effect of form deviations

When assessing roundness, straightness, flatness or cylindricity according to ISO 1101 [43], it is clear that these values will be influenced by form, waviness as well as roughness. In case of CMM measurements, the influence of the roughness will partially be filtered out by the probe tip. The amount of (mechanical) filtering will be determined by the diameter of the probe tip. In most practical situations the roundness, straightness, flatness and cylindricity values will be dominated by the effect of form.

To illustrate the dominating effect of form, Figure 3.3(a) shows the roundness deviation of a circular part manufactured by turning (full red line). The figure on the left plots the deviation from the least squares circle against the angular position along the circle, clearly showing the 3-lobed form deviation due to the clamping of the workpiece. The amplitude spectrum on the right, obtained by taking the Fourier transform of the roundness deviation, also shows a large peak at 3 UPR (undulations per revolution). The second order term (2 UPR) accounts for the non-uniform magnitude of the three lobes. The dotted blue line in the plot of the roundness deviation is a reconstruction of the original profile in which higher order harmonics (above 15 UPR) have been removed. The roundness value of the reconstructed profile (0.071 mm) equals 93% of the original profile (0.076 mm). Neglecting roughness and waviness seems to have little influence on the roundness value.

This hypothesis does not only hold for workpieces with very regular form deviations. Figure 3.3(b) illustrates the same for a less regular form deviation. In this case the roundness value of the reconstructed profile (0.013 mm) equals 87% of the original value (0.015 mm). It is important to know that in most applications the roundness value is dominated by lower order harmonics. This knowledge can be used for modelling form deviations .

To further illustrate the dominance of lower order harmonics, a random test set of 30 circular features from different technical workpieces is analysed. Analogous to

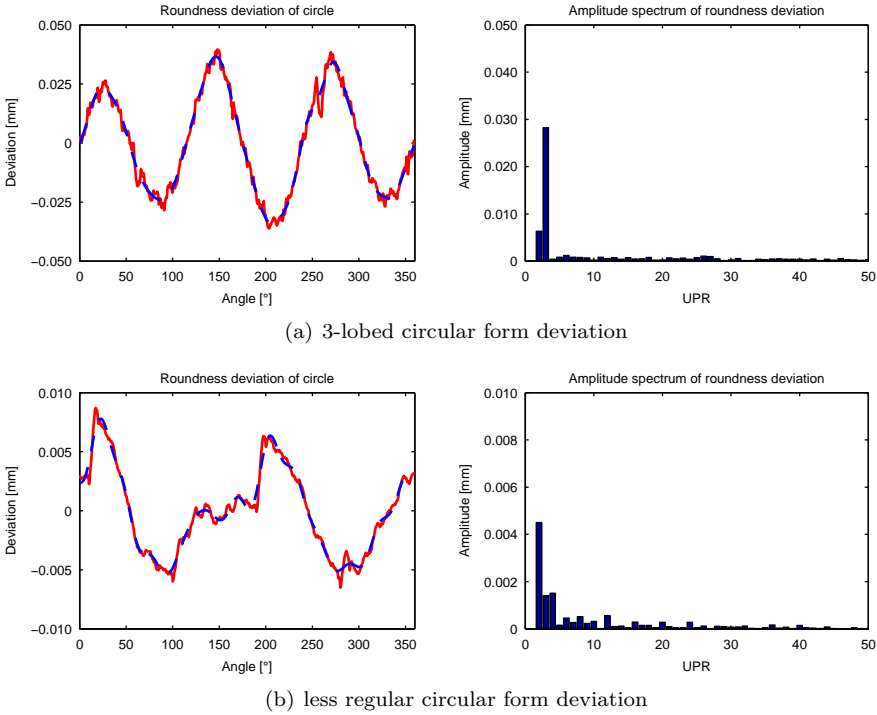


Figure 3.3: Frequency analysis of measured circular form deviations (full red line: original profile, dotted blue line: low pass (15 UPR) filtered profile).

the two examples above, the roundness value is calculated twice: once based on the original deviations and once based on the filtered data (low pass filter of 15 UPR). For each of these profiles the ratio of both values is calculated. The histogram of all ratios is given in Figure 3.4. For 25 of the 30 circular profiles the difference between measured and filtered profile is smaller than 5%. None of the deviations was larger than 15 %. This supports the hypothesis that profile deviations are dominated by lower order harmonics (longer wavelengths).

Although no systematic analysis has been carried out on lines, planes and cylinders, it can be assumed that this hypothesis also holds for other types of features. Of course examples can be found in practice where the form deviation value is dominated by waviness or roughness, but those will be exceptions.

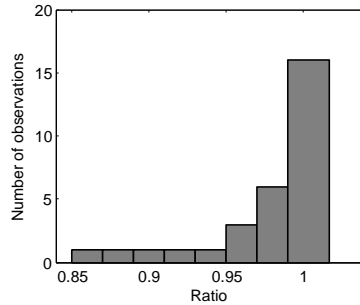


Figure 3.4: Histogram of ratios between filtered (low pass of 15 UPR) and original roundness values for 30 random circular features.

### 3.3 Former research on the influence of form deviations

One of the earliest contributions describing the influence of feature form deviations on the uncertainty of CMM measurements is by Wirtz [44]. This publication clearly illustrates the influence of a circular form deviation on diameter and position uncertainty. Also the relation between the measurement uncertainty and the harmonic content of the form deviation is mentioned. A very extensive study concerning the influence of feature form deviations on measurement uncertainty has been carried out by Weckenmann et al. [45, 46]. They expressed the uncertainties relative to the true form deviations, because relative uncertainties are independent of the magnitude of the true form deviation, as long as no hardware uncertainties of the measuring equipment are taken into account. These studies were mainly focussed on typical form deviations for circular features. Choi et al. investigated the influence of the form error distribution function and the number of sampling points on the measurement uncertainty [47]. Baldwin et al. proposed a software to evaluate task-specific measurement uncertainties for CMMs that also allows to evaluate the influence of feature form deviations based on ‘what if’ scenarios [26]. This software (PUNDITCMM) has already been discussed in Section 2.4.2.

Instead of focussing on calculating measurement uncertainties for conventional uniform sampling strategies, other authors focussed on optimised sampling strategies to reduce measurement uncertainties. This can be done by either using a priori defined sampling patterns or by using adaptive sampling patterns [48, 49]. Summerhays et al. provide an extensive literature review on this topic [48]. They also analysed a large set of holes, produced by different machining techniques, in order to model form deviations. They compared two ways to do this modelling: based on a combination of Fourier series and Chebyshev polynomials, and based on eigenshapes of the deviations obtained by principal component analysis. Based on



these models, optimised sampling strategies are defined. The effectiveness of this approach seemed to be very dependent on how well these models describe the true deviation. Building accurate models usually requires a large set of representative dense sampled form deviations, which makes such strategies only applicable for measurements of series.

### 3.4 Error simulation method

This section introduces an error simulation method which allows to determine the influence of form deviations on the measurement errors. The method is based on Monte Carlo simulations and is schematically shown in Figure 3.5. The method is illustrated for circles, but is also valid and has also been implemented for other features like lines, planes and cylinders. In order to focus on form deviations, CMM hardware and environmental influences are initially neglected. Chapter 4 explains how this method can be extended to incorporate CMM hardware uncertainties.

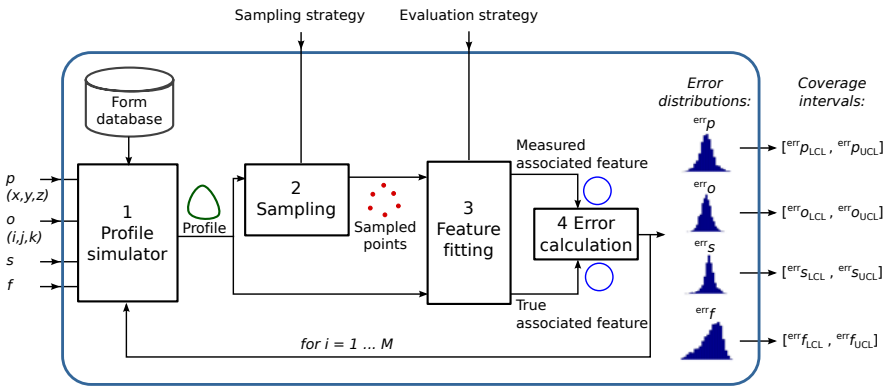


Figure 3.5: Scheme of Monte Carlo method to simulate influence of form deviations on measurement errors (illustrated for a circle measurement).

The method consists of four main modules (rectangular boxes in Figure 3.5):

1. *Profile simulator*: simulates a profile<sup>3</sup> with a form deviation based on a given position ( $\mathbf{p}$ ), orientation ( $\mathbf{o}$ ), size ( $s$ ) and form deviation value ( $f$ ). Profile simulation for circles and other features is explained in Section 3.5.

<sup>3</sup>The word ‘profile’ is used in this thesis for circles, lines, planes as well as cylinders and represents a dense set of points (x,y,z) that describe the surface or contour of the feature, including the form deviation and possibly also waviness and roughness.

2. *Sampling*: simulates the sampling of measurement points on the given profile. Points are taken based on a user defined sampling strategy (equidistant, partial circle measurement etc.). Section 3.6 discusses the sampling of features.
3. *Feature fitting*: fits an associated feature through a set of points. This is done twice, once for the sampled points (coming from the sampling module) and once for the complete original profile (coming straight from the profile simulator and defined by a large ( $> 100$ ) set of points). This results in two associated features: a *measured* (i.e. sampled) associated feature and a *true* associated feature (Section 3.7).
4. *Error calculation*: parameters of the measured associated feature are compared with the parameters of the true associated feature and the errors on position ( ${}^{err}p$ ), orientation ( ${}^{err}o$ ), size ( ${}^{err}s$ ) and form deviation ( ${}^{err}f$ ) are calculated (Section 3.8).

Since no CMM hardware errors are added, the calculated errors are only due to the effect of limited sampling. If all points of the original profile are sampled, all errors will be zero. These four steps are repeated multiple times in order to obtain error distributions for the different feature parameters (see Figure 3.5). These error distributions can be used to calculate upper (UCL) and lower confidence limits (LCL) for the errors of the different feature parameters. These confidence limits define the coverage interval for a given parameter: e.g.  $[{}^{err}s_{LCL}, {}^{err}s_{UCL}]$  represents the coverage interval for size (see Figure 3.5). Usually 95% is chosen as level of confidence.

The shape and width of the error distributions obtained by the error simulation are determined by the sampling strategy, the evaluation strategy and the profiles that are simulated by the profile simulator. E.g. using 3-lobed profiles will result in other distributions than irregularly shaped profiles. In order to produce realistic error distributions, the profiles that are simulated should also be realistic.

## 3.5 Profile simulator

The profile simulator simulates profiles based on a form database. Figure 3.6 depicts two ways to build this form database (illustrated for circular profiles). The first one is based on measured profiles. The second is based on simulation. Both methods are explained in Section 3.5.1 and 3.5.2 for different types of features. Section 3.5.3 describes how the form databases are used to generate profiles with a given magnitude of form deviation.

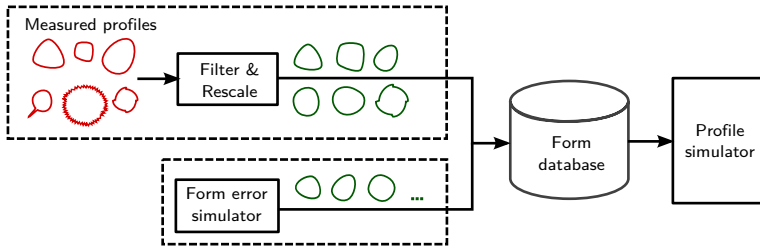


Figure 3.6: Two possible strategies to build the form database (illustrated for circular profiles).

### 3.5.1 Form databases based on measured form deviations

A pragmatic solution to generate realistic profiles is to do this based on real measured profiles. If enough real profiles are gathered, these profiles can be used to build a form database. The data can be obtained from CMM measurements, but also from a roundness or profile measuring device because only form deviation information is needed. If reference profiles are measured by a CMM, it is preferred to use uniform sampling densities and enough sampling points. Measurement errors should be small compared to the measured form deviations. Usually deviations from a least squares substitute element are used, but deviations from other associated features (like e.g. minimum zone elements) can also be used. The deviations can be represented as arrays,  $n \times 1$  arrays for circles and lines,  $n \times m$  arrays for planes and cylinders. If measurement points are not belonging to a uniform sampling pattern (e.g. in case of point clouds obtained by laser scanning) or if the number of sampled points is not equal to the number of points to be stored in the form deviation arrays, the measured profiles need to be resampled. This is done by linear interpolation of neighbouring points.

Since the interest lies in the influence of form deviation on measurement uncertainty, roughness and local defects which distort the results, are to be avoided. Therefore every profile is filtered. Section 3.2.2 already showed that the roundness deviation is dominated by low order harmonics. Therefore low pass filters will be used to preserve the deviations due to form and to remove deviations due to roughness and local defects. Several filtering techniques in *space* and *frequency* domain have been considered. These techniques are well established for digital signal processing and image processing applications. Eventually filtering with a Gaussian weighting function seemed to be most suited. This technique is nowadays the most common filtering technique for surface texture and roundness measurements. Another important advantage is that it can be applied to all types of features, 1D

features<sup>4</sup> (circles and lines) as well as 2D features (planes and cylinders).

### Filtering of 1D features

For lines the deviation can be expressed as a function of the distance along the line and for circles as a function of the angle. This makes that form deviation of lines and circles can be treated similar with respect to filtering.

According to ISO 11562 the Gaussian weighting function for circular and line profiles, with cutoff wavelength  $\lambda_c$ , looks as follows [50]:

$$w(x) = \frac{1}{\alpha\lambda_c} e^{-\pi\left(\frac{x}{\alpha\lambda_c}\right)^2}, \quad \alpha = \sqrt{\frac{\ln 2}{\pi}} \quad (3.1)$$

The filtered profile  $d(x)$  can be obtained by a convolution of the original profile  $p(x)$ , with  $x$  the distance along the line, and the weighting function  $w(x)$ :

$$d(x) = p(x) * w(x)$$

The amplitude transmission characteristic can be obtained from the Fourier transform of  $w(x)$ :

$$H(\lambda) = \frac{a_1}{a_0} = e^{-\pi\left(\frac{\alpha\lambda_c}{\lambda}\right)^2}$$

Figure 3.7 shows the weighting function  $w(x)$  and its transmission characteristic.

When the filter is applied to a discrete measured profile the weighting function also needs to be a discrete form that approximates the Gaussian weighting function. The width of the filtering window is determined by the sampling distance of the measured profile and the cutoff wavelength. A well known drawback of discrete convolution is that some points (corresponding to the half-width of the filter) in the beginning and at the end of the measured profile are lost. For surface texture measurements this is solved by measuring over a somewhat larger distance. If the filtered signal is used to represent the form deviation any loss of information on the borders is unwanted. An alternative to prevent length reduction of the measured profile is to make use of *padding values*. These are additional values that are added in the beginning and at the end of the data set. Lines can be padded with the border value of respectively the first and last measured point. Since measured profiles of circles are periodic, the end of the profile can be padded periodically with values of the beginning and vice versa.

---

<sup>4</sup>The term 1D feature is used to describe circles and lines since these are considered as 1D manifolds in mathematics. Planes and cylinders, but also spheres and cones, are 2D manifolds.

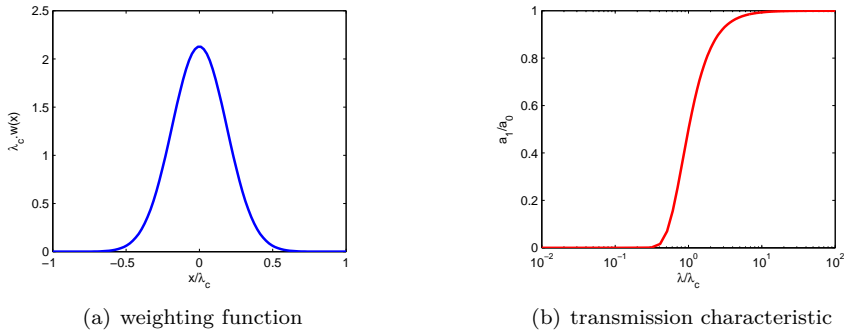


Figure 3.7: Profile filtering with weighting function: (a) Gaussian weighting function, (b) transmission characteristic of a Gaussian weighting function.

Considering the cutoff wavelength  $\lambda_c$ , it is important to choose a value that removes the roughness and keeps the form deviation. It is difficult to define clear borderlines between roughness, waviness and form deviation, as already mentioned in Section 3.2. For interpretation of the results it should be clear how the filtering is performed since the used filter values can have an important influence on the calculated uncertainties. In case of circle measurements it is common practice to use cutoff frequencies ( $f_c$ , expressed as UPR, undulations per revolution) instead of cutoff wavelengths (expressed in mm) [51]. ISO/TS 12181-2 specifies some default values for cutoff frequencies; the smallest value equals 15 UPR. For several reasons, among others understandability, it was found desirable to use also a cutoff frequency instead of cutoff wavelengths for lines, although this is not common practice for (line) profile measurements. This cutoff frequency ( $f_c$ ) can be expressed as undulations per length (UPL). 1 UPL corresponds with one period of a sine wave over the complete length of the line. 15 UPL seemed to be a good value that in most situations keeps almost the complete form deviations and removes the influence of roughness. Figure 3.8 illustrates the filter for a measured circle and a measured line.

Figure 3.8(a) also shows the drawback of using filtering. The original profile clearly shows the deviations due to reversal errors of the milling machine. In the filtered profile these deviation are partially flattened. In a certain sense this profile can be seen as an exception since most other investigated profiles showed almost no difference between original and filtered profile. This supports the hypothesis that roundness values are mainly dominated by lower order harmonics. In this work, most raw profiles are measured by a CMM equipped with a touch trigger probe with a sphere tip of 4 mm diameter. This means that the ‘raw’ profile has already been filtered mechanically. When one wants to include the effects of specific local deviations like reversal errors, it is advisable not to use filtering on the raw profiles,

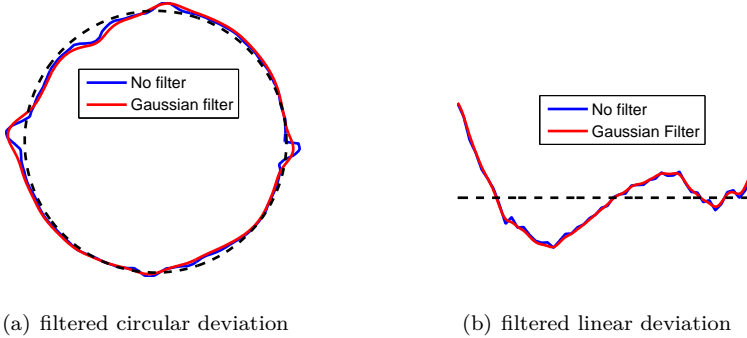


Figure 3.8: Profile filtering with Gaussian weighting function: (a) applied to a circle ( $f_c = 15$  UPR) (b) applied to a line ( $f_c = 15$  UPL).

or to use higher cutoff frequencies.

### Filtering of 2D features

The 2D Gaussian weighting function is represented as follows [52]:

$$w(x, y) = \frac{1}{\alpha^2 \lambda_{cx} \lambda_{cy}} e^{-\pi \left[ \left( \frac{x}{\alpha \lambda_{cx}} \right)^2 + \left( \frac{y}{\alpha \lambda_{cy}} \right)^2 \right]}, \quad \alpha = \sqrt{\frac{\ln 2}{\pi}} \quad (3.2)$$

and has following amplitude transmission characteristic [53]:

$$H(\lambda_x, \lambda_y) = e^{-\pi \left[ \left( \frac{\alpha \lambda_{cx}}{\lambda_x} \right)^2 + \left( \frac{\alpha \lambda_{cy}}{\lambda_y} \right)^2 \right]}$$

$\lambda_{cx}$  and  $\lambda_{cy}$  are the cutoff wavelength in the two orthogonal directions. Figure 3.9 shows the weighting function  $w(x, y)$  and its transmission characteristic.

In order to apply the filter to measured planes and cylinders a coordinate transformation of the measurement points will be necessary in order to make the deviation direction correspond to the z-direction, while the position in the plane or cylinder are represented by x and y. For planes this can be obtained by a rotation, for cylinders a transformation to cylindrical coordinates is performed.

The filtered profile  $d(x, y)$  is now also obtained by convolution of the original profile  $p(x, y)$  with the weighting function  $w(x, y)$ :

$$d(x, y) = p(x, y) * w(x, y)$$

Again a discrete and truncated version of the Gaussian filter is used, and just as for circles and lines, padding values will be needed to prevent data loss. Cylinders will

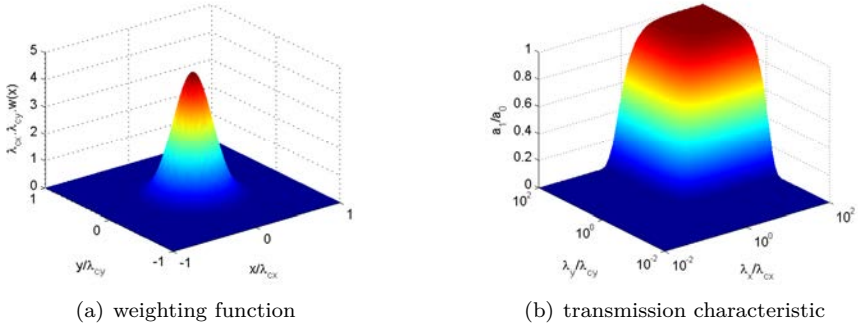


Figure 3.9: Surface filtering with weighting function: (a) 2D Gaussian weighting function, (b) transmission characteristic of a 2D Gaussian weighting function.

be padded *periodically in radial direction* and padded by *border values in length direction*. Planes are padded in *both directions by border values*.

Similar to lines and circles cutoff frequencies are used instead of cutoff wavelengths. For planes a default cutoff frequency of 15 UPL is used in both directions. For cylinders the default cutoff frequencies in radial and length directions are respectively 15 UPR and 15 UPL. Other values can be used as cutoff frequencies if necessary.

Figure 3.10 shows the results of the filter when it is applied to a laser line scanned plane. It clearly shows the noise removal capabilities of the filter, while preserving form deviation information.

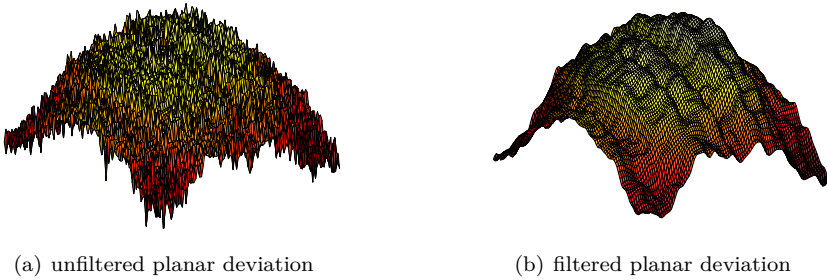


Figure 3.10: Profile filtering with Gaussian weighting function applied to a plane ( $f_{cx} = f_{cy} = 15$  UPL).

### Scaling of the profiles

The measured (and possibly filtered) profile is characterized by a shape and a specific magnitude of form deviation. The profile simulator needs to simulate profiles with different shapes and different magnitudes of form deviation, that can be specified by the user. Therefore every form deviation is rescaled to a standard dimensionless form deviation of 1. This can be done easily by dividing each array with deviations by its range (= magnitude of the form deviation):

$$\mathbf{d} \leftarrow \frac{\mathbf{d}}{\max(\mathbf{d}) - \min(\mathbf{d})} \quad (3.3)$$

Once these deviations are standardized, only the information about the shape of the form deviation is left. They are stored in what is called a form database. With these standardized deviations, profiles with a form deviation of whatever magnitude can be generated, simply by multiplying the form deviations with a given value of form deviation magnitude. This means that the data of one measured profile with a certain form deviation magnitude (and feature size) is used to generate form deviations of varying magnitudes. This approach assumes that the shape of the form deviation is not correlated with the magnitude of the form deviation or size of the feature (diameter of circle, length of a line etc.). Probably this assumption is a simplification of reality.

Since the profiles used to construct the form database are measured with a CMM or a roundness or profile measuring device, they will inevitably also be influenced by measuring hardware errors. For profiles with large form deviations, the relative influence will be negligible. For very small form deviations one should make sure that the measured profile is not distorted by hardware errors of the measuring device.

One can use the constructed form database in several ways. All filtered and rescaled profiles can be collected in one large database. Alternatively they can be stored in *sub-databases* according to the used manufacturing process, since the manufacturing process will have an important influence on the shape of the form deviations. Each process will leave a so-called *manufacturing signature*. One could use sub-databases for features produced by turning, milling, electrical discharge machining or other manufacturing processes. In case of series production, even a sub-database for one type of product could be built.

### 3.5.2 Form databases based on simulated form deviations

Building a form database based on measured profiles will be quite time consuming if one wants to collect a large amount of measured profiles. As an alternative, one could *simulate* standardized deviations that will be stored in the database. Although



the deviations are simulated, they should represent realistic form deviations; just generating random noise will not result in realistic deviations. Circles, lines, planes and cylinders all have their typical types of form deviation. The generation of simulated profiles for these features will be discussed below.

### Simulation of circular form deviations

For circles it is known that they often have important second, third and fourth order harmonics in their roundness deviations. A typical second order form deviation is visible in Table 3.1 on page 41, and a measured third order deviation is represented in Figure 7.4(a) on page 131. A combination of second and third order deviation is illustrated in Figure 7.4(b). Second order harmonics represent 2-lobed (elliptic) deviations and can be due to different scaling factors for x- and y-scales or squareness errors of the CNC machine tool, two sided clamping of the workpiece during machining of the circular feature etc. Third order harmonics represent 3-lobed deviations and can be related to clamping in a three-jaw chuck, straightness errors of the machine slides etc. Fourth order harmonics represent 4-lobed deviations and can be addressed to clamping in a four-jaw chuck, straightness errors of the machine slides, backlash at reversal of slide movement etc.

In literature sometimes one principal harmonic order is selected and all other orders are neglected, resulting in purely sinusoidal deviations, which are not a good representation of reality [45, 49]; see for instance Figure 7.4(b) on page 131 that clearly combines a second and third order deviation. As an alternative one can add, besides the principal component, also some random harmonics. The roundness deviation  $d(x)$  is built up as a *Fourier series*:

$$d(x) = \sum_{n=1}^N a_n \cos(nx + \phi_n) \quad \text{for } x \in [0, 2\pi[ \quad (3.4)$$

with

$$a_1 = 0 \quad \text{and} \quad \sum_{n=2}^N a_n = 1$$

To obtain a deviation array, Eq. 3.4 should be evaluated for a discrete set of equidistant points from the interval  $[0, 2\pi[$ . The values of the coefficients  $a_n$  should be determined in such way that realistic form deviations are obtained. The first order component is never taken into account for circles because this will cause a shift of the centre point of the circle: roundness deviations from a least squares circle will never contain a first order component (this can also be seen in Figure 3.3. As a consequence  $a_1$  is always 0. The amplitude  $a_n$  of the principal harmonic order component (second, third or fourth order depending on type of form deviation) is

chosen as a value between 0 and 1. All other amplitudes are distributed randomly but in such a way that all amplitudes sum up to 1. A Dirichlet distribution can be used to do this. When the principal harmonic order component equals 1, this results in a perfect sinusoidal deviation. The smaller the value of the principal component the more ‘randomness’ will be added. The value that was chosen as *maximum harmonic order*  $N$  is 15 because analysis of real roundness deviations showed that the roundness deviation is dominated by harmonics lower than 15 UPR (Section 3.2.2). Values for *phase shifts*  $\phi_n$  are chosen *randomly* between 0 and  $2\pi$ . This is a simplification of reality because it does not take into account the possible correlation between the phases of different orders. Due to the random distribution of amplitudes and phases, the simulated roundness value will never be exactly the same. Therefore every simulated profile is also rescaled to a standard dimensionless roundness deviation of 1 (cf. Eq. 3.3 on page 54).

After rescaling, the profiles are stored in the form database. In case of simulated profiles as many form deviation profiles as wanted can be added. Alternatively, profiles could also be simulated in real time by the profile simulator, without storing them in a database. However, calculating them in advance and storing them in a form database saves time during the Monte Carlo simulation.

Figure 3.11 shows different examples of simulated roundness profiles. Each example also shows the value used for the principal harmonic order. In Figure 3.11(d) and 3.11(e) two principal harmonic orders were defined. Combining third or fourth order principal harmonics with a second order results in ‘asymmetric’ 3- and 4-lobed deviations. As much principal harmonics as wanted can be defined, as long as their sum does not exceed 1. For Figure 3.11(f) no principal order was specified, which means that all orders (up to 15 UPR) were determined randomly.

### Simulation of linear form deviations

Because lines are also 1D features and since they are treated similar to circles when building measured form databases (Section 3.5.1), it would also be interesting to treat both 1D features similar with respect to simulated profiles. To do this, linear form deviations would need to be simulated by means of Fourier series. A typical linear form deviation is the bending or curving of a line (as in Figure 3.12(a)). Although it is perfectly possible to *describe* a curved profile by means of Fourier series it is much more difficult to *simulate* it based on Fourier series, since this involves high order harmonics and strong correlation between the phases of the different harmonics (which means they can not be chosen random as in the case of circles).

Therefore it is difficult to treat linear form deviations completely similar to circular form deviations. An interesting way to describe linear deviations, that has also been used by other authors, is to make use of Chebyshev polynomials [54, 48].

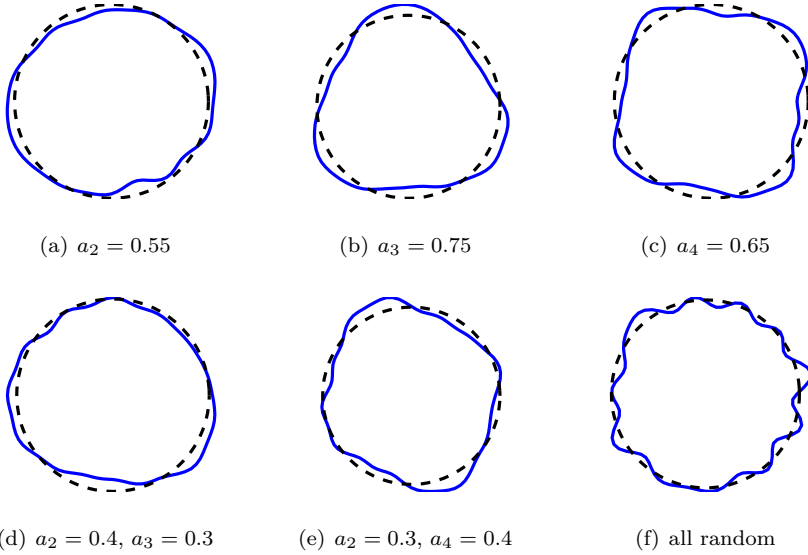


Figure 3.11: Examples of simulated circular form deviations.

Chebyshev polynomials of the first kind can be generated recursively:

$$T_0(x) = 1 \qquad T_1(x) = x \qquad T_n(x) = 2xT_{n-1}(x) - T_{n-2}(x)$$

The first 5 Chebyshev polynomials of the first kind are as follows:

$$\begin{aligned} T_0(x) &= 1 \\ T_1(x) &= x \\ T_2(x) &= 2x^2 - 1 \\ T_3(x) &= 4x^3 - 3x \\ T_4(x) &= 8x^4 - 8x^2 + 1 \end{aligned}$$

Chebyshev polynomials are usually used on the  $[-1, 1]$  interval. On this interval Chebyshev series can be used to approximate any continuous function, similar to Fourier series. When using Chebyshev series to simulate a linear form deviation,  $T_2(x)$  can be used to represent the curvature component of the form deviation. However when the form deviation would be generated by randomly assigning values to the coefficients of the Chebyshev series this results in unrealistic form deviations (very large deviations at the beginning and the end of the  $[-1, 1]$  interval). Eventually the best solution seemed to take only  $T_1(x)$  and  $T_2(x)$  into account and to combine these two terms with a Fourier series. Alternatively one could state that a linear and quadratic term are added to a Fourier series. Mathematically this

can be expressed as follows:

$$d(x) = sx + c(2x^2 - 1) + \sum_{n=1}^N a_n \cos(n\pi x + \phi_n) \quad \text{for } x \in [-1, 1] \quad (3.5)$$

with

$$s + c + \sum_{n=1}^N a_n = 1$$

To obtain a deviation array, Eq. 3.5 should be evaluated for a discrete set of equidistant points from the interval  $[-1, 1]$ . Coefficient  $s$  represents the amount of slope and coefficient  $c$  the amount of curvature. For linear form deviations  $s$  will always be zero, but Eq. 3.5 will also be used further on to generate planar and cylindrical form deviations, where  $s$  will not be zero. Preliminary analysis showed that for most real form deviations the *curvature component* is dominant [55]. Therefore the curvature is usually taken as principal component for the simulated linear form deviations. The curvature can be convex or concave, this is determined by the sign of coefficient  $c$ . Since in most practical situations both situations can occur, coefficient  $c$  is usually multiplied by a random sign (-1 or +1). The remaining amplitude coefficients are, just as for circles, determined randomly but in such a way that they sum up to 1. The default value for maximum harmonic order  $N$  is taken as 15, since these orders seem to be dominating the straightness value [55]. Again every generated profile is rescaled to a standard dimensionless value of 1 before being stored in the form database.

Some examples of simulated linear form deviations are shown in Figure 3.12. Figure 3.12(c) shows that combining a curvature component with the first order harmonic can generate an ‘asymmetric’ curvature. For Figure 3.12(d) no principal order was specified, which means that all terms (up to  $a_{15}$ , 15 UPL) were determined randomly. Notice that Eq. 3.5 also can be used for generating circular form deviations, when coefficients  $s$ ,  $c$  and  $a_1$  are taken zero.

### Simulation of planar form deviations

Since form deviations for circles and lines are modelled as Fourier series (extended with a curvature component in case of linear form deviation) it would be logical to look for 2D Fourier series or to series of 2D polynomials to model form deviations for planes. These 2D series have proven to be very useful for analysis purposes by means of decompositions (e.g. Zernike polynomial decomposition is used to analyse optical aberrations [56]). But when using these kinds of functions to model form deviations by (semi-)random synthesis, it is very difficult to obtain realistic form deviations.

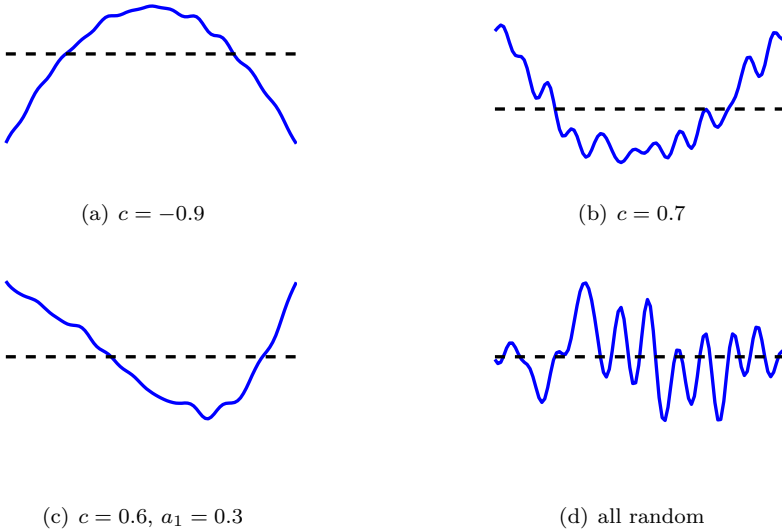


Figure 3.12: Examples of simulated linear form deviations.

Eventually a method was found to simulate planar form deviations based on simulated form deviations for lines. Four such form deviations for lines are generated. These four form deviations represent the borders of the plane. The form deviations inside the plane are calculated as a weighted sum of the border values. The weighting functions for the different borders all have value 1 at the respective border side and decrease linearly to reach 0 at the opposite border. Mathematically this looks as follows:

$$d(u, v) = d_1(u)w_1(v) + d_2(u)w_2(v) + d_3(v)w_3(u) + d_4(v)w_4(u) \tag{3.6}$$

with

$$w_1(v) = 1 - v, \quad w_2(v) = v, \quad w_3(u) = 1 - u, \quad w_4(u) = u$$

The planar form deviation, expressed in  $u - v$  parameters, is represented by  $d(u, v)$ . The linear form deviation  $d_1$  corresponds to border  $v = 0$ ,  $d_2$  to  $v = 1$ ,  $d_3$  to  $u = 0$  and  $d_4$  to  $u = 1$ . Figure 3.13 illustrates the different weighting functions graphically in the  $u - v$  space. The total weight will sum up to 2. This does not matter since the outcome will be rescaled to a standard dimensionless form deviation of 1, just as for circles and lines.

It makes sense to take form deviations of the border lines as basis for planar form deviations because measured lines are often part of a plane for actual CMM

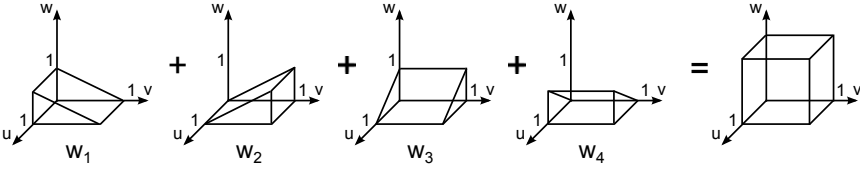


Figure 3.13: Graphical illustration of weighting functions used to build planar form deviations.

measurements. Since the linear form deviations for the borders all have magnitude 1, the magnitude of the form deviation along the  $u$ -direction of the plane will be equal to the magnitude of the form deviation along the  $v$ -direction. In practice the form deviation of a plane is often concentrated in one of the two directions. To account for this, the ratio  $r$  is introduced. This user-determined ratio can be used to rescale the deviation along the  $u$  and  $v$ -direction. Eq. 3.6 will adapt to:

$$\begin{aligned}
 d(u, v) = & r [d_1(u)w_1(v) + d_2(u)w_2(v)] \\
 & + (1 - r) [d_3(v)w_3(u) + d_4(v)w_4(u)]
 \end{aligned}
 \tag{3.7}$$

The simplicity of this method is considered as one of its major advantages. It can reuse the profile simulation method for lines. Once the four line profiles are obtained as  $n \times 1$  arrays the result can be calculated as a sum of outer products of vectors, corrected with ratio  $r$ :

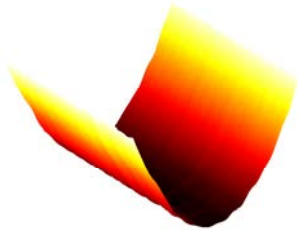
$$\mathbf{d} = r [\mathbf{w}_{01} \otimes \mathbf{d}_1 + \mathbf{w}_{10} \otimes \mathbf{d}_2] + (1 - r) [\mathbf{d}_3 \otimes \mathbf{w}_{10} + \mathbf{d}_4 \otimes \mathbf{w}_{01}]$$

where  $\mathbf{w}_{01}$  represents a vector with  $n$  values increasing linearly from 0 to 1, and  $\mathbf{w}_{10}$  represents a vector with values decreasing linearly from 1 to 0.

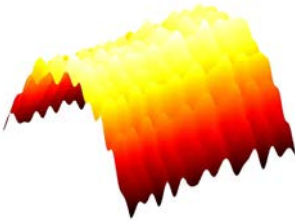
Figure 3.14 shows some examples of simulated form deviations. Typical form deviations like single curved and double curved form deviations can be obtained. Therefore, to create the linear form deviations, the right combination of parameters needs to be chosen. The *summarizing parameters* are shown in the figure captions. Table 3.3 explains how these summarizing parameters are used to simulate the four linear form deviations. The example with the twisted form deviation (Figure 3.14(e)) shows why the *slope* component  $s$  in Eq. 3.5 is necessary.

**Simulation of cylindrical form deviations**

Almost completely analogous to the way how planar form deviations can be built based on four linear form deviations, cylindrical form deviations can be built based



(a) u-curved,  $c = 0.95, r = 0.95$



(b) v-curved,  $c = -0.8, r = 0.2$



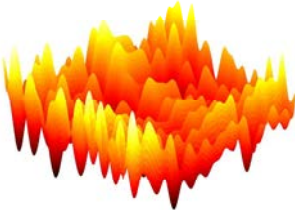
(c) uv-curved,  $c = -0.9, r = 0.7$



(d) saddle-curved,  $c = -0.9, r = 0.5$



(e) twist,  $s = -0.95, r = 0.8$



(f) random,  $r = 0.5$

Figure 3.14: Examples of simulated planar form deviations.

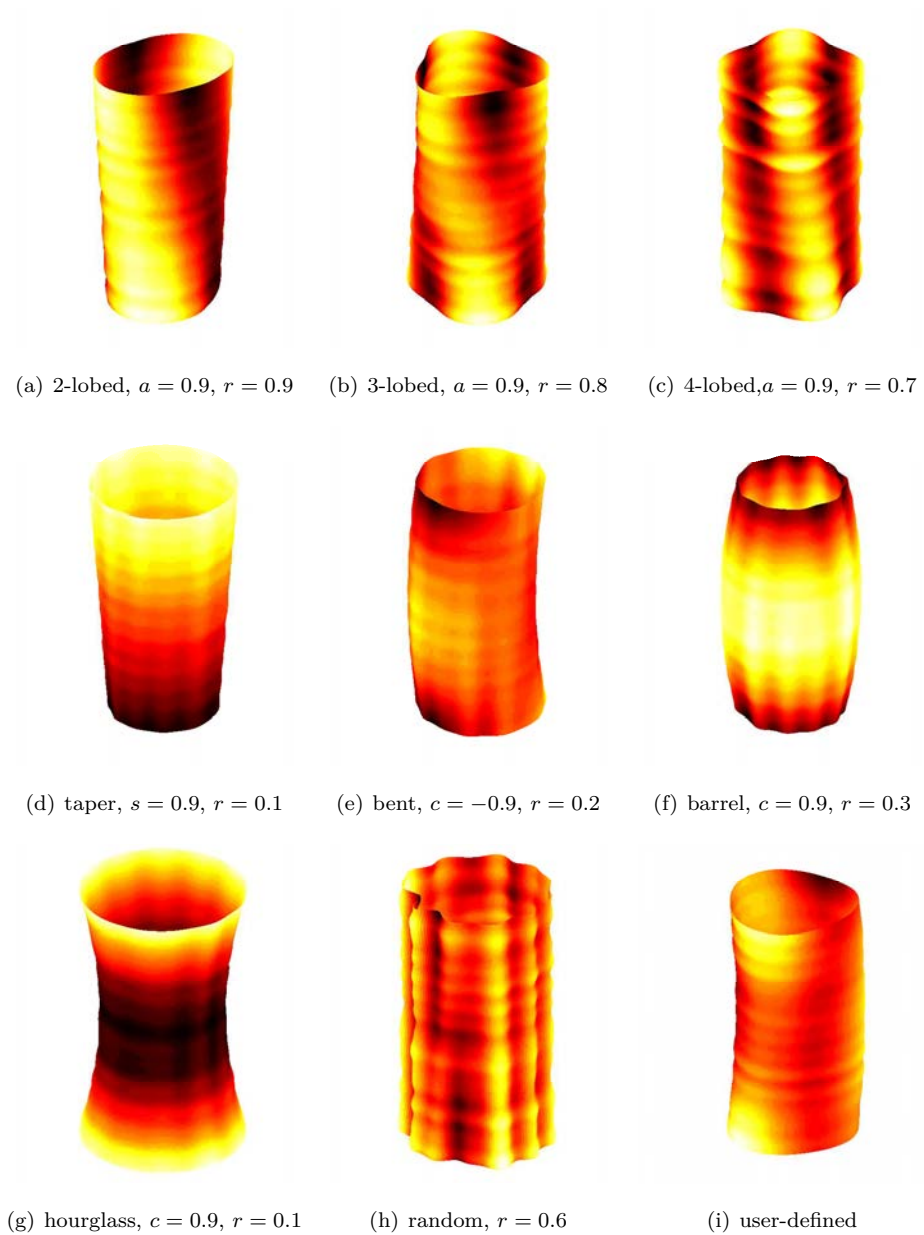


Figure 3.15: Examples of simulated cylindrical form deviations.



Summarizing parameters	ratio	$d_1$	$d_2$	$d_3$	$d_4$
(a) ucurved $c = 0.95, r = 0.95$	$r = 0.95$	$c = 0.95$	$c = 0.95$	random	random
(b) vcurved $c = -0.8, r = 0.2$	$r = 0.2$	random	random	$c = -0.8$	$c = -0.8$
(c) uvcurved $c = -0.9, r = 0.7$	$r = 0.7$	$c = -0.9$	$c = -0.9$	$c = -0.9$	$c = -0.9$
(d) saddlecurved $c = -0.9, r = 0.5$	$r = 0.5$	$c = -0.9$	$c = -0.9$	$c = 0.9$	$c = 0.9$
(e) twist $s = -0.95, r = 0.8$	$r = 0.8$	$s = -0.95$	$s = 0.95$	random	random
(f) random $r = 0.5$	$r = 0.5$	random	random	random	random

Table 3.3: Parameters used to simulate the linear form deviations for building the planar form deviations of Figure 3.14.

on two circular form deviations and two linear form deviations. The circular form deviations will correspond to the circumference on both ends of the cylinder, while the linear form deviations will be used for the axial direction of the cylinder. The values for different positions on the surface of the cylinder are, just as for planes, determined as a weighted sum of the four simulated 1D form deviations. The mathematical function describing the process also looks very similar to its planar counterpart (Eq. 3.6):

$$d(\theta, z) = d_1(\theta)w_1(z) + d_2(\theta)w_2(z) + d_3(z)w_3(\theta) + d_4(z)w_4(\theta) \tag{3.8}$$

The cylindrical form deviation  $d(\theta, z)$  is expressed in cylindrical coordinates. The linear form deviation  $d_1$  corresponds to the circumference for  $z = 0$ ,  $d_2$  for  $z = 1$ , while  $d_3$  corresponds to a surface line in axial direction for  $\theta = 0$  and  $d_4$  for  $\theta = \pi$ . The shape of the weighting functions  $w_3$  and  $w_4$  is slightly different as before:

$$w_1(z) = 1 - z, \quad w_2(z) = z,$$

$$w_3(\theta) = \begin{cases} 1 - \theta/\pi & \text{for } \theta \in [0, \pi] \\ \theta/\pi - 1 & \text{for } \theta \in [\pi, 2\pi] \end{cases}, \quad w_4(\theta) = \begin{cases} \theta/\pi & \text{for } \theta \in [0, \pi] \\ 2 - \theta/\pi & \text{for } \theta \in [\pi, 2\pi] \end{cases}$$

Figure 3.16 illustrates the different weighting functions graphically. The total weight will again sum up to 2. Weighting functions  $w_3$  and  $w_4$  have this triangular shape because the weight for  $\theta = 0$  needs to be the same as the weight for  $\theta = 2\pi$  since it describes the same position on the cylinder.

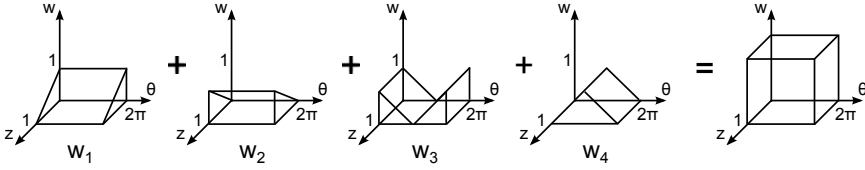


Figure 3.16: Graphical illustration of weighting functions used to build cylindrical form deviations.

Again the ratio  $r$  is introduced to determine the relative importance of the angular versus the axial component of the form deviation. This changes Eq. 3.8 into:

$$\begin{aligned}
 d(\theta, z) = r [d_1(\theta)w_1(z) + d_2(\theta)w_2(z)] \\
 + (1 - r) [d_3(z)w_3(\theta) + d_4(z)w_4(\theta)]
 \end{aligned}
 \tag{3.9}$$

Just as for planes this can be implemented as a sum of vector outer products.

Figure 3.15 gives some examples of simulated cylindrical form deviations. Most typical form deviations can be obtained by the right combination of parameters. The summarizing parameters are shown in the figure captions. Table 3.4 shows the parameters that are used for the two circular form deviations and the two linear form deviations.

Since circular form deviations are generated with random phase, the lower circular form deviation  $d_1$  is *rotated* with respect to the top circular form deviation  $d_2$  as can be seen in Figures 3.15(a) to 3.15(c). For real measured form deviations this rotation will seldom be observed, although some manufacturing processes, like drilling, show spiral shaped form deviations [54]. Taking the phase of the principal component ( $\phi_i$  with  $i = 2, 3$  or  $4$  for  $d_1$  and  $d_2$ ) equal will allow to simulate a non-twisted 2-lobed, 3-lobed or 4-lobed cylinder. Taking the curvature parameter  $c$  of the same sign for  $d_3$  and  $d_4$  results in a barrel shape (both negative) or a hourglass shape (both positive). Taking both curvature parameters of the opposite sign results in bending. Instead of using predefined shapes it is also possible to specify all parameters separately as done for Figure 3.15(i). The *slope* component for the linear form deviation is necessary to model taper (Figure 3.15(d)).

**Concluding remarks on simulated form deviations**

The methods described in this section showed how feature form deviations for circles, lines, planes and cylinders can be simulated. An important advantage of the proposed method is its simplicity: all form deviations can be built with the linear form deviation simulator. Circles can be simulated as linear form deviations

Summarizing parameters	ratio	$d_1$	$d_2$	$d_3$	$d_4$
(a) lobe2 $a = 0.9, r = 0.9$	$r = 0.9$	$a_2 = 0.9$	$a_2 = 0.9$	random	random
(b) lobe3 $a = 0.9, r = 0.8$	$r = 0.8$	$a_3 = 0.9$	$a_3 = 0.9$	random	random
(c) lobe4 $a = 0.9, r = 0.7$	$r = 0.7$	$a_4 = 0.9$	$a_4 = 0.9$	random	random
(d) taper $s = 0.9, r = 0.1$	$r = 0.1$	random	random	$s = 0.9$	$s = 0.9$
(e) bent $c = -0.9, r = 0.2$	$r = 0.2$	random	random	$c = -0.9$	$c = 0.9$
(f) barrel $c = 0.9, r = 0.3$	$r = 0.3$	random	random	$c = -0.9$	$c = -0.9$
(g) hourglass $c = 0.9, r = 0.1$	$r = 0.1$	random	random	$c = 0.9$	$c = 0.9$
(h) random $r = 0.6$	$r = 0.6$	random	random	random	random
(i) user-defined	$r = 0.6$	$a_3 = 0.9$	$a_3 = 0.9$	$c = 0.8$	$c = -0.8$

Table 3.4: Parameters used to simulate the circular and linear form deviations for building the cylindrical form deviations of Figure 3.15.

without a curvature ( $c$ ) and first order harmonics ( $a_1$ ) component. Form deviations for planes and cylinders can be built as a weighted sum of linear and circular form deviations.

Most typical form deviations can be simulated, although there are also shapes of form deviations that will be difficult to simulate (e.g. reversal errors). Surface discontinuities are not considered as part of the form deviation (see Section 3.2) and should not be simulated either. It should be emphasized that it is not the main objective to model all form deviations as realistically as possible. The level of detail should be sufficient to provide reliable uncertainty statements. If completely unrealistic simulated form deviations would produce reliable uncertainty statements it would be no problem to use these. Proving that the calculated uncertainties, obtained from simulated form deviations, are reliable asks for sufficient measurement data. In Section 3.10 this is carried out for two sets of 30 circles measurements: calculated errors based on measured profiles are compared to errors obtained from simulated profiles.

### 3.5.3 Profile simulation based on form database

Once the form databases for the different features are built, based on measured form deviations or on simulated form deviations, they can be used to simulate feature profiles based on given feature parameters. Below this process is illustrated for a circle.

In case of a circle, the position, orientation, diameters and roundness value of the circle are given by the user. A random form deviation  $\mathbf{d}$  is taken from the form database or from one of the sub-databases. The standardized deviation array  $\mathbf{d}$  is multiplied with the given roundness value  $f$  and added to a perfect circle with given position  $\mathbf{p}$ , orientation  $\mathbf{o}$ , and diameter  $s$ . The length  $n$  of the form deviation array determines the number of points of the profile. The  $i$ th point  $\mathbf{C}_i$  of the circular profile can be calculated as follows:

$$\mathbf{C}_i = \mathbf{N}_i + \mathbf{D}_i$$

where  $\mathbf{N}_i$  represents the nominal point on the profile

$$\mathbf{N}_i = \mathbf{p} + \frac{s}{2} (\sin(\theta_i)\mathbf{n}_1 + \cos(\theta_i)\mathbf{n}_2) \quad \text{with} \quad \theta_i = i \frac{2\pi}{n} \quad \text{for} \quad i = 1 \dots n$$

and  $\mathbf{D}_i$  contains the scaled deviation vector

$$\mathbf{D}_i = f d_i (\sin(\theta_i)\mathbf{n}_1 + \cos(\theta_i)\mathbf{n}_2)$$

$d_i$  is the value of  $d(x)$  (Eq. 3.4) for  $\theta_i$ .  $\mathbf{n}_1$  and  $\mathbf{n}_2$  are determined in such way that they form an orthogonal set of unit vectors with orientation vector  $\mathbf{o}$ . The orientation vector  $\mathbf{o}$  is the vector normal to the projection plane of the circle:

$$\mathbf{o} = \mathbf{n}_1 \times \mathbf{n}_2 \quad \text{with} \quad \|\mathbf{n}_1\| = \|\mathbf{n}_2\| = 1$$

The number of points  $n$  should be limited because it will influence the calculation time of the next steps significantly. Nevertheless enough points are needed for realistic representations of surfaces. Taking a number of profile points  $n$  between 100 and 500 seems to give satisfying results for circular profiles. For other features the profile generation procedure is very similar. The detailed implementation can be found in the source files.

## 3.6 Sampling module

Once a profile is generated, points can be sampled from this profile according to a given sampling strategy (cf. overview scheme on page 47). These sampling point

locations are represented by array  $\mathbf{l}$ , containing a set of numbers between 0 and 1. For circles this array can be obtained by dividing the probing angles by  $2\pi$ . An equidistant sampling pattern of  $m$  points for a circle can be denoted as follows:

$$\mathbf{l} = \left[ 0 \quad \frac{1}{m} \quad \frac{2}{m} \quad \dots \quad \frac{m-1}{m} \right]$$

Based on the sampling pattern  $\mathbf{l}$  the probed points  $\mathbf{P}_i$  can be obtained from the profile array  $\mathbf{C}$  of a circle:

$$\mathbf{P}_i = \mathbf{C}_j \quad \text{with} \quad j = \lfloor \mathbf{l}_i n \rfloor + 1 \quad \text{for} \quad i = 1 \dots m$$

$\lfloor \mathbf{l}_i n \rfloor$  represents the floor rounded value (i.e. largest preceding integer) of the  $i$ th element of array  $\mathbf{l}$  multiplied by  $n$ . Since the number of points of the true profile  $n$  is limited the actual probing positions will generally be between two points of the true profile, that is why calculated index values of the true profile are rounded to the closest lower integer. Alternatively interpolation between the surrounding points of the true profile can be used. When using interpolation one should be careful because linearly interpolated points will no longer lie on the true circle profile. For a circle of diameter  $s$  without form deviation, the maximum error  $\delta$  made by linear interpolation is equal to the height of the circle sector described by two subsequent points of the profile:

$$\delta = \frac{s}{2} \left( 1 - \cos \left( \frac{\pi}{n} \right) \right)$$

For a circle with a diameter of 100 mm almost 500 points are necessary to make the interpolation error  $\delta$  smaller than  $1 \mu\text{m}$ . For  $n = 200$  the interpolation error is  $6.2 \mu\text{m}$ . To avoid these interpolation errors the closest trailing point on the true profile is used. It would be more exact to use the closest point or a kind of circular interpolation. Experiments showed that taking the closest trailing point had almost no effect on the results, as long as the number of points composing the true circle profile is sufficiently large ( $> 100$ ). Therefore it was decided to stay with this approach in order to save calculation time.

The implementation for sampling lines, planes and cylinders is analogue to circles. For 2-D features (planes and cylinders) the size of the array  $\mathbf{l}$ , representing the probing locations, is  $m \times 2$ , with  $m$  the number of sampling points. For lines, planes and for the height direction of cylinders it is no problem to use linear interpolation. In order to avoid interpolation errors linear interpolation should also be avoided for the circumference direction of cylinders.

### 3.7 Feature fitting module

After virtual probing of the profile, the probed points can be used to fit an associated feature (cf. overview scheme on page 47). The kind of fitting algorithm is subjected to the choice of the user. Several fitting criteria can be used. Table 3.5 shows which fitting criteria can be applied for the different feature types [37].

Fitting criterion	Circle	Line	Plane	Cylinder
Least Squares (LSQ)	•	•	•	•
Minimum Zone (MZ)	•	•	•	•
Maximum Inscribed (MI)	•			•
Minimum Circumscribed (MC)	•			•

Table 3.5: Applicable fitting criteria to different types of features.

In order to be able to compare the *virtually measured* values (limited number of sampling points) with the *true* values (all points) the same fitting algorithm should be applied to the points representing the true profile, as already illustrated in the scheme of Figure 3.5 on page 47. Since the number of sampled points is usually much lower than the number of points representing the true profile, overall calculation time during the Monte Carlo simulation is dominated by the calculation of the true associated feature.

That is also the reason why all examples in the thesis are illustrated for the LSQ fitting criterion. LSQ fitting algorithms for circles, lines, planes and cylinders are well developed, fast and always have a unique solution. Other fitting criteria, like e.g. MZ, MC and MI, are usually much slower and have bad convergence. In practice almost always the LSQ fitting criterion is used (although it often would be better to use more functional fitting criteria). Despite the fact that the LSQ fitting criterion is very suited for its time efficiency, calculation times are often still too large to be used in an online Monte Carlo method. An efficient way to improve calculation time of the fitting algorithms is to adapt the convergence parameters. Usually convergence criteria do not need to be as stringent for uncertainty calculation as for other purposes. It is for instance no problem to have an error of 0.1  $\mu\text{m}$  on the calculated parameters of the LSQ feature if the measurement uncertainties of the parameters are several micrometers.

### 3.8 Error calculation module

Once the measured and true associated feature parameters are known, these can be used to calculate the errors. This results in an error on position, orientation, size and form deviation (cf. overview scheme on page 47). The error of a given

parameter  $\chi$  is simply calculated as follows:

$${}^{err}\chi = {}^{meas}\chi - {}^{true}\chi$$

These error values are stored and the whole process shown in Figure 3.5 is repeated, starting with the profile generation. This is repeated until the preferred number of Monte Carlo iterations  $M$  is reached.  $M$  needs to be sufficiently high in order to obtain representative error distributions (cf. right side of Figure 3.5). However, an increasing number of iterations will raise the calculation time. Once the number of iterations is reached, coverage intervals for the measurement errors of the parameters can be determined from the distribution functions. Usually a (probabilistically symmetric<sup>5</sup>) coverage interval with a 95% level of confidence used. All uncertainty results in this text are calculated for a confidence level of 95% unless otherwise specified.

For errors on size and form deviation the error calculated after each iteration is one single value. For position and orientation this is an error vector  $(x, y, z)$  or  $(i, j, k)$ . To obtain a single error value for position, the distance error can be calculated:

$${}^{err}d = \sqrt{{}^{err}p_x^2 + {}^{err}p_y^2 + {}^{err}p_z^2}$$

The angle error  ${}^{err}a$  can also be derived from the orientation error vector  ${}^{err}\mathbf{0}$ .

Instead of just calculating the error, also a relative error can be calculated. Appendix A explains why it can be useful to express the measured error of a given parameter  $\chi$  relative to the measured form deviation  ${}^{meas}f$ . This relative error is calculated as follows:

$${}^{relerr}\chi = \frac{{}^{meas}\chi - {}^{true}\chi}{{}^{meas}f} \quad (3.10)$$

### 3.9 The number of Monte Carlo iterations, $M$

Due to the stochastic nature of a Monte Carlo method (MCM), calculated uncertainties (expressed as coverage intervals) will never be exactly the same when calculations are repeated. This means that there is an *uncertainty on the calculated measurement uncertainty*. The larger the number of Monte Carlo iterations  $M$ , the more repeatable the calculated coverage intervals will be. How many iterations are needed:  $10^2$ ,  $10^3$ ,  $10^6$ ?

---

<sup>5</sup>A coverage interval is not unique for a given confidence level. For probabilistically symmetric coverage intervals the probability that the quantity is smaller than the smallest value of the interval is equal to the probability that the quantity is larger than the largest value of the interval. Alternatively the shortest coverage interval can be used. For symmetric probability density functions both coverage intervals are the same.

In this perspective it is interesting to look at the distribution of the sample standard deviation. Since the sample standard deviation is a random variable on itself one can determine its standard deviation. The standard deviation  $\sigma_S$  of the sample standard deviation  $S$  of a normal parent population (with standard deviation  $\sigma$ ) is determined as follows [57]:

$$\sigma_S = \sqrt{1 - c_4^2} \sigma \quad \text{with} \quad c_4 = \sqrt{\frac{2}{n-1}} \left[ \frac{\Gamma\left(\frac{n}{2}\right)}{\Gamma\left(\frac{n-1}{2}\right)} \right]$$

with  $n$  the number of samples and  $\Gamma$  representing the Gamma function.

For large  $n$  the factor  $\sqrt{1 - c_4^2}$  is close to  $\sqrt{1/(2n)}$ . This means that for  $n = 200$ ,  $\sigma_S$  almost equals 5% of  $\sigma$ . This equation could be used to select the number of Monte Carlo iterations if one could assume normal output distributions. In practice output distributions will often be non-normal. Because of this reason the number of Monte Carlo iterations  $M$  is often determined experimentally by calculating the measurement uncertainty multiple times. If the standard deviation of the width of the coverage interval does not exceed 5% of the average width of the coverage interval, the number of Monte Carlo iterations is considered to be sufficient. This number will strongly depend on the type of measurand and other parameters (like the used form database, confidence level of coverage interval, etc.). In most situations taking a value of  $M$  between 200 and 500 gives satisfactory results.

An interesting alternative to calculate the uncertainty on the measurement uncertainty is the use of resampling methods, like jackknife and bootstrap methods [58, 59]. These methods are often used in statistics and have the advantage that the uncertainties on the statistics (in this case the percentiles) can be calculated on the same set of sample data ( $M$  simulated measurement errors in this case) used to calculate the statistics. This means that the measurement uncertainty just has to be calculated once. Since the time that these resampling methods take is neglectable compared to the time that the error simulation takes, one can easily calculate the uncertainty for every calculated measurement uncertainty.

**Remark 3.1** *The supplement to the GUM regarding Monte Carlo methods also gives some directions for the choice of the number of Monte Carlo iterations  $M$  [21]. It is mentioned that the value of  $M$  should at least be  $10^4$  times greater than  $1/(1-p)$ , with  $p$  the coverage probability. This means that for a 95% coverage probability the value of  $M$  should be larger than  $200 \times 10^3$ . This number is unreasonably large for uncertainty calculations with some level of complexity like the one used in this research. It is also mentioned in the document that for some applications (like e.g. finite element calculations) only a limited number of Monte Carlo iterations can be performed; in these situations the probability distribution of the output value will be less reliable.*



*Another directive in that document suggests to determine  $M$  adaptively. It states that the uncertainty result can be considered as been stabilized if twice its related standard deviation is smaller than the least significant digit of the uncertainty value. This means that if the width of the uncertainty interval equals  $89\ \mu\text{m}$  the standard deviation on the width of this coverage interval (when calculated multiple times) should be smaller than  $0.5\ \mu\text{m}$ . In the author's opinion it makes no sense to calculate the width of a coverage interval up to sub-micrometer accuracy if the width of the interval is larger than  $10\ \mu\text{m}$ . Expressing the desired calculation accuracy relative to the width of the uncertainty interval seems a very natural choice but is surprisingly not mentioned in this GUM supplement.*

### 3.10 Results of the error simulation method

The error simulation method illustrated in Figure 3.5 and described in the previous sections can be used to determine upper and lower confidence limits for the errors due to limited sampling. This section illustrates the method for circular profiles.

Figure 3.17(a) shows the confidence limits of the measurement error, as a function of the number of equidistant sampling points, for a circle with a circular form deviation of  $0.1\ \text{mm}$ . Remember that the errors are only due to the interaction of sampling strategy and feature form deviation. CMM hardware errors are not taken into account. If the true form deviation of the circle would be zero, all simulated errors would also be zero. Only the magnitude of the roundness is determined by the user, not the shape and not the phase. For every Monte Carlo run another shape is taken from the form database. The user can determine the content of the database that is used in order to account for a known manufacturing signature: e.g. only third order principal harmonics for rings clamped in a three-jaw chuck.

Results of Figure 3.17(a) were calculated for two types of form databases, based on measured profiles:

**MEAS1** A form database containing 30 filtered and rescaled circular profiles from a series production of turned workpieces. All workpieces had a kind of 3-lobed form deviation.

**MEAS2** A form database containing 30 rescaled circular profiles from several varying production techniques.

Notice that, for database MEAS1, the lower confidence limit for position is larger than  $0.03\ \text{mm}$  for four equidistant measurement points, and much larger than for five or more points. This means that in case of 3-lobed deviations the error on position, for 4-points measurements, will be at least 30% of the true roundness ( $0.1\ \text{mm}$ ). Similarly the possible errors on diameter and position with MEAS2 are

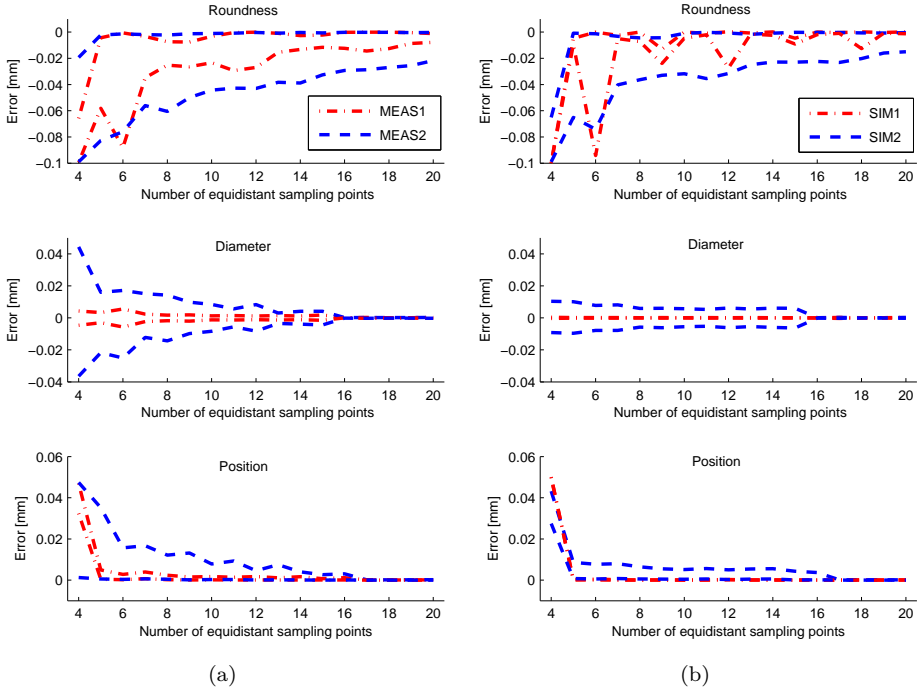


Figure 3.17: Upper and lower confidence limits (95%) of simulated errors on the parameters of the LSQ circle for two types of measured form databases (a) and for two types of simulated form databases (b).

much larger for four points than for other numbers of sampling points. It is also clear that the confidence limits from database MEAS2 bound the confidence limits of MEAS1 (except for 6-points measurements on roundness).

Instead of using measured form databases, one could also use simulated form databases, as described in Section 3.5. Figure 3.17(b) is created in the same way as Figure 3.17(a) but two databases built by simulated form deviations are used instead:

**SIM1** A form database containing 3-lobed form deviations generated by using a perfect third order harmonic deviation ( $a_3 = 1$ ). The shape of all form deviations is in this case the same, only the phase will vary.

**SIM2** A form database containing 3-lobed form deviations generated by using a third order harmonic deviation ( $a_3 = 0.5$ ) combined with other orders of random magnitudes.

It is clear, from the results in Figure 3.17(b), that the confidence limits for the errors, while using a perfect 3-lobed sinusoidal deviation (SIM1), do not agree with the confidence limits for measured 3-lobed form deviations (MEAS1 in Figure 3.17(a)). This type of model should therefore not be used to model realistic form deviations. When a third order harmonic deviation is combined with other random orders (SIM2) the agreement with the results obtained from measured 3-lobed deviations is much better (compare SIM2 and MEAS1). When using simulated form deviations, one should make sure that the modelled deviations are realistic. Notice that, in Figure 3.17(a) as well as Figure 3.17(b), the errors for diameter and position are becoming zero once the number of sampling points is larger than 15, corresponding to the limiting frequency content for the measured as well as the simulated profiles (15 UPR)<sup>6</sup>.

This section showed that simulations allow to calculate the confidence limits of the measurement errors for a given (assumed) value of true roundness and a given measurement strategy (number of equidistant sampling points). Such simulations can then be used to define the confidence limits for other values of true roundness, because the measurement errors are directly proportional to the true roundness value as long as hardware and environmental uncertainty contributors can be neglected. The measurement errors will not only be directly proportional to the true roundness value but also to the measured roundness value. Appendix A shows that this knowledge can be used to determine measurement uncertainties for all feature parameters based on the measured form deviation value. The described approach is a new and theoretical interesting but is only valid if other uncertainty contributors can be neglected. This implies that measurement uncertainties calculated according to this approach will be underestimated in case of actual measurements. Chapter 5 describes how the error simulation method of this chapter can be used to determine measurement uncertainties that combine the influence of feature form deviation and CMM hardware uncertainties.

## 3.11 Conclusions

This chapter started with a case study to illustrate that the influence of form deviations on the measurement result can be more important than all other influences. The case shows that the form deviation may have a very large influence on the measured position, diameter and form deviation. If the measurement points

---

<sup>6</sup>When the filtering of the measured profiles database is performed by using a Gaussian weighting function as described in Section 3.5.1 the errors will not become completely zero once the number of sampling points exceeds the filtering frequency, since frequencies larger than the limiting frequency are not completely removed. In this example a filtering technique based on the Fourier transform was used. This filtering technique works well for circles but not for other features. For reasons of uniformity Gaussian filtering is eventually used for all kinds of measured features.

are always taken at the same location, measurement results are quite reproducible. However, if the measurement points are taken at varying locations, the form deviation largely influences the outcome and the dispersion of the measurement results becomes twice as large as if the number of sampling points is smaller than 10. Also for a larger number of sampling points the influence of form deviation can not be neglected. For high accuracy CMMs the relative influence of form deviations on the measurement uncertainty will become even more important.

It is difficult to define what should be considered as form deviation. Current standards do not define hard boundaries between form, waviness and roughness. It is clear that local defects should not be considered as part of the form deviation. A study on circular form deviations showed that the *form deviation value is mostly dominated by the lower order harmonics*. It can be assumed that lower order terms will also be dominant for linear, planar and cylindrical form deviations.

The objective of this research is to develop an uncertainty evaluation software that integrates the influence of form deviation. This chapter was mainly devoted to the error simulation method that simulates errors due to limited sampling on profiles with a form deviation. CMM hardware errors were neglected in this chapter. An important part of the error simulation method is the profile simulator which allows to generate profiles based on measured form deviations or based on simulated form deviations. Gaussian filtering was used to *filter measured profiles* in order to remove effects of measurement noise and roughness. It was shown that form deviations for circles, lines, planes as well as cylinders can all be *simulated* based on the method to simulate linear form deviations. Measured and simulated form deviations are rescaled to a standard dimensionless form deviation value of 1, and stored in a form database. This form database is used to simulate feature profiles based on given position, orientation, size and form deviation values.

The generated feature profiles are sampled according to a given sampling strategy (e.g. six equidistant points) and the sampled points are used to create a *measured* associated feature. Through comparison with the associated feature of the *true* (unsampled) profile, errors on position, orientation, size and form deviation are calculated. The process is repeated multiples times in order to obtain error distributions for each of these feature parameters. The number of Monte Carlo simulations will determine the calculation time. The optimal number will dependent on the measured parameters, the level of confidence, used form database, etc. Taking between 200 and 500 iterations is sufficient under most circumstances. The chapter ended with some examples of error simulations for circles.

The next chapter will propose a method to model hardware errors of a CMM. Chapter 5 will explain how the error simulation method of this chapter can be extended to incorporate the modelled CMM hardware errors of Chapter 4 and how this updated error simulation method can be used to calculate task-specific measurement uncertainties.

# Chapter 4

## Modelling CMM hardware errors

In the error simulation method, presented in the previous chapter, CMM hardware errors were neglected. In order to obtain full task-specific measurement uncertainties, also the influence of CMM hardware uncertainties needs to be taken into account. This chapter presents a method to model geometric errors and probing errors of the CMM. The next chapter shows how the error simulation method can be extended to incorporate these hardware uncertainties.

### 4.1 Hardware uncertainty contributors

Although they are not the only measurement uncertainty contributors, CMM hardware errors are often regarded as a very important source of measurement uncertainty. For a conventional CMM, hardware errors can be divided into two main categories:

**Geometric errors** Due to mechanical imperfections of guideways and carriages of a Cartesian CMM, linear motions along the axes will not be perfectly straight. These error motions are called geometric errors of the CMM.

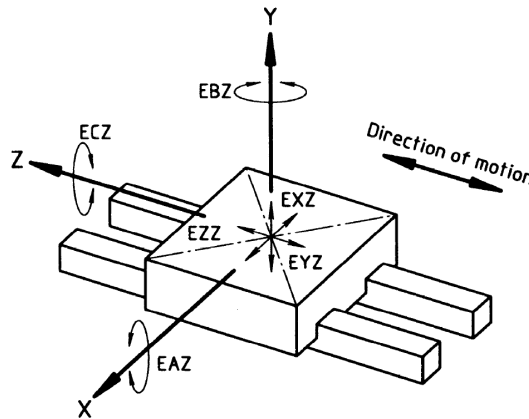
**Probing system and probe head errors** Apart from the CMM geometric errors, the probing system, possibly mounted on an indexable probing head, will usually have a notable influence on the measurement uncertainty. The influence of probing errors will depend much on the type of probing system that is used.

It should be clear that CMM hardware uncertainties can never be treated without considering environmental influences, as already indicated in Section 1.7.1. Environmental conditions (like temperature and vibrations) will have an important influence on hardware uncertainties [60]. The next two sections will describe the terminology regarding geometric errors and probing system configuration.

### 4.1.1 Geometric errors

For a conventional CMM, three linear motions are used to cover a Cartesian space. Every linear motion involves six elements of deviation [61]:

- *One positional deviation* in the direction of motion (positioning error).
- *Two linear deviations* of the moving component (straightness errors).
- *Three angular deviations* of the moving component (pitch, roll and yaw errors).



- EXZ: Straightness error motion of the z-axis in x direction  
 EYZ: Straightness error motion of the z-axis in y direction  
 EZZ: Positioning error of the z-axis  
 EAZ: Tilt error motion of the z-axis around x (pitch)  
 EBZ: Tilt error motion of the z-axis around y (yaw)  
 ECZ: Roll error motion of the z-axis

Figure 4.1: Error components for a straight line motion along the z-axis. Adapted from [61].

In this thesis the conventions according to ISO 230-1 are used<sup>1</sup>; these are illustrated in Figure 4.1 for a motion along the  $z$ -axis. Besides the 6 errors of motion for each axis, usually three additional squareness errors are defined because the three axes are not perfectly perpendicular to each other. This means that the geometric errors of a CMM can be described by 21 ( $3 \times 6 + 3$ ) parametric errors, if the rigid body assumption is valid [62].

### 4.1.2 Probing system configuration

Figure 4.2 shows the different components of a probing system as they are referred to in this thesis. Notice that not all probing systems will contain an articulating system (also called articulated probe head). The figure is illustrated with a tactile probe but the probe can also be optical (e.g. a laser line scanner); in that case there will of course be no stylus or stylus extension.

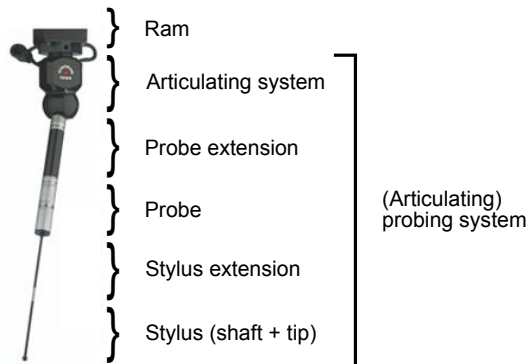


Figure 4.2: Different components of a probing system.

## 4.2 Measuring geometric errors

When simulating CMM geometric errors, these errors should be realistic. Usually measured geometric errors are not random; mostly a typical pattern can be recognised in the geometric errors. In order to get acquainted with different geometric errors of a CMM and to get an idea of the relative importance of the different geometric errors, the parametric errors of the  $x$ -motion of the Coord3 MC16 CMM were measured by means of a laser interferometer (Renishaw ML10).

<sup>1</sup>according to ISO 230-1 the different deviations are denoted by capital letters; further in this text lower case is used for reasons of readability (e.g. *exx* instead of *EXX*).

Figure 4.3 shows the results for the positioning error  $exx$  and pitch error  $ebx$ . The measurements were carried out as close as possible ( $y = 963, z = -691$  in machine coordinates) to the  $x$ -scale, that is glued to the granite table. Under these measurement conditions the positioning error  $exx$  is (almost) not influenced by the yaw error  $ecx$  and pitch error  $ebx$ .

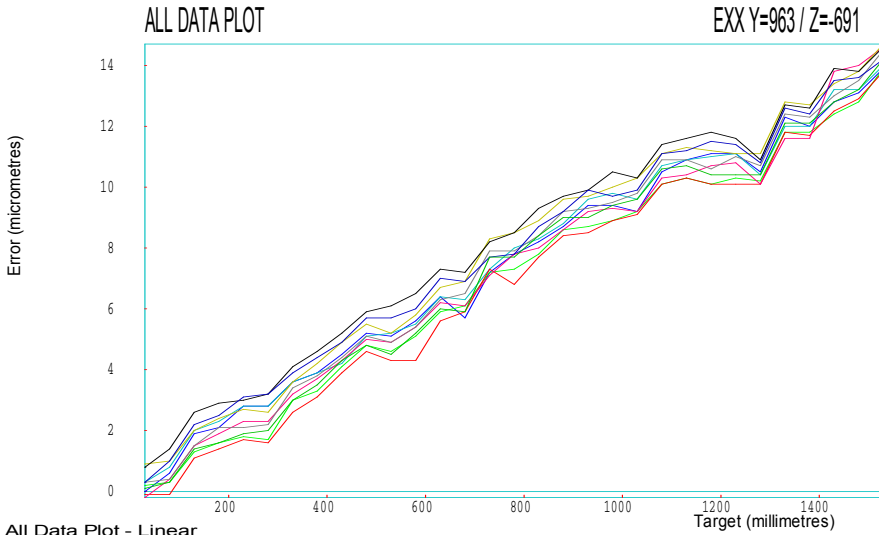
The measurement showed a considerable positional deviation of about  $14\ \mu\text{m}$  over the travel of the  $x$ -axis (1500 mm). This is large for a CMM in a temperature controlled environment. It should be noticed that the temperature, in the metrology room where the measurements took place, may deviate up to  $1\ ^\circ\text{C}$ , because of people entering the room and imperfect temperature control. Since the CMM is not equipped with thermal compensation, this affects the positioning error. Taking into account the expansion coefficient of granite ( $6 \times 10^{-6}\ \text{K}^{-1}$ ) learns that the deviation can not be completely attributed to a temperature difference from  $20^\circ\text{C}$ . It is very likely that a large part of the error can be removed by recalibrating the CMM. However it will never be possible to remove the (linear) error completely since (even small) temperature changes and drift of the machine will still cause positional errors. A considerable amount of drift can be observed during the quite limited time of measurement ( $\pm 10\ \text{min}$ ); target position 0 has an error of  $0\ \mu\text{m}$  for the first measurement and an error of  $\pm 1\ \mu\text{m}$  for the last measurement.

It is remarkable that also the pitch error  $ebx$  has a ‘mainly linear’ behaviour. The maximum observed pitch error over the measured range equals about ( $14\ \mu\text{m}/\text{m}$ ). The monotonically raising pitch error is caused by bending of the granite table which also serves as guideway for the  $x$ -motion (see Figure 1.1).

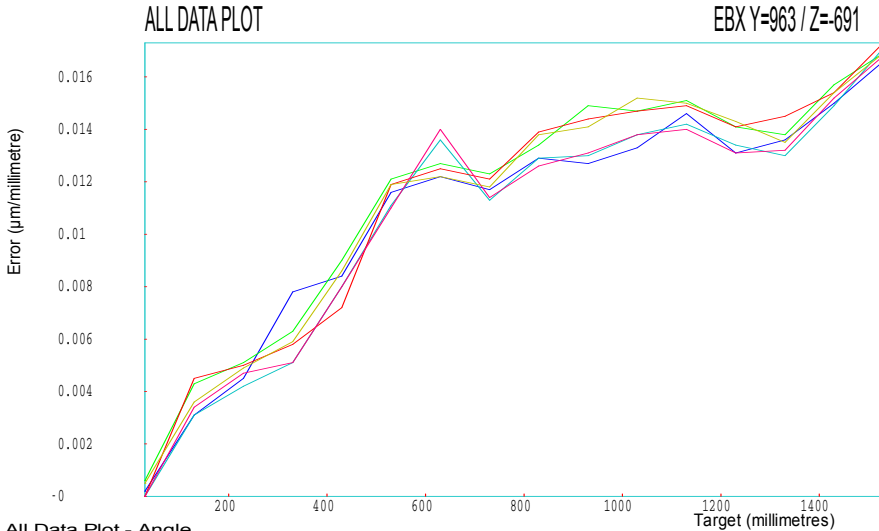
The bending of the granite table can also be observed from the straightness measurement  $ezx$  depicted in Figure 4.4. Here is no linear component present since for straightness measurements the start point and end point are set at zero by definition.

The results of the other parametric errors of the  $x$ -motion are given in Appendix B. This appendix contains also the results of a second measurement executed at the same height ( $z$ -value) but as far away from the  $x$ -scale as possible. The roll error motion  $eax$  was not measured since this one can not be measured with a laser interferometer. Roll error motions can be measured by means of electronic levels. Squareness errors were also not measured.





<p>All Data Plot - Linear                  Machine:Coord3 MC 16                  Serial No:219 0.0 632                  Date:13:20 Jan 30 2009                  By:JVK &amp; NVG</p>	<p>Axis:X                  Location:Labo PMA                  Filename: track1_exx.rtl                  Bidirectional</p>
--	---



<p>All Data Plot - Angle                  Machine:Coord3 MC 16                  Serial No:219 0.0 632                  Date:14:09 Jan 30 2009                  By:JVK &amp; NVG</p>	<p>Axis:X                  Location:Labo PMA                  Filename: track1_ebx.rta                  Bidirectional</p>
---	---

Figure 4.3: Measurement of positioning error ( $exx$ ) and pitch error ( $ebx$ ) along  $x$ -axis.

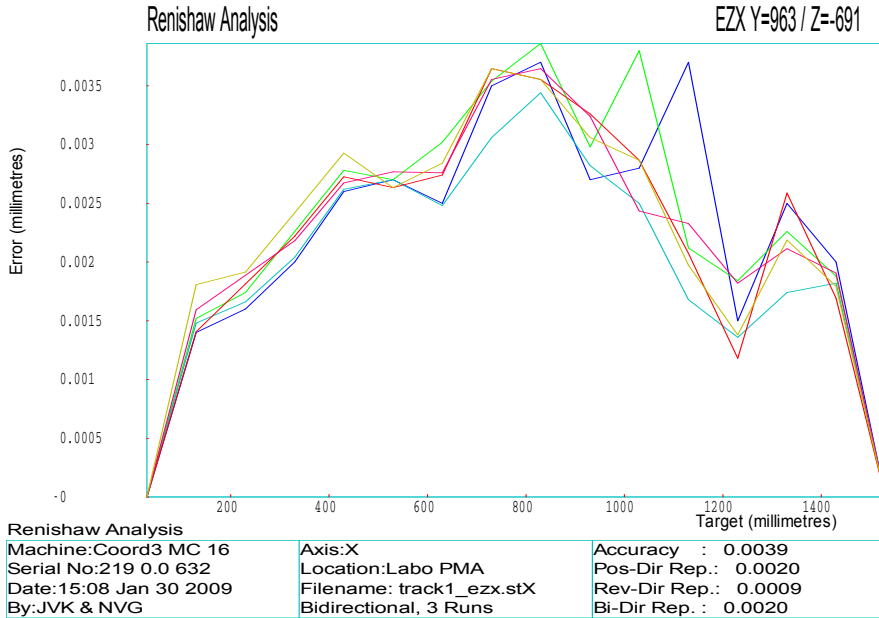


Figure 4.4: Measurement of straightness error ( $ezx$ ) along  $x$ -axis.

## 4.3 Modelling geometric errors

### 4.3.1 Kinematic model of CMM-measurement

Most conventional CMMs can be modelled as a kinematic chain of 4 rigid bodies connected by 3 prismatic joints. To each of the four rigid bodies a frame can be assigned. The kinematic chain of the Coord3 CMM is depicted in Figure 4.5; the frames are assigned as follows:

- Frame  $\{0\}$  is connected to the fixed CMM structure (granite table), and corresponds to the machine coordinate system (MCS).
- Frame  $\{1\}$  is connected to the  $x$ -carriage (portal structure).
- Frame  $\{2\}$  is connected to the  $y$ -carriage (saddle).
- Frame  $\{3\}$  is connected to the  $z$ -ram.

The motion of the frames relative to each other, through the prismatic joints, can be described by homogeneous transformation matrices. In case of error-free

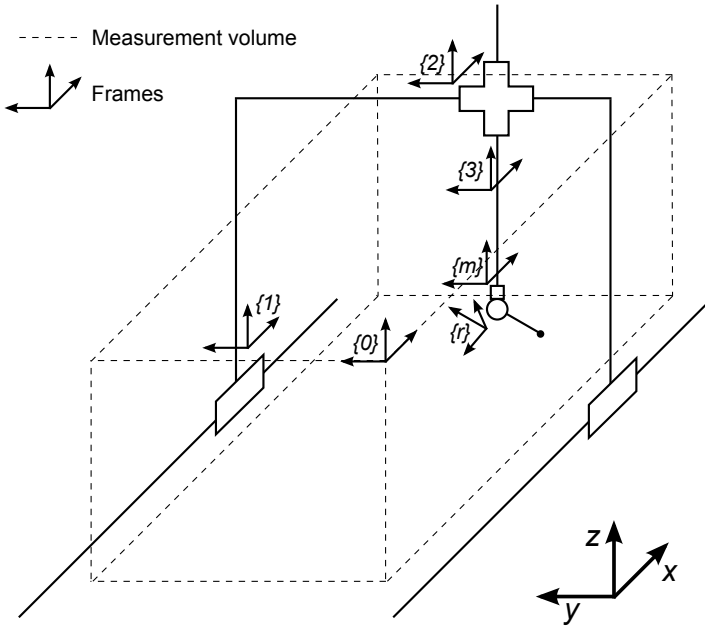


Figure 4.5: The kinematic chain of the Coord3 MC16 CMM.

prismatic joints, the homogeneous transformation matrix describing the pose of frame  $\{1\}$  with respect to frame  $\{0\}$ , expressed in frame  $\{0\}$ , is as follows:

$${}^1_0T = \begin{bmatrix} 1 & 0 & 0 & | & {}_0x0x + x_{enc} \\ 0 & 1 & 0 & | & {}_0y0x \\ 0 & 0 & 1 & | & {}_0z0x \\ \hline 0 & 0 & 0 & | & 1 \end{bmatrix} \quad (4.1)$$

This homogeneous transformation matrix is describing a simple translation.  $x_{enc}$  represents the value read from the  $x$ -scale (linear encoder of the  $x$ -scale).  $({}_0x0x, {}_0y0x, {}_0z0x)$  corresponds to the beginning (home position) of the  $x$ -scale, expressed in frame  $\{0\}$ . This means that the origin of frame  $\{1\}$  is connected to the reference point of the scale reading unit mounted on the  $x$ -carriage. If the coordinates  $({}_1x, {}_1y, {}_1z)$  of a point with respect to frame  $\{1\}$  are known, the

coordinates  $({}_0x, {}_0y, {}_0z)$  with respect to frame  $\{0\}$  are calculated as:

$$\begin{bmatrix} {}_0x \\ {}_0y \\ {}_0z \\ 1 \end{bmatrix} = {}^1_0T \begin{bmatrix} {}_1x \\ {}_1y \\ {}_1z \\ 1 \end{bmatrix} \quad (4.2)$$

If the error motions of the  $x$ -carriage are taken into account, Eq. 4.1 extends to:

$${}^1_0T = \left[ \begin{array}{ccc|c} 1 & -ecx & ebx & {}_0x0x + x_{enc} + exx \\ ecx & 1 & -eax & {}_0y0x + eyx \\ -ebx & eax & 1 & {}_0z0x + ezx \\ \hline 0 & 0 & 0 & 1 \end{array} \right] \quad (4.3)$$

It should be noticed that the error motions  $e*x$  ( $*$  is used as wildcard character) of Eq. 4.3 are no single values but that they depend on the position of the  $x$ -axis (cf. Figure 4.3 and 4.4); this means that they are function of  $x_{enc}$ . Instead of  $e*x(x_{enc})$  the short notation  $e*x$  is used. The short notation is also used to refer to the  $y$ - and  $z$ -error motions.

The motion of the  $y$ -carriage, frame  $\{2\}$ , with respect to the  $x$ -carriage can be described by a completely analogue transformation matrix:

$${}^2_1T = \left[ \begin{array}{ccc|c} 1 & -ecy & eby & {}_1x0y + exy \\ ecy & 1 & -eay & {}_1y0y + y_{enc} + eyy \\ -eby & eay & 1 & {}_1z0y + ezy \\ \hline 0 & 0 & 0 & 1 \end{array} \right]$$

$y_{enc}$  represents the value read from the  $y$ -scale.  $({}_1x0y, {}_1y0y, {}_1z0y)$  corresponds to the beginning (home position) of the  $y$ -scale expressed in frame  $\{1\}$ . The origin of frame  $\{2\}$  is connected to the reference point of the scale reading unit mounted on the  $y$ -carriage. The transformation matrix describing the motion of the  $z$ -ram frame  $\{3\}$  with respect to the  $y$ -carriage, frame  $\{2\}$  is again completely analogue:

$${}^3_2T = \left[ \begin{array}{ccc|c} 1 & -ecz & ebz & {}_2x0z + exz \\ ecz & 1 & -eaz & {}_2y0z + eyz \\ -ebz & eaz & 1 & {}_2z0z + z_{enc} + ezz \\ \hline 0 & 0 & 0 & 1 \end{array} \right]$$

$({}_2x0z, {}_2y0z, {}_2z0z)$  corresponds to the position of the reference point of the scale reading unit for the  $z$ -scale, expressed in frame  $\{2\}$ . This scale reading unit is

mounted on the  $y$ -carriage.<sup>2</sup> The origin of frame  $\{3\}$  is connected to the beginning (home position) of the  $z$ -scale.

Frame  $\{3\}$  is not suited to be used as reference frame since its position has no practical value. It is better to use the end of the  $z$ -ram as reference frame (frame  $\{m\}$  in Figure 4.5). This position is called the *probe head mounting point*, because that is the position where the probe head is mounted. Since this is a position on the  $z$ -ram, the transformation matrix describing the pose of frame  $\{m\}$  with respect to frame  $\{3\}$  represents a simple translation:

$${}^m_3T = \left[ \begin{array}{ccc|c} 1 & 0 & 0 & 3x0m \\ 0 & 1 & 0 & 3y0m \\ 0 & 0 & 1 & 3z0m \\ \hline 0 & 0 & 0 & 1 \end{array} \right] \quad (4.4)$$

$(3x0m, 3y0m, 3z0m)$  corresponds to the position the probe head mounting point, expressed in frame  $\{3\}$ .

Based on  ${}^m_3T$ ,  ${}^3_2T$ ,  ${}^2_1T$  and  ${}^1_0T$ , the homogeneous transformation matrix describing the pose of frame  $\{m\}$  with respect to frame  $\{0\}$  can be calculated:

$${}^m_0T = {}^1_0T {}^2_1T {}^3_2T {}^m_3T$$

Calculating this set of matrix multiplications, and neglecting second order effects ( $e^{**} \cdot e^{**} \approx 0$ ) gives following extensive matrix:

$${}^m_0T = \left[ \begin{array}{c|c} {}^m_0R & {}_0P^{0,m} \\ \hline \mathbf{0}_{1 \times 3} & 1 \end{array} \right]$$

with

$${}^m_0R = \left[ \begin{array}{ccc} 1 & -ecz - ecy - ecx & ebz + eby + ebx \\ ecx + ecy + ecz & 1 & -eaz - eay - eax \\ -ebx - eby - ebz & eax + eay + eaz & 1 \end{array} \right]$$

<sup>2</sup>For the  $x$ - and  $y$ - axes the scale reading units are connected to the moving  $x$ - and  $y$ -carriages while the scales stay fixed. For the  $z$ -axis the scale is mounted on the moving ram and the scale reading unit stays fixed on the  $y$ -carriage. This subtle difference does not matter for the description of the kinematic model.

and

$${}^0\mathbf{p}^{0,m} = \begin{bmatrix} x_{enc} + x0x + x0y + x0z + x0m + e_{xx} + e_{xy} + e_{xz} \\ -e_{cz} y0m + e_{bx} z0y + e_{bz} z0m - e_{cx}(y0y + y_{enc}) \\ -(e_{cy} + e_{cx})(y0m + y0z) + (e_{by} + e_{bx})(z0m + z_{enc} + z0z) \\ y_{enc} + y0x + y0y + y0z + y0m + e_{yx} + e_{yy} + e_{yz} \\ +e_{cz} x0m + e_{cx} x0y - e_{ax} z0y - e_{az} z0m \\ +(e_{cx} + e_{cy})(x0m + x0z) - (e_{ay} + e_{ax})(z0m + z_{enc} + z0z) \\ z_{enc} + z0x + z0y + z0z + z0m + e_{zx} + e_{zy} + e_{zz} \\ -e_{bz} x0m + e_{az} y0m - e_{bx} x0y + e_{ax}(y0y + y_{enc}) \\ -(e_{bx} + e_{by})(x0m + x0z) + (e_{ax} + e_{ay})(x0m + y0m + y0z) \end{bmatrix} \quad (4.5)$$

${}^m\mathbf{R}$  represents the total angular errors of the  $z$ -ram expressed with respect to frame  $\{0\}$ . It can be calculated as the sum of the angular errors of all separate axes.  ${}^0\mathbf{p}^{0,m}$  represents the position of the probe head mounting point<sup>3</sup>. Errors on this position depend on the positioning and straightness errors of the different axes, but also on the angular error motions of these axes. These latter errors are the so called ‘*Abbe-errors*’ and depend on the position of the probe head mounting point with respect to the different scales. The closer to the scales, the smaller the effect of these errors [63].

The position of the probe head mounting point is usually not the position of interest when using the CMM. For tactile sensors the center of the stylus tip is determined as reference, for optical sensors usually the center point of the field of view is determined as reference point. The position of this reference point is important to calculate the effect of the angular errors. The position of the probe tip, with respect to the probe head mounting point can be expressed by following homogeneous transformation matrix:

$${}^p_mT = \left[ \begin{array}{ccc|c} 1 & 0 & 0 & mx_p \\ 0 & 1 & 0 & my_p \\ 0 & 0 & 1 & mz_p \\ \hline 0 & 0 & 0 & 1 \end{array} \right]$$

${}^p_mT$  does not include errors due to the probing system. The modelling of probing errors is discussed in Section 4.4. To calculate the effect of CMM geometric errors on the probe reference point  $(x_p, y_p, x_p)$ , only its nominal position is needed. The transformation matrix describing the complete kinematic chain of the CMM is then calculated as:

$${}^p_0T = {}^m_0T {}^p_mT = \left[ \begin{array}{c|c} {}^p_0\mathbf{R} & {}^0\mathbf{p}^{0,p} \\ \hline \mathbf{0}_{1 \times 3} & 1 \end{array} \right]$$

<sup>3</sup>In Eq. 4.5 the parameters \*0\* are no longer accompanied by the leading subscripts (as in Eq. 4.3 to 4.4) for reasons of readability.

with

$${}^p_0\mathbf{R} = {}^m_0\mathbf{R}$$

and

$${}_0\mathbf{p}^{0,p} = {}_0\mathbf{p}^{0,m} + \begin{bmatrix} m x_p - m y_p(ecx + ecy + ecz) + m z_p(ebx + eby + ebz) \\ m y_p + m x_p(ecx + ecy + ecz) - m z_p(eax + eay + eaz) \\ m z_p - m x_p(ebx + eby + ebz) + m y_p(eax + eay + eaz) \end{bmatrix} \quad (4.6)$$

One could wonder why squareness errors are not included in all equations above; the equations only show 18 instead of 21 error components. In the model presented above it is assumed that squareness errors are included in the straightness errors. When measuring geometric errors, one usually considers straightness errors and squareness errors as two different error components because they are usually measured in different setups. In that case the straightness errors in the beginning and at the end of the axis are always zero (see Figure 4.4). However, the squareness error can be added to the straightness error by adding the squareness value (expressed as  $\mu\text{m}/\text{m}$ ) as a linear component to the straightness error. This approach was followed in the present work.

### Need for scale positions

Vector  ${}_0\mathbf{p}^{0,m}$  (Eq. 4.5) is quite complicated because the real positions of the scales (\*0\*) are taken into account. If the scales are treated as coincident with the axes of the MCS (frame {0}) all \*0\* values are zero, and Eq. 4.5 simplifies to:

$${}_0\mathbf{p}^{0,m} = \begin{bmatrix} x_{enc} + exx + exy + exz - y_{enc} ecx + z_{enc}(ebx + eby) \\ y_{enc} + eyx + eyy + eyz - z_{enc}(eax + eay) \\ z_{enc} + ezx + ezy + ezz + y_{enc} eax \end{bmatrix} \quad (4.7)$$

This equation looks more like results obtained by other authors [64, 65, 66]. Eq. 4.7 shows that the only angular error that creates an error in  $z$ -position of the probe head mounting point corresponds to the roll errors of the  $x$ -axis. Yet, more angular errors will influence the total error on  $x$ - and  $y$ -position.

One could wonder why the position of the scales is usually not taken into account when modelling CMM geometric errors. Most articles describing geometric errors deal with compensating geometric errors of a CMM, or other machine tools. It is the purpose to compensate the systematic errors as good as possible and not to model the remaining errors after compensation. To illustrate that the position of the scales does not matter for error compensation, Figure 4.6 shows a simplified example for the compensation of an error motion of one axis ( $x$ -axis).

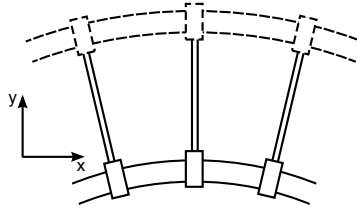


Figure 4.6: Two axes configurations that describe the same error motion.

Figure 4.6 shows an axis that is bent, resulting in a yaw error  $ecx$ . The positioning error of the axis is represented by  $exx$ . The  $x$ -errors can be calculated as follows:

$${}^{err}x = exx + ecx y$$

If the positioning errors are considered to be zero, the errors will rise with increasing  $y$ -value, as illustrated in Figure 4.6. The measured geometric errors can be used to compensate for the error motions. The geometric errors  $exx$ ,  $ecx$  could be measured with a laser interferometer that is positioned as close as possible to the  $x$ -guideway ( $y = 0$ ). However, if the laser interferometer is positioned further away from the  $x$ -guideway ( $y = y_1$ ) positive positioning errors will be measured by the laser interferometer. This measured positioning error  $exx'$  can not be considered as a scale error since it is the consequence of the straightness error of the  $x$ -guideway. The measured yaw error  $ecx'$  will stay the same. It can be considered as a virtual guideway with following geometric errors:

$$exx' = exx + ecx y_1$$

$$ecx' = ecx$$

The  $x$ -errors induced by this virtual guideway are the same as the one of the actual guideway:

$${}^{err}x = exx' + ecx'(y - y_1) = exx + ecx y$$

This example shows that the position of the axes in the CMM model is not important for the compensation of systematic error motions. It does not matter whether or not the measured positional and linear deviations are also influenced by angular errors of the guideway. As long as the geometric errors do not change the calculated compensations will be the same. However, in order to determine the measurement uncertainty (after calibration of the CMM) the position of the axis is really important. If there are uncompensated yaw-errors in the example above, they will hardly influence measurements close to the  $x$ -scale ( $y \approx 0$ ) while they



can have an important influence for measurements further away from the  $x$ -scale ( $y \gg 0$ ).

If one wants the CMM model to reflect the ‘Abbe-errors’ [67] correctly, the position of the scales should be integrated in the CMM model. Measurement positions further from the scales will have higher measurement uncertainties than positions close to the scales. This should be integrated in the uncertainty calculations. Therefore it is important that the positions of the scales are modelled correctly.

When geometric errors are simulated (see next section), positioning errors are considered as caused by the scales while straightness and angular error motions are considered as caused by the straightness of the guideways. If the position of the simulated axes does not correspond with the actual position of the scales, errors due to ‘Abbe-offsets’ are not reflected correctly by the simulated geometric errors. For this reason it is very important to integrate the positions of the scales in the kinematic model of the CMM.

### 4.3.2 Simulating geometric error components

Equations 4.5 and 4.6 can be used to simulate errors on the position of the *probe head mounting* point and the *probe tip position*. In order to do so, information about the configuration of the CMM (position of the scales) is needed and information about the geometric errors of the CMM. Information about the configuration of the CMM can be easily obtained (see further in Section 4.3.3). Obtaining information about the geometric errors of the CMM is not so obvious. Measuring the geometric errors of a CMM can be done in several ways: e.g. by laser interferometer and electronic levels or by means of multilateration techniques [68]. Regardless of the used method, measuring all 21 geometric errors is very time consuming. But knowing the true geometric errors is not essential for uncertainty modelling :

- If the measured geometric errors are known, they should be compensated. This can be done by changing the compensation table of the CMM or by compensating the measurement result (based on the available kinematic model of the CMM). The concept that known systematic errors should be compensated, and not included in the measurement uncertainty, is one of the basic principles of the GUM [13].
- Measured geometric errors can seldom be considered as invariable. In a limited time period, geometric errors often stay quite constant, but when geometric errors are remeasured after a longer period, they can look very different due to drift of the machine. Section 4.2 showed that this drift can already be significant for a very small time slot ( $\pm 10$  min).

- For measurement uncertainty determination it is important that the obtained measurement uncertainties are reliable. The actual values of the true geometric errors are not known and do not matter, as long as the calculated measurement uncertainties are reliable. The actual values of the true geometric errors are needed for calibration, but not for measurement uncertainty determination.

The central idea of the proposed approach is that it is impossible and unnecessary to know the true geometric errors of a CMM for uncertainty calculations. This is in contrast to the approach used in current implementations of uncertainty evaluation software for CMMs (see Section 2.4.2). Although it is unnecessary to know the *true* geometric errors, this does not mean that it is unnecessary to be able to simulate *realistic* geometric errors. Realistic geometric errors will be necessary to simulate realistic measurement errors in order to obtain reliable measurement uncertainties.

Before starting to model geometric errors, one should first have a look at some measured geometric errors. Remember that the geometric errors are no single value but that they depend on the position of the related axes:  $e*x$  on  $x$ -position,  $e*y$  on  $y$ -position and  $e*z$  on  $z$ -position. Section 4.2 shows that the measured positioning and angular errors can be considered as mainly linear with some added curvature. No extensive study of geometric errors of CMMs was carried out during this research. However based on in-house experience on other machine tools and examples from literature [3, 65, 28] the hypothesis that geometric errors are dominated by linear and curvature components seems to be valid. Simulated geometric errors should have similar properties as measured geometric errors. Simulating these kinds of error profiles shows similarities with simulating linear form deviations (Section 3.5.2). This is not surprising since several geometric errors are also due to straightness deviation of the guideways. Therefore it was decided to use Eq. 3.5, which was applied in Chapter 3 to model linear form deviations ( $d(x)$ ), also for modelling geometric errors ( $e(x)$ ):

$$e(x) = sx + c(2x^2 - 1) + \sum_{n=1}^N a_n \cos(n\pi x + \phi_n) \quad \text{for } x \in [-1, 1] \quad (4.8)$$

with

$$s + c + \sum_{n=1}^N a_n = 1$$

The values of parameters  $s$  and  $c$  will determine the importance of respectively the linear and curvature component of the geometric error.  $N$  determines the maximum harmonic order, expressed in undulations per length (UPL). The simulation of geometric errors by means of Fourier series has already been applied in Monte Carlo simulations for machine tools and CMMs [29, 30].

The values for  $a_n$  can be specified by the user but are usually determined randomly. A geometric error will be represented by a vector  $\mathbf{e}$ . It describes a geometric error (e.g. *exx*) over the length of the respective axis. For simulated *linear form deviations*, this simulated error vector is rescaled to a (dimensionless) *range* of 1. In contrast, to simulate *geometric errors* the *maximum absolute value* of the error vector  $\mathbf{e}$  is rescaled to 1. Additionally, and also different from the situation for linear form deviations, the first value is put at zero because geometric errors are zero by definition at the origin of the scale. This zeroing is implemented by subtracting the first value from the complete error vector; the scaling by dividing the vector by its maximum absolute value:

$$\mathbf{e} \leftarrow \mathbf{e} - \mathbf{e}(1)$$

$$\mathbf{e} \leftarrow \frac{\mathbf{e}}{\max(|\mathbf{e}|)}$$

The advantage of having this rescaled error vector is that it can be rescaled to a error vector of whatever magnitude, just by multiplying it by a given error value  $e_{tot}$ . This will be the largest value of the geometric error over the total range of the axis:

$$\mathbf{e} \leftarrow e_{tot} \mathbf{e}$$

A realistic value for  $e_{tot}$  should be chosen. In reality the geometric error will be strongly dependent on the length. The longer the travel of the axis, the larger the error can be. Therefore it would be logical to choose these values proportional to the length of the axis. One can choose these values based on the ISO 10360 specification of the CMM. E.g. a CMM with a specification of  $5 \mu\text{m} + 5 \mu\text{m}/\text{m}$  will not show positioning errors of  $20 \mu\text{m}/\text{m}$ . Based on the performance specification one can roughly estimate the maximum possible value for the geometric error  $e_{max}$  that represents the maximum error value per travel length.<sup>4</sup> Once  $e_{max}$  is known,  $e_{tot}$  can be determined by multiplying  $e_{max}$  with the total travel  $t$  of the axis (in meter). Not every simulated geometric error component needs to have the maximum value, errors will often be smaller. The sign of the errors can also be positive or negative. That is why  $e_{tot}$  is determined by additionally multiplying  $e_{max}$  with a random value, ranging between  $-1$  and  $1$ :

$$e_{tot} = \text{rand}(-1, 1) t e_{max}$$

Figure 4.7 shows the simulated positioning and straightness errors for one virtual CMM. Figure 4.8 shows the angular errors. Table 4.1 shows the parameter settings that were used to generate the geometric errors.

<sup>4</sup> $e_{max}$  is expressed in  $\mu\text{m}/\text{m}$  for positional and linear deviation and is expressed in  $\mu\text{m}/\text{m}^2$  for angular deviations.

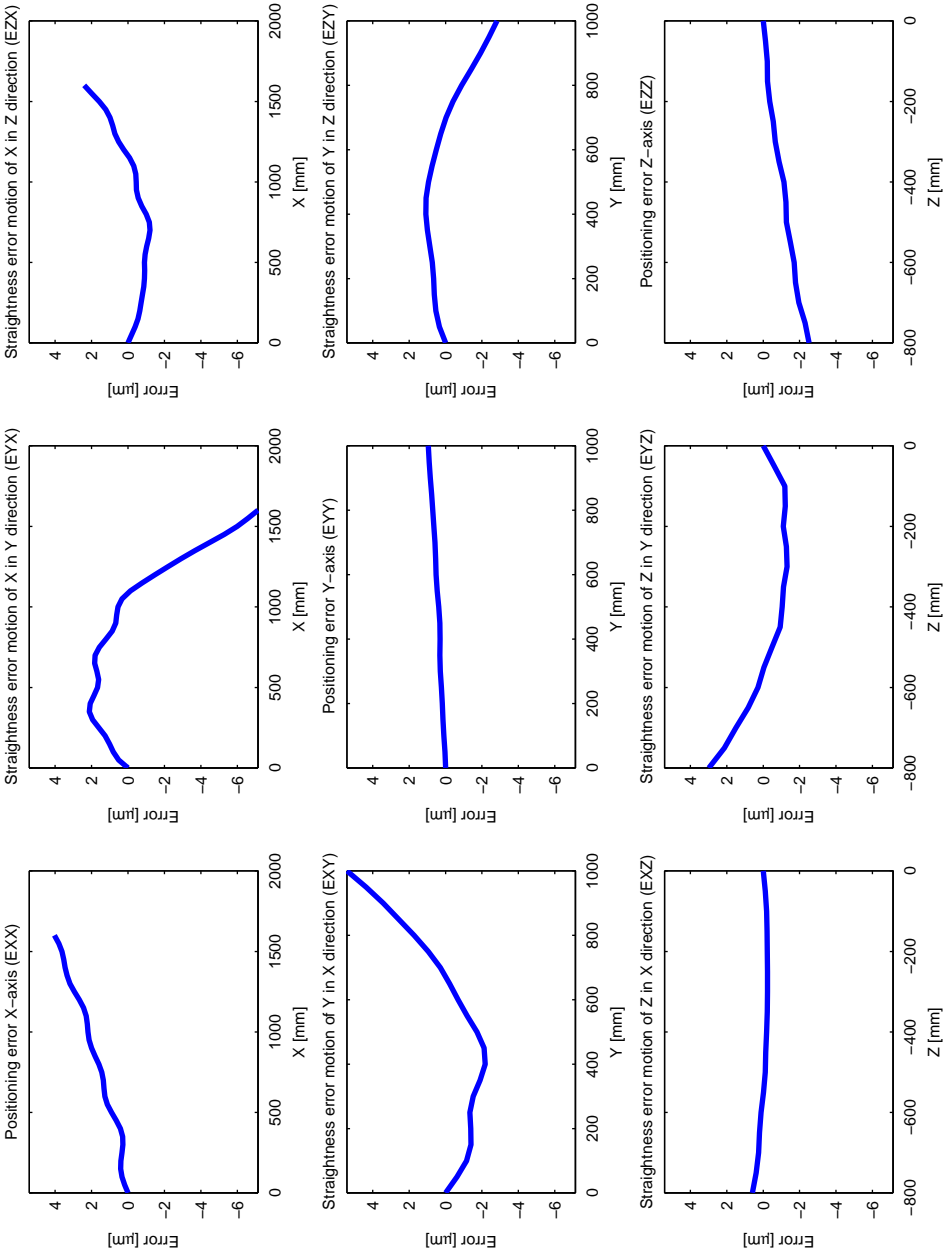


Figure 4.7: Simulated positioning and straightness errors for a virtual CMM.

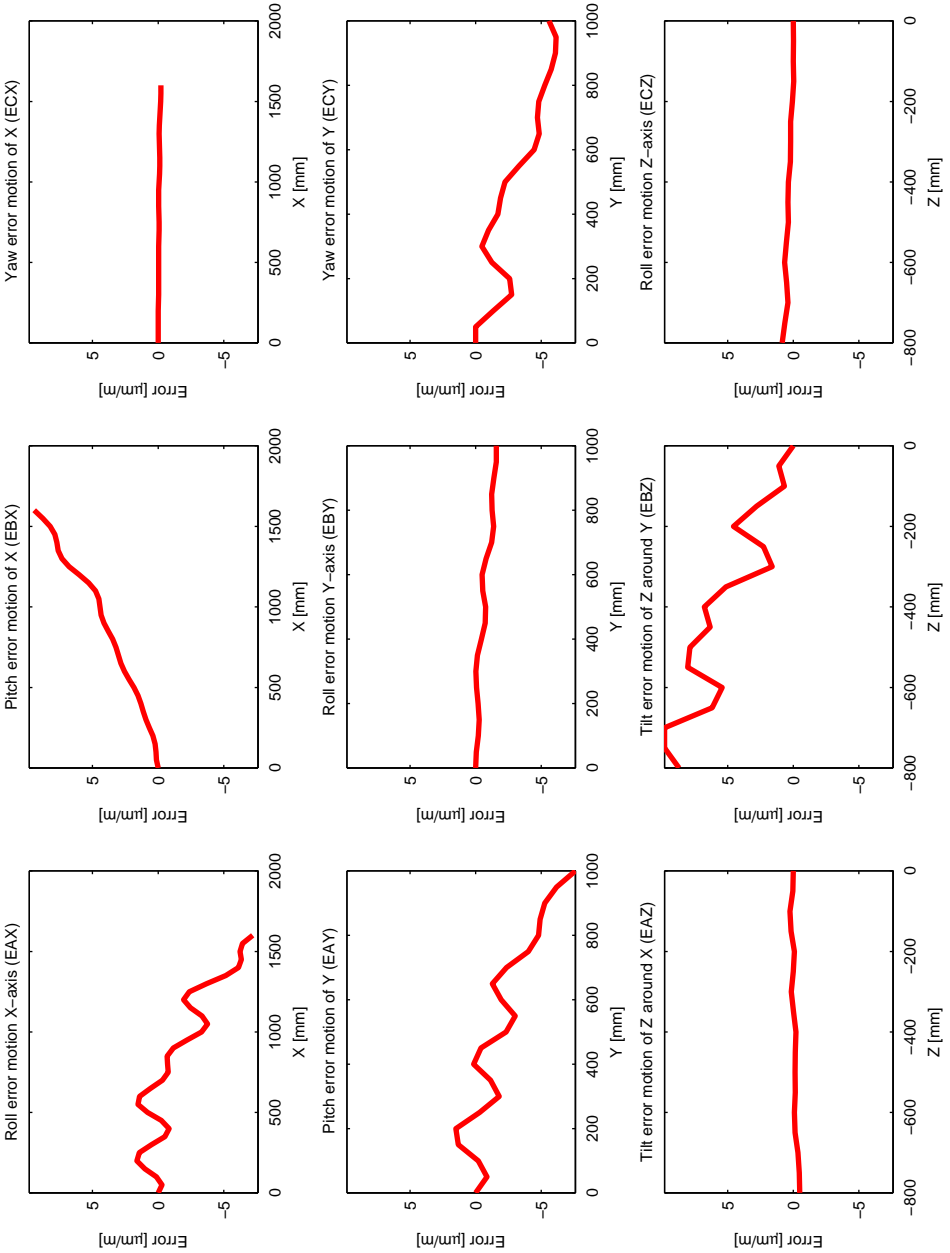


Figure 4.8: Simulated angular errors for a virtual CMM.

	$s$	$c$	$N$	$t$	$e_{max}$		$s$	$c$	$N$	$t$	$e_{max}$
$exx$	0.8	0.1	7	1.6 m	7 $\mu\text{m}/\text{m}$	$eax$	0.6		7	1.6 m	10 $\mu\text{m}/\text{m}^2$
$eyx$	0.5	0.4	7	1.6 m	7 $\mu\text{m}/\text{m}$	$ebx$	0.6		7	1.6 m	10 $\mu\text{m}/\text{m}^2$
$ezx$	0.5	0.4	7	1.6 m	7 $\mu\text{m}/\text{m}$	$ecx$	0.6		7	1.6 m	10 $\mu\text{m}/\text{m}^2$
$exy$	0.5	0.4	7	1.0 m	7 $\mu\text{m}/\text{m}$	$eay$	0.6		7	1.0 m	10 $\mu\text{m}/\text{m}^2$
$eyy$	0.8	0.1	7	1.0 m	7 $\mu\text{m}/\text{m}$	$eby$	0.6		7	1.0 m	10 $\mu\text{m}/\text{m}^2$
$ezy$	0.5	0.4	7	1.0 m	7 $\mu\text{m}/\text{m}$	$ecy$	0.6		7	1.0 m	10 $\mu\text{m}/\text{m}^2$
$exz$	0.5	0.4	7	0.8 m	7 $\mu\text{m}/\text{m}$	$eaz$	0.6		7	0.8 m	10 $\mu\text{m}/\text{m}^2$
$eyz$	0.5	0.4	7	0.8 m	7 $\mu\text{m}/\text{m}$	$ebz$	0.6		7	0.8 m	10 $\mu\text{m}/\text{m}^2$
$ezz$	0.8	0.1	7	0.8 m	7 $\mu\text{m}/\text{m}$	$ecz$	0.6		7	0.8 m	10 $\mu\text{m}/\text{m}^2$

Table 4.1: Parameters used to simulate the geometric errors of Figure 4.7 and 4.8.

All geometric errors are generated independently from each other, so there will be no correlation between different geometric errors. This is a simplification of reality because:

- Several errors are mainly due to thermal deviations, which makes these errors positively correlated. If the temperature of the axes is too high, all axes will usually have positive positioning errors. The proposed method could be adapted to account for this shortcoming.
- Straightness errors are normally strongly linked with pitch and yaw errors. These angular errors are usually caused by the straightness deviation of the axis. Roll and yaw errors often approximate the derivatives of the straightness profiles. This connection is not taken into account by the proposed method.

### 4.3.3 Calculating error states of virtual CMMs

Once all geometric errors are simulated, Eq. 4.5 can be used to calculate the resulting errors on the probe head mounting point in the measurement space of the CMM. The representation of all errors in the measurement space of the CMM is called the *error state*. To calculate this error state, information about the position of the axes is needed. Table 4.2 shows the values of the axes position parameters used to calculate the error state for the Coord3 MC16 CMM.

${}_0x0x$	-120 mm	${}_0y0x$	1400 mm	${}_0z0x$	-950 mm
${}_1x0y$	0 mm	${}_1y0y$	-1410 mm	${}_1z0y$	1085 mm
${}_2x0z$	95 mm	${}_2y0z$	-30 mm	${}_2z0z$	265 mm
${}_3x0m$	25 mm	${}_3y0m$	40 mm	${}_3z0m$	-400 mm

Table 4.2: Axes position parameters used to simulate the error state.

The leading subscripts in Table 4.2 are used to indicate that the axes positions are expressed relative to the preceding frame; for reasons of readability these subscripts were not used further on. From equation (4.5) the relationship between the *nominal* (error free) position of probe head mounting point, expressed in the MCS, and the values read from the scales  $x_{enc}, y_{enc}, z_{enc}$  can be derived:

$$\begin{aligned} {}_0x_m &= x_{enc} + x_0x + x_0y + x_0z + x_0m \\ {}_0y_m &= y_{enc} + y_0x + y_0y + y_0z + y_0m \\ {}_0z_m &= z_{enc} + z_0x + z_0y + z_0z + z_0m \end{aligned} \quad (4.9)$$

It is assumed that the home position of the scales ( $x_{enc}, y_{enc}, z_{enc} = 0$ ) corresponds to the nominal home position of the probe head mounting point expressed in the MCS ( ${}_0x_m, {}_0y_m, {}_0z_m = 0$ ). This means that the sum of all axes translations should be zero:

$$\begin{aligned} x_0x + x_0y + x_0z + x_0m &= 0 \\ y_0x + y_0y + y_0z + y_0m &= 0 \\ z_0x + z_0y + z_0z + z_0m &= 0 \end{aligned}$$

The values of Table 4.2 meet this requirement. If these axes position parameters are known and the 18 geometric errors are simulated, Eq. 4.5 can be used to calculate the errors on the position of the probe head. If the effect of geometric errors on the center of the probing tip needs to be known, Eq. 4.6 should be used. Figure 4.9 shows the calculated state spaces for the axes position parameters of Table 4.2 and the geometric errors represented in Figure 4.7 and 4.8.

These figures represent the  $x$ ,  $y$ , and  $z$ -errors of a virtual CMM with the same measurement volume and the same configuration of its axes as the Coord3 CMM. The ‘intersection’-planes dividing the measurement volume into eight sub-volumes do not have a specific meaning. They are used for better visualisation of the errors. All errors are zero for  $({}_0x_m, {}_0y_m, {}_0z_m) = (0, 0, 0)$  since all geometric errors are zero (by default) at the home position of the axis. The bottom-right figure, representing the 3D-error state, indicates the total distance error that is calculated as follows:

$${}^{err}d = \sqrt{{}^{err}x^2 + {}^{err}y^2 + {}^{err}z^2}$$

Therefore this error will always be positive. This distance error is only included for visualisation purposes and to have a measure for the total error. This error will not be used further on.

Although the positions close to the origin show small errors, and positions further from the origin mostly show larger errors, this does not mean that the CMM will measure more accurately in zones that show small errors. The error gradients are

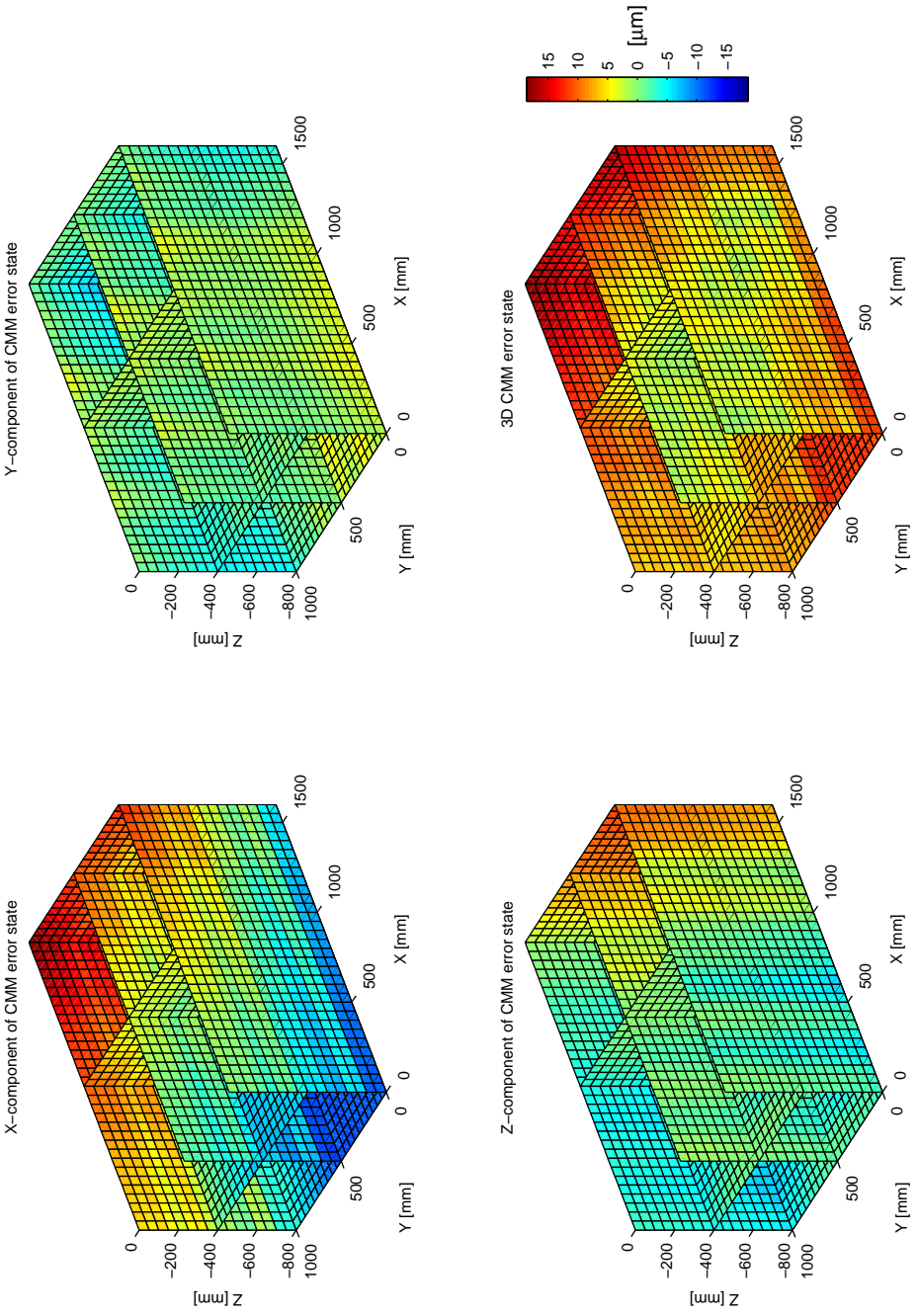


Figure 4.9: Simulated error state for a virtual CMM.



important for the error on the measurement result, not the magnitude of the error. This can be explained most easily with an example: suppose that a small circle is measured in a zone with large errors but with small spatial gradients in the error. If only CMM geometric errors are taken into account, this will lead to very small errors on diameter and roundness because the errors on the separate measured points are (almost) all the same. There will be an error on the position of the circle when its position is expressed in the MCS but this error is not important. If a second circle is measured close to the first one, this circle will show the same error on position (expressed in the MCS) which means that there will be (almost) no error on the distance between the two circles. If a third circle is measured far away from the first one, in a zone with low errors and low spatial gradients, it will show very small errors on diameter, roundness as well as position (expressed in the MCS). The measurement error on the distance between circle 1 and circle 3 will be large, as might be expected for a large distance measurement.

#### 4.3.4 Selecting representative virtual CMMs

Although the error states, calculated in the previous section, represent the  $x$ ,  $y$ , and  $z$ -errors of a virtual CMM with the same measurement volume and the same configuration as an actual CMM, it is not guaranteed that the error will be representative for the actual CMM. The simulated errors should not be the same as the errors of the actual CMM but should be representative for this CMM. This means in the first place that their magnitude should be approximately the same. The chosen magnitude of the geometric errors will determine the magnitude of the errors at the probe mounting point (and probe tip center). One could check if the magnitude of the errors of the actual CMM corresponds to the magnitude of the simulated errors by comparing an actually measured reference artefact (e.g. gauge block) with a simulated measurement of that object. Yet performing actual measurements can take a lot of time.

It is not necessary to make use of actual measurements if one uses the ISO 10360 performance specification for length measurements. If there is a valid ISO 10360 specification, one knows that every length measurement (according to ISO 10360) will have an error lower than the given limit. This information can be used to check if measurements of the virtual CMM fall within these limits. Every virtual CMM will be subjected to a virtual ISO 10360-2 test. This test is used to check if the virtual CMM is representative for the true CMM.

Details about ISO 10360-2 were already discussed in Section 2.2. A set of five material standards of size (step gauge or gauge blocks) needs to be measured in seven different orientations on the CMM, and each measurement is repeated three times. The shortest material of size should be smaller than 30 mm, the longest should be longer than 66% of the largest spatial diagonal of the measuring

volume of the CMM. For each of the 105 measurements, the error on size E is calculated. All errors are plotted on a graph as a function of the measured length. Figure 4.10 shows the graph of such a simulated measurement for the virtual CMM represented in Figure 4.9. Measurements labelled as d1, d2, d3 and d4 represent measurement errors along the four diagonals; measurement labelled x, y and z represent measurement errors along the respective axes. Every length is only measured one time instead of three times, since no random geometric errors or probing errors are included. Performing the same measurement three times would yield three times the same result. This means that only 35 virtual measurements are done rather than the 105 (35 × 3) measurements required by ISO 10360-2.

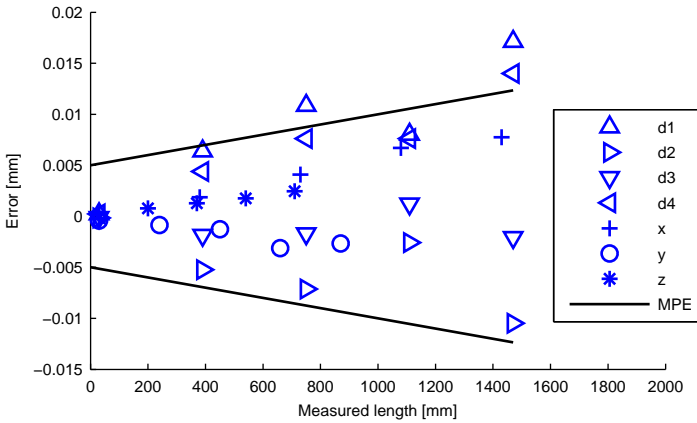


Figure 4.10: ISO 10360-2 test for the virtual CMM of Figure 4.9.

The results in Figure 4.10 show that not all virtual measurements fall within the MPE-limits of the actual CMM (5 μm ± 5 μm/m). But the errors are also not extremely large compared to the MPE. Other virtual CMMs, created with the same parameters showed errors that were all lower than the specified MPE. This means that the chosen parameters for the simulated geometric errors  $e_{max}$  are satisfying. In order to measure how well the simulated CMM corresponds to the performance specification of the actual CMM, a performance indicator  $v$  for each virtual CMM is calculated:

$$v = \min \left( \left| \frac{mpe_l}{err_l} \right| \right) \quad \text{for all 35 measured lengths}$$

where  $err_l$  represents the virtually measured error on a given length and  $mpe_l$  represents the maximum permissible error for that length. If the performance indicator  $v$  is lower than 1, the virtual CMM has not passed the ISO 10360 test and is considered as unsuited for simulation purposes. If the value of  $v$  is higher

than 2, which means that no measured error is larger than half its MPE, the errors are considered as too small. In this case the virtual CMM is not representative for the actual CMM, because its errors are too low.

If virtual CMMs are used for error simulation in a Monte Carlo method, multiple virtual CMMs will be needed. It is impossible to choose the parameters for the geometric errors in such way that all simulated CMMs have values of  $v$  between 1 and 2, because the generated geometric errors have a large degree of randomness. If too much (e.g. more than 50%) virtual CMMs fail because their errors are too low or too high, the parameters for the generation of the geometric errors are probably wrongly selected and should be adapted.

## 4.4 Modelling probing system errors

### 4.4.1 Modelling the nominal position of the probe tip

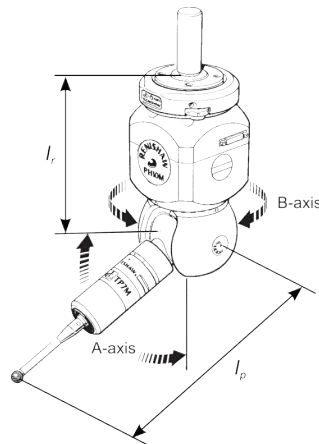


Figure 4.11: Representation of an articulating system with two angles (Renishaw PH10M), adapted from [69].

In order to complete the kinematic model of the CMM, the position of the probe tip with respect to the probe head mounting point is needed (see Eq. 4.6). Therefore the dimensions and the configuration of the probing system have to be known. Figure 4.11 shows a drawing of the articulating probe head, equipped with probe and stylus, used on the Coord3 CMM. The nominal position of the probe tip with respect to frame  $\{m\}$  ( $m x_p, m y_p, m z_p$ ) can be easily expressed as a function of the

$A$  and  $B$  angles  $(\theta_A, \theta_B)$  of the articulating probe head system:

$$\begin{bmatrix} m x_p \\ m y_p \\ m z_p \\ 1 \end{bmatrix} = \left[ \begin{array}{c|c} \begin{matrix} r \\ m \end{matrix} \mathbf{R} & m \mathbf{P}^{m,r} \\ \hline \mathbf{0}_{1 \times 3} & 1 \end{array} \right] \begin{bmatrix} r x_p \\ r y_p \\ r z_p \\ 1 \end{bmatrix} \quad (4.10)$$

with

$${}^r_m \mathbf{R} = \begin{bmatrix} \cos(\theta_A) \cos(\theta_B) & -\sin(\theta_B) & -\sin(\theta_A) \cos(\theta_B) \\ \cos(\theta_A) \sin(\theta_B) & \cos(\theta_B) & -\sin(\theta_A) \sin(\theta_B) \\ \sin(\theta_A) & 0 & \cos(\theta_A) \end{bmatrix}$$

and

$$m \mathbf{P}^{m,r} = \begin{bmatrix} m x_r \\ m y_r \\ m z_r \end{bmatrix}$$

$(r x_p, r y_p, r z_p)$  represents the position of the center of the stylus tip, expressed in frame  $\{r\}$ . The origin of frame  $\{r\}$  corresponds to the center of rotation of the articulating probe head. This frame is connected to the last linkage of the articulating probe head (linkage where probe is mounted); this means that the position of the probe tip with respect to frame  $\{r\}$  does not change with changing  $A$  or  $B$  angle.  ${}^r_m \mathbf{R}$  is a rotation matrix representing the  $A$  and  $B$  rotation of the articulating probe head. This matrix is valid for the mounting configuration of the PH10M probe head on the Coord3 CMM ( $\theta_B$  corresponding to a rotation around the positive  $z$ -axis,  $\theta_A$  to a rotation around negative  $y$ -axis when  $\theta_B = 0$ ). For other mounting configurations, matrix  ${}^r_m \mathbf{R}$  will look slightly different.  $m \mathbf{P}^{m,r}$  represents the position of the center point of the articulating probe head, with respect to the probe head mounting point. This is the intersection of the  $A$ -axis and  $B$ -axis and is usually only offset in negative  $z$ -direction with respect to the probe head mounting point:

$$(m x_r, m y_r, m z_r) = (0, 0, -l_r)$$

For straight styli the nominal center position of the stylus tip  $(r x_p, r y_p, r z_p)$  is usually only offset in negative  $z$ -direction over a length  $l_p$ :

$$(r x_p, r y_p, r z_p) = (0, 0, -l_p)$$

In this specific situation Eq. 4.10 results in:

$$\begin{bmatrix} m x_p \\ m y_p \\ m z_p \end{bmatrix} = \begin{bmatrix} \sin(\theta_A) \cos(\theta_B) l_p \\ \sin(\theta_A) \sin(\theta_B) l_p \\ -l_r - \cos(\theta_A) l_p \end{bmatrix} \quad (4.11)$$

These calculated nominal positions of the center of the stylus tip can be used in Eq. 4.6 to calculate the errors on the center point of the probe tip due to the geometric errors of the CMM. Knowing the nominal position will be sufficient. Information about the position of the probe tip is needed to know the actual Abbe-distances to the different axes. E.g. the errors on probe position due to the roll of the  $z$ -axis ( $ecz$ ) can be neglected for  $\theta_A = 0$ , but can not be neglected for  $\theta_A > 0$ . The errors of the articulating probe head will hardly influence the effect of geometric errors on the position of the probe tip. Errors of the probe and probe head can be modelled separately and added to the probe tip errors caused by geometric errors.

#### 4.4.2 Modelling errors of the articulating probe head

The angles  $\theta_A$  and  $\theta_B$  of most articulating systems cannot be changed continuously but will be changed in discrete steps of fixed angles ( $7.5^\circ$  for the PH10M). These angular positions are not sufficiently accurate to determine the position of the probe tip. However, the repeatability of the different angular positions is very good. This means that the relative position of the probe tip can be calibrated before the start of the measurement. This is also the used procedure in practice. All necessary probing system configurations are calibrated in advance. Once calibrated, all available probe configurations can be used with a very good repeatability. Although the repeatability of the articulating system is very good, the introduced errors can not be neglected, certainly when probe or stylus extensions (see Figure 4.2) are used. The influence of angular deviations from the nominal positions on the probe position can be obtained from Eq. 4.11. The angular errors  $^{err}\theta_A$  and  $^{err}\theta_B$  are considered as the only relevant errors for the articulating probe head. This is a simplification of reality, since the real rotations around the  $A$ -axis as well as the  $B$ -axis exhibit three linear and three angular errors.

In order to quantify the errors of the articulating probe head, the manufacturer's specifications are used. Repeatability values for the angles  $\theta_A$  and  $\theta_B$  are not specified. Instead the repeatability of the probe tip is specified for a given probe and stylus length. For a length  $l_p$  of 62 mm the specified repeatability of the probe tip is  $0.5 \mu\text{m}$  ( $2\sigma$ ) for the used probe head [69]. From these specifications an *approximating* value for the standard deviations of the angular errors  $^{err}\theta_A$  and  $^{err}\theta_B$  can be obtained:

$$\sigma(^{err}\theta_A) = \sigma(^{err}\theta_B) = \arctan\left(\frac{0.5/2 \cdot 10^{-3}}{62}\right) = 0.83''$$

These values are used to model probe position errors due to the articulating probe head. These errors stay the same as long as the probe orientation is not changed; so in that case they can be considered as a kind of systematic errors. Errors of the

articulating probe head will have no influence on the hardware uncertainties if only one probe configuration is used during the measurement.

### 4.4.3 Modelling errors of the probe

Besides geometric errors and errors of the articulating probe head, there are also the errors of the probe itself that will have an influence on the hardware uncertainties. Multiple probes, and probe configurations, can be used on one CMM. For modelling probe errors in detail, a dedicated model for every type of probe is needed. Modelling probe errors can be very difficult due to the large number of parameters and settings that will influence the probe errors: measurement speed, contact force, stylus length, probe tip diameter ... Modelling uncertainties of optical probing systems, like vision probes or laser line scanners, becomes even more complicated because the errors will strongly depend on environmental conditions (lighting) and surface properties of the measured objects (reflection, translucency) [70, 6]. Because of these difficulties, a pragmatic solution was chosen. The probe errors are modelled as random errors defined by given standard deviations for three orthogonal directions:

$$[\sigma(^{err}_r x_p), \sigma(^{err}_r y_p), \sigma(^{err}_r z_p)]$$

These values are determined by the user and can be derived from actual tests or from specifications (e.g. ISO 10360 specification  $MPE_P$  for the probing error). Considering probe errors as purely random errors does not comply with the real behaviour of most probing system: e.g. switching touch-trigger probes exhibit systematic errors due to the varying pre-travel distance, laser line scanners have important systematic errors as a function of scanning depth [71, 6]. Although it is possible to model the probe error as a combination of a systematic and random component it was decided to model the probe error as a purely random error to reduce the complexity.

## 4.5 Conclusions

This chapter discussed the modelling of CMM hardware errors. The measurement accuracy of the CMM will vary over the measurement volume, mainly because of the varying Abbe-offset to the scales. In order to model this behaviour accurately, the position of the scales needs to be incorporated in the kinematic model of the CMM. Based on the kinematic model and the 21 geometric error components, the error state of the complete CMM volume can be determined. It is impossible and unnecessary to know the true non-compensated geometric error components, but one should be able to model realistic geometric error components.

The method used to model these geometric error components is similar to the one used to model linear form deviations in Chapter 3. Based on the kinematic model of the CMM and simulated geometric error components, virtual CMMs can be built. In order to check if a virtual CMM exhibits errors that are representative for the actual CMM, a virtual ISO 10360-2 test is performed. Besides the modelling of CMM geometric errors, this chapter also describes the modelling of probe and probe head errors.

The next chapter describes how the modelled hardware errors can be included in the error simulation method of the previous chapter.





# Chapter 5

## Determining task-specific measurement uncertainties

This chapter shows how the error simulation method of Chapter 3 can be extended to incorporate the modelled hardware errors of Chapter 4 and how this updated error simulation method can be used to calculate task-specific measurement uncertainties.

### 5.1 Error calculation method extended with hardware uncertainties

The methods to simulate the CMM geometric errors and probing system errors, described in Section 4.3 and 4.4, can be used to integrate CMM hardware uncertainties into the error simulation method. This is realised by extending the sampling module of the error simulation method (see Figure 3.5 on page 47). Instead of just sampling the points and sending the sampled points directly to the feature fitting module, hardware errors are added to the sampled points. These hardware errors consist of CMM geometric errors and probing system errors. An updated schematic presentation can be found in Figure 5.1.

The hardware uncertainty database consists of a set of virtual CMMs equipped with virtual probing systems. These virtual CMMs are generated in advance, according to the methods of Section 4.3 and 4.4, and show possible behaviour of the actual CMM. The coordinates of the points that are sampled from the true simulated profile will be expressed in the MCS. Simulated measurement errors due to geometric errors, errors of the articulating probe head and probe errors will be added to the sampled points.

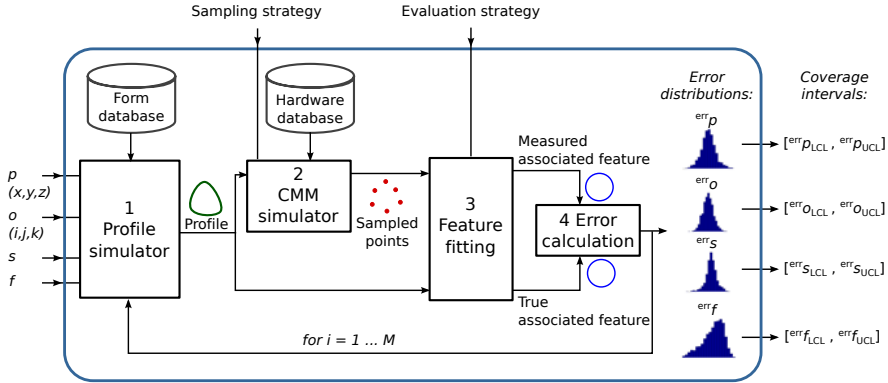


Figure 5.1: Scheme of Monte Carlo method to simulate influence of form deviations and hardware uncertainties on measurement errors.

Every Monte Carlo run, another virtual CMM is selected. Enough virtual CMMs are needed, but the number of virtual CMMs  $N_{CMM}$  does not necessarily need to be the same as the number of Monte Carlo runs  $M$ . However, it is important that each separate Monte Carlo run (denoted by index number  $i_M$ ) is connected to a predefined virtual CMM (denoted by index number  $i_{CMM}$ ). This is important if the measurement uncertainty on distances between features and geometrical tolerances needs to be determined (see Chapter 6). Suppose the uncertainty of the distance between two measured circles needs to be evaluated. When the error simulation method is used for both circles this will result in  $M$  virtual measurements for circle 1 and circle 2. One can also calculate  $M$  virtual distances and  $M$  virtual errors on the distances. A virtual error on distance will only be representative if both circles are measured by the same virtual CMM.

In Figure 5.1 the input of the error calculation method stays the same as in Figure 3.5: actual position, orientation, size and form deviation of the feature. In order to add the correct CMM geometric errors, it is important that the position and orientation of the feature are expressed in the MCS. The output of the error calculation method are distributions of errors on position, orientation, size and form deviation. From these distributions, upper and lower confidence limits for measurement errors can be defined.

## 5.2 Uncertainty calculation method

The method described in the previous section allows to simulate the measurement errors on feature parameters. It takes into account sampling strategy, hardware

errors and the influence of form deviations. To determine these errors, the true parameters of the feature need to be known. Usually only the measured parameters are known. Using measured values as input for the error calculation method will hardly affect the result, if the form deviation of the feature is negligible. Unfortunately the form deviation is seldom negligible. The true form deviation influences the measurement errors but is not known in advance.

In Appendix A it was suggested to express the simulated errors relative to the measured form deviation. Measurement uncertainties seem to be proportional to the measured roundness as long as hardware uncertainties are neglected. When hardware errors are taken into account, measurement uncertainties will no longer be proportional to the form deviation. Hardware errors will be more important for small form deviations than for large form deviations. This is shown in Figure 5.2. This figure shows the confidence limits of simulated measurement values for a circle with diameter 500 mm measured with 10 points in the middle of the CMM volume. If only the form deviation is taken into account the confidence limits of the measurement values are linearly proportional to the true roundness value. If hardware errors are taken into account the situation is different. For very small form deviations the hardware errors become the major uncertainty contributor. For large form deviations (and a limited number of used sampling points) the hardware errors are only minor contributors.

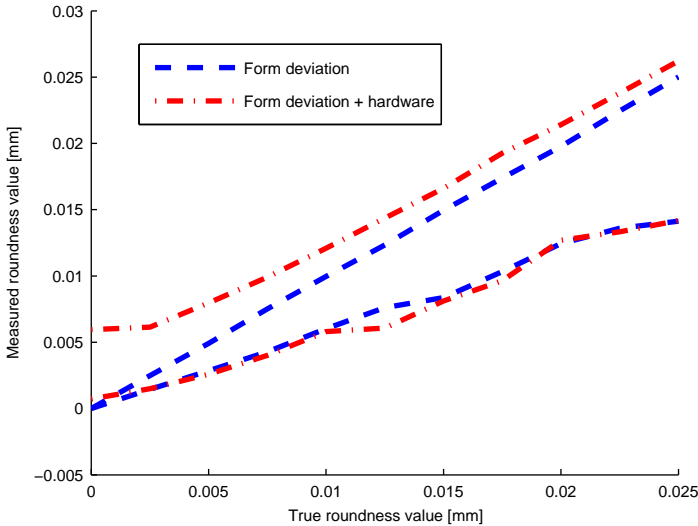


Figure 5.2: Confidence limits of simulated measured roundness values for a circle measurement. Form deviation: no hardware uncertainties are taken into account. Form deviation + hardware: hardware uncertainties are taken into account.

By expanding the previous error simulation method it is possible to obtain reliable uncertainty statements when the true form deviation is unknown. It will be necessary to determine first the form deviation uncertainty. Once the form deviation uncertainty is known, the range of possible form deviations (defined by the form deviation uncertainty) can be used to determine the uncertainties on the other feature parameters, like position, orientation or size. Section 5.2.1 explains how the confidence limits of the true form deviation can be obtained based on the actual measured form deviation. Section 5.2.2 explains how these confidence limits can be used to determine the measurement uncertainties of all feature parameters.

### 5.2.1 Form deviation uncertainty by likelihood criterion

A way has to be found to determine the LCL and UCL for the form deviation based on the actual measured form deviation. The error simulation method can be used to simulate measurement errors for features where the true parameters are known. For actual measurements only the measured parameters are known. The actual measured form deviation can not be used as input for the error simulation because the measured form deviation can highly underestimate the true form deviation while the true form deviation influences the magnitude of the simulated errors. A solution to this problem can be found if the error simulation method is ran three times with three *chosen* (instead of measured) form deviation values.

Three values for the true form deviations ( ${}^{\text{true}}f$ ) are chosen:  $f_{\min}$ ,  $f_{\text{med}}$  and  $f_{\max}$  (see abscissa of Figure 5.3), where  $f_{\min}$  and  $f_{\max}$  are very rough estimates of the minimum and maximum possible form deviation, and  $f_{\text{med}}$  is the average of the aforementioned two. This will result in three coverage intervals for the parameter errors. The coverage intervals for measured form deviations can be determined by adding the chosen true form deviation to the calculated confidence limits of the form deviation errors:

$$[{}^{\text{meas}}f_{\text{LCL}}, {}^{\text{meas}}f_{\text{UCL}}] = [{}^{\text{true}}f + {}^{\text{err}}f_{\text{LCL}}, {}^{\text{true}}f + {}^{\text{err}}f_{\text{UCL}}] \quad (5.1)$$

evaluated for the three chosen form deviation values:

$${}^{\text{true}}f = f_{\min}, f_{\text{med}} \text{ and } f_{\max}$$

The three calculated coverage intervals for measured form deviation are drawn in red in Figure 5.3. The next steps can be further illustrated graphically. Second order polynomial interpolation between the three lower limits and three upper limits allows to determine coverage intervals (of measured form deviations) for every value of true form deviation between  $f_{\min}$  and  $f_{\max}$ . The interpolated confidence limits in Figure 5.3 show which measured form deviations can be expected for a given magnitude of true form deviation. These limits will depend on the type of

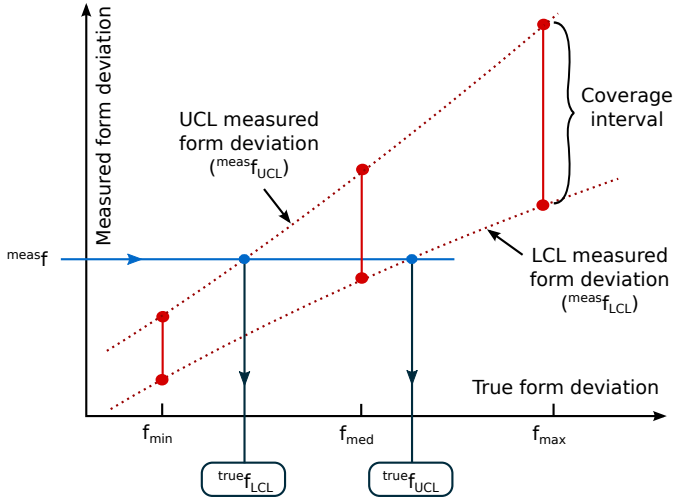


Figure 5.3: Determination of lower and upper confidence limits for form deviations, based on the actually measured form deviation.

form deviations included in the form deviation database, the applied sampling strategy, and the CMM hardware uncertainties included in the CMM hardware database. The true form deviation is not known, but since the actually measured form deviation ( $^{meas}f$ ) is known (see ordinate on Figure 5.3), the range of true form deviations that allow this measurement result can be determined. In other words: the *likelihood* of the true form deviation is determined, given the actually measured form deviation. The LCL and UCL for the true form deviation [ $^{true}f_{LCL}, ^{true}f_{UCL}$ ] can be determined by calculating the intersection point with the upper and lower limits of the coverage intervals for the measured form deviations (Figure 5.3). These upper and lower confidence limits of the true form deviation ( $^{true}f_{LCL}$  and  $^{true}f_{UCL}$ ) define the form deviation uncertainty.

One could also use more than three chosen values for true form deviation. However, tests showed that this does not improve calculated coverage intervals significantly. To limit calculation time it was decided to use only three chosen values for true form deviation by default.

It could happen that in Figure 5.3 the horizontal line determined by  $^{meas}f$  does not intersect with the interpolated upper and lower confidence limits over the interval [ $f_{min}, f_{max}$ ]. This means that the actually measured form deviation is too low or too high. According to the simulations it is then very unlikely that the true form deviation belongs to the interval [ $f_{min}, f_{max}$ ]. This results in a warning to the user and  $f_{min}$  or respectively  $f_{max}$  is taken as value for both confidence limits. It can also be that only an intersection with one of the interpolated confidence limits

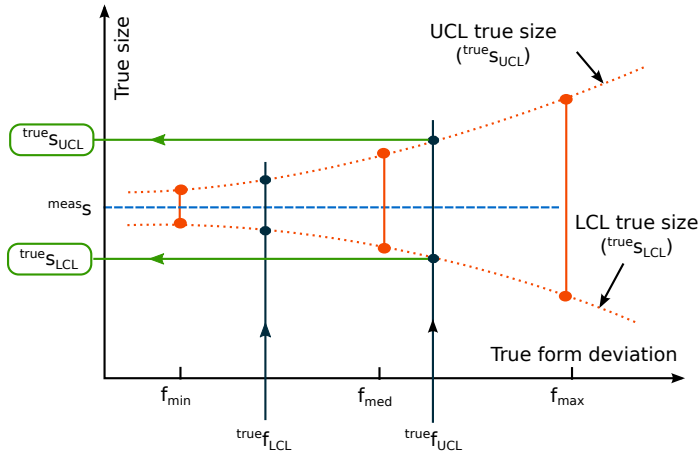


Figure 5.4: Determination of lower and upper confidence limits for size (e.g. diameter) based on confidence limits for form deviation.

(LCL or UCL) can be found. In this case the missing value for  $\text{true } f_{\text{LCL}}$  or  $\text{true } f_{\text{UCL}}$  is also set as  $f_{\text{min}}$  or respectively  $f_{\text{max}}$ .

## 5.2.2 Uncertainty of other parameters, based on form deviation uncertainty

Once the form deviation uncertainty is known, this can be used to determine the measurement uncertainties of the other feature parameters. Two methods to calculate the other measurement uncertainties have been developed: one that is based on the simulation results for the form deviation uncertainty, that needs no additional Monte Carlo simulation and one that still needs a final Monte Carlo simulation step.

### Uncertainty of other parameters, based on simulation results for form deviation uncertainty

The LCL and UCL for true form deviation, calculated in the previous paragraph, can be used to determine LCL and UCL for the other parameters. First, the coverage intervals for position, orientation and size errors are retrieved for the three Monte Carlo simulations performed in the previous step (Section 5.2.1) for  $f_{\text{min}}$ ,  $f_{\text{med}}$  and  $f_{\text{max}}$ . The output of these simulations are not only the coverage

intervals for the form deviation (red bars on Figure 5.3), but also for size, position and orientation. This is illustrated in Figure 5.4 for the true size of a hole (i.e. true diameter): the coverage intervals on true size for  $f_{\min}$ ,  $f_{\text{med}}$  and  $f_{\max}$  are represented by the red bars. The confidence limits are calculated as follows:

$$[\text{true } s_{\text{LCL}}, \text{true } s_{\text{UCL}}] = [{}^{\text{meas}}s - {}^{\text{err}}s_{\text{UCL}}, {}^{\text{meas}}s - {}^{\text{err}}s_{\text{LCL}}] \quad (5.2)$$

Second order interpolation between the three lower limits and three upper limits allows to determine coverage intervals (for true size) at every value of true form deviation. Then the lowest and highest limit is searched by calculating the coverage intervals over the interval  $[\text{true } f_{\text{LCL}}, \text{true } f_{\text{UCL}}]$ . The lowest and highest possible value are the LCL and UCL for true size:  $\text{true } s_{\text{LCL}}$  and  $\text{true } s_{\text{UCL}}$ . The calculations of the coverage intervals for position and orientation are similar.

One could wonder why it is necessary to evaluate the coverage intervals over the complete interval  $[\text{true } f_{\text{LCL}}, \text{true } f_{\text{UCL}}]$  since the width of the uncertainty interval for size will always be the largest for  $\text{true } f_{\text{UCL}}$ . However, this is not always the case; under certain circumstances (e.g. in case of maximum inscribed or minimum circumscribed associated features) it is sometimes possible that upper or lower confidence limit for size, obtained for  $\text{true } f_{\text{LCL}}$  will be outside the coverage interval obtained for  $\text{true } f_{\text{UCL}}$ .

### Uncertainty of other parameters, based on additional Monte Carlo simulations

The previous method has the advantage that the uncertainty for the other parameters can be calculated immediately after the calculation of the form deviation uncertainty. No further simulation is necessary. However, there are also two important drawbacks to this approach:

- The actual confidence level for the calculated uncertainties for size (and position and orientation) will be higher than the confidence level for the form deviation. Suppose that the confidence level for form deviation is 95%, and that  $\text{true } f_{\text{UCL}}$  determines the upper confidence limit for size (as in Figure 5.4). The likelihood that the actual form deviation is larger than  $\text{true } f_{\text{UCL}}$  is only 2.5%. It is for this value of form deviation that the 95% coverage interval for size (and other parameters) is determined. This means that the provided uncertainty for size (position and orientation) is calculated for the ‘worst case’ form deviation. Therefore the coverage interval of these parameters is (largely) overestimated.
- In order to provide also uncertainties for inter-feature distances and geometrical tolerances like perpendicularity, concentricity, etc. the simulated errors should be stored. This means that all three sets of simulated errors

(for  $f_{\min}$ ,  $f_{\text{med}}$  and  $f_{\max}$ ) need to be stored. It would be easier if only one set of errors for each feature needs to be stored. This will be explained in Chapter 6.

A solution to both drawbacks mentioned above is to do one additional Monte Carlo simulation in which the value for (true) form deviation is sampled from a distribution. This form deviation distribution is determined based on the calculated upper and lower confidence limits for form deviation [ ${}^{\text{true}}f_{\text{LCL}}$ ,  ${}^{\text{true}}f_{\text{UCL}}$ ]. Since it will be difficult to obtain information about the distribution of the actual form deviation, a straightforward solution is to treat it as a rectangular distribution (Figure 5.5(a)). This does not take into account that there is a probability of 5% that the true form deviation is outside the [ ${}^{\text{true}}f_{\text{LCL}}$ ,  ${}^{\text{true}}f_{\text{UCL}}$ ] interval. Alternatively one could use a normal distribution with a mean equal to the average of the UCL and LCL and a standard deviation equal to a quarter of the width of the uncertainty interval (Figure 5.5(b)). In this case it is assumed that values close to the middle of the uncertainty interval are most likely. There is no reason to assume this. A third possibility is to use a kind of flattened normal distribution (Figure 5.5(c)). This type of distribution can be obtained as a convolution of a rectangular and normal distribution. Probably this is the most correct solution, however for the ease of implementation and the small difference in final results with the rectangular distribution, the rectangular distribution was chosen.

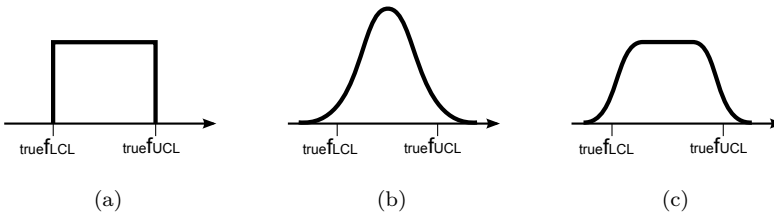


Figure 5.5: Distribution assigned to the true form deviation used to determine uncertainties of other feature parameters: (a) rectangular (b) normal (c) flattened normal.

Once a distribution is assigned to the uncertainty interval of the form deviation, one can use this distribution to sample random form deviation values during a new full Monte Carlo simulation. The same number of Monte Carlo runs as before can be taken. The uncertainty intervals are then obtained directly from the simulated error distributions. The uncertainty interval for size can be obtained by means of Eq. 5.2. Uncertainties intervals for position and orientation are calculated in a complete analogue way.

This alternative method to calculate the measurement uncertainty for feature parameters other than form deviation, will take somewhat more time but will result



in more correct uncertainty intervals. Besides, there will be less data to store and it will be easier to calculate uncertainties for inter-feature distances and geometrical tolerances.

### 5.3 Conclusions

This chapter described how the hardware errors of the previous chapter can be integrated in the error simulation method from Chapter 3. Simulated hardware errors of a virtual CMM will be added to the sampled points.

The error simulation method can be used to determine the measurement uncertainties of feature parameters. First the form deviation uncertainty is calculated based on the measured feature parameters. Three Monte Carlo simulations are executed for three different values of assumed roundness. These results can be used to determine the form deviation uncertainty based on the likelihood criterion.

Once the form deviation uncertainty is known it can then be used to calculate the uncertainties of the other feature parameters. The uncertainty of the other feature parameters can be calculated from the simulation results that are used to determine the form deviation uncertainty. Alternatively an additional Monte Carlo simulation can be used. For this simulation the value for (simulated true) form deviation is sampled from a distribution. This form deviation distribution is determined based on the calculated upper and lower confidence limits for form deviation  $[\text{}^{\text{true}}f_{\text{LCL}}, \text{}^{\text{true}}f_{\text{UCL}}]$ .



# Chapter 6

## Derived uncertainties, software layout and implementation

Chapter 3 and 4 explained how task-specific measurement uncertainties that incorporate the influence of feature form deviations and CMM hardware, can be calculated for CMM measurements. However, the uncertainty output of the described methods is not always useful in practice. The uncertainty results for the position and orientation parameters of the feature are expressed in the machine coordinate system (MCS). In practice measurement results are usually expressed in the part coordinate system (PCS). Besides, the orientation of one single feature is often of minor interest; the orientation of one feature with respect to another is usually more relevant, like e.g. in case of perpendicularity, parallelism and angularity tolerances. This chapter explains how uncertainties on part coordinate systems and uncertainties on measurements of geometrical tolerances can be calculated from the results obtained by the uncertainty calculation method described in the previous chapters. Furthermore this chapter describes the object oriented software layout of the developed uncertainty evaluation software (UES), and the interface to the available commercial measurement software.

### 6.1 Uncertainty on part coordinate systems

#### 6.1.1 Datum, datum features and part coordinate systems

For geometrical product specifications (GPS) the use of datums in tolerancing is a very important concept. According to ISO 5459 the definition of a datum is [72]:

**Definition 6.1** *A theoretically exact geometric reference (such as axes, planes, straight lines, etc.) to which toleranced features are related. Datums may be based on one or more datum features of a part.*

A group of two or more datums can also be used as a composed datum, this is called a datum system. Datums and datum systems are used for establishing geometric relationships of related features. The quality of relevant datum features must be adequate for functional requirements [72]. The example of the introductory chapter, depicted in Figure 1.13, already illustrated that the choice of the datum feature has an important influence on the measurement results and measurement uncertainties. Interchanging datum and toleranced feature will never yield the same results. Every kind of feature can be used as a datum feature.

Measurement results are seldom reported in the machine coordinate system (MCS); usually a part coordinate system (PCS) is defined. The part coordinate system is defined by a set of features from the workpiece. The part coordinate system is also called the datum reference frame<sup>1</sup> in the DMIS standard [19]. According to DMIS, the part coordinate system is defined by multiple datums, a datum can be defined by one or more datum features.

For the construction of a measured datum reference frame, several features can be used. A datum reference frame has three positional degrees of freedom and three orientational degrees of freedom. These six degrees of freedom should be ‘locked’ by the features that compose the datum reference frame, only then the datum reference frame will be fully constrained.

### 6.1.2 Datum matrix

A fully constrained datum reference frame can be represented by a homogeneous transformation matrix, that describes the transformation from the PCS (frame {d}) to the MCS (frame {0}):

$${}^d_0\mathbf{T} = \left[ \begin{array}{c|c} {}^d_0\mathbf{R} & {}_0\mathbf{p}^{0,d} \\ \hline \mathbf{0}_{1 \times 3} & 1 \end{array} \right]$$

The three columns of  ${}^d_0\mathbf{R}$  contain the coordinates of the  $x$ ,  $y$  and  $z$ -unit vectors along the axes of the PCS expressed in the MCS.  ${}_0\mathbf{p}^{0,d}$  represents the origin of the PCS expressed in the MCS.

Since it is the purpose to express the measurements, that are stored in machine coordinates, in part coordinates, the inverse transformation matrix will be needed.

<sup>1</sup>In this thesis also the short term ‘datum’ will be used to refer to a part coordinate system. A datum has to be seen as a reference. This reference can be a single feature, multiple features or a datum reference frame.

This matrix is called the datum matrix:

$${}^0_d\mathbf{T} = {}^d_0\mathbf{T}^{-1} = \left[ \begin{array}{c|c} {}^0_d\mathbf{R} & {}^d\mathbf{P}^{d,0} \\ \hline \mathbf{0}_{1 \times 3} & 1 \end{array} \right]$$

In order to build this datum matrix based on measured features, two feature orientations and three feature position parameters are needed:

- The first feature orientation is used for the orientation of the primary axis of the datum.
- The second feature orientation is used for the alignment of the secondary axis of the datum.
- A feature position is needed constrain the  $x$ -origin of the datum.
- A feature position is needed constrain the  $y$ -origin of the datum.
- A feature position is needed constrain the  $z$ -origin of the datum.

After orienting the first axis, one rotational degree of freedom is left. This is locked by the second feature orientation. While the first feature orientation will be exactly the same as the orientation of the primary axis of the PCS, this is not the case for the second feature orientation. Measured orientation vectors are never perfectly perpendicular, that is why the secondary axis of the PCS will correspond to the projection of the second feature orientation vector into a plane with the primary axis as its normal. The third axis of the PCS has to be perpendicular to the primary and secondary axis and its sense is defined by the ‘right hand rule’. One feature can determine one or more of the coordinates of the origin of the PCS. E.g. in the developed software, one can use following command to construct a datum (labeled Datum1) from a measured plane, line and circle:

```
addDatum('Datum1', 'Plane1', 'ZDIR', 'ZPOS', 'Line1', 'XDIR',
        'Circle1', 'XPOS', 'YPOS')
```

The primary axis is the  $z$ -axis which is determined by the orientation of **Plane1**. The secondary axis is the  $x$ -axis which is determined by the orientation of **Line1**. The position of **Circle1** determines the  $x$ - and  $y$ -origin of the PCS, while the  $z$ -origin corresponds to the position of **Plane1**.

Once the datum matrix is built, this can be used to express positions ( ${}^0\mathbf{p}$ ) and orientations  ${}^0\mathbf{o}$ , that were measured in the MCS, with respect to this datum:

$${}^d\mathbf{p} = {}^0_d\mathbf{R} {}^0\mathbf{p} + {}^d\mathbf{P}^{d,0}$$

$${}_d\mathbf{o} = {}^0_d\mathbf{R}_0 \mathbf{o}$$

Feature parameters like size ( $s$ ) and form deviation ( $f$ ) are independent from the used coordinate system and do not need to undergo a transformation.

### 6.1.3 Determining uncertainty on part coordinate systems

Reporting the measured features with respect to a given (i.e. measured) PCS is relatively straightforward, but expressing the measurement uncertainties on the parameters of these features with respect to the measured PCS is more complicated. The uncertainty of the measured parameters expressed in a measured PCS will depend on the uncertainty of the PCS. Since the PCS is constructed from measured features that have a certain measurement uncertainty, the PCS itself will also have an uncertainty. If the same datum is measured twice, the datum matrix will not be the same due to the uncertainty. The measurement uncertainty of the datum matrix depends on the measurement uncertainty of the underlying features. The higher the measurement uncertainty of the datum features, the higher the uncertainty of the datum matrix. Figure 6.1 illustrates possible causes of this uncertainty.

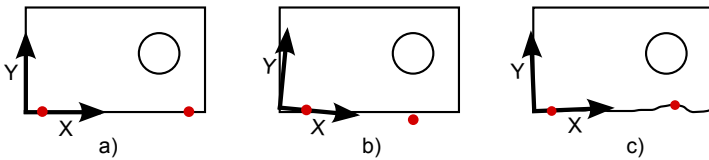


Figure 6.1: Orientation uncertainty of a line influencing datum uncertainty.

Figure 6.1a shows that an error free measurement of a line along the long edge will lead to an error free alignment of the part. The datum matrix will be error free. Figure 6.1b shows that a measurement error along the edge results in an error on the alignment. For the same absolute measurement error the resulting alignment error will be smaller if the distance between the measured points is larger. The resulting measurement uncertainty on the PCS will not only depend on the sampling strategy but also on the form deviation of the line, as illustrated in Figure 6.1c. Since sampling strategy and form deviations have an influence on the orientation uncertainty of the measured line, they will also influence the datum uncertainty. The higher the uncertainty on the PCS, the higher the uncertainty on the position of the circle expressed in the measured PCS.

How can we take into account the uncertainty on the PCS? To calculate the feature uncertainties,  $M$  (the number of Monte Carlo trials) simulated features are created, for every actual measured feature. These simulated features are sampled

according to the applied sampling strategy and this results  $M$  simulated measured features. The simulated errors are used to calculate the uncertainties of the feature parameters, as explained in the previous chapters.

If all these virtual features (true and measured) are stored, they can also be used to create simulated *true* datums and simulated *measured* datums. For every actually measured feature,  $M$  true features and  $M$  measured features are simulated. For every actually measured datum,  $M$  true datums and  $M$  measured datums are created based on, respectively, the simulated true features and simulated measured features.

### 6.1.4 Uncertainty of parameters expressed in part coordinate systems

Since the uncertainty on feature parameters depends on the PCS in which they are expressed, the error calculation can only be done after every simulated true feature and simulated measured feature parameter is expressed in the corresponding simulated true datum and simulated measured datum. The errors for position and orientation can be calculated as follows:

$$\begin{aligned} \text{err } {}_d\mathbf{p} &= \text{meas } [{}_d^0\mathbf{R}_0\mathbf{p} + {}_d\mathbf{p}^{d,0}] - \text{true } [{}_d^0\mathbf{R}_0\mathbf{p} + {}_d\mathbf{p}^{d,0}] \\ \text{err } {}_d\mathbf{o} &= \text{meas } [{}_d^0\mathbf{R}_0\mathbf{o}] - \text{true } [{}_d^0\mathbf{R}_0\mathbf{o}] \end{aligned}$$

Uncertainties for size and form deviations do not depend on the used datum.

This error calculation will be done  $M$  times, whereafter confidence limits for the errors can be determined, which can be used to determine the measurement uncertainties. This way of working allows that the position and orientation uncertainty for a given feature will be higher when it is expressed relative to a datum that is based on datum features with a higher measurement uncertainty.

## 6.2 Constructed feature uncertainty

When executing a measurement program, it regularly occurs that features need to be constructed from one or more measured features: e.g. the intersection point<sup>2</sup> of two measured lines, the intersection line of two measured planes, the connecting line of two measured circles, the symmetry line of two measured lines ... The position, orientation and size of the measured (constructing) features can be used to calculate the parameters of the constructed feature.

<sup>2</sup>A point is also considered as a feature, although it has only a position and no orientation, size or form deviation.

Due to the measurement uncertainties of the measured (constructing) features, the constructed feature will also have a measurement uncertainty. It is impossible to obtain the measurement uncertainty for the constructed feature based on the calculated values of the measurement uncertainties of the constructing features.

The measurement uncertainty on constructed features can be calculated similar to the datum matrix uncertainty. Based on the simulated true features, simulated constructed true features can be calculated. Based on the simulated measured features, simulated constructed measured features can be calculated. Thereafter, simulated errors can be calculated for every parameter of the constructed feature, these simulated errors can be used to calculate the measurement uncertainty.

### 6.3 Uncertainty on measurement of geometrical tolerances

Geometrical tolerances are often used on technical drawings. Table 6.1 shows the geometrical tolerances defined by ISO 1101. These geometrical tolerances are divided into 4 different categories: form, orientation, location and run-out. The last three categories need a datum and are therefore also called *related geometrical tolerances* while form tolerances are called *unrelated geometrical tolerances* [37].

#### 6.3.1 Unrelated geometrical tolerances

The form deviations used in the uncertainty calculation method, presented in the previous chapters, are calculated based on the least squares (LSQ) fitting criterion. According to ISO 1101 straightness, roundness, flatness and cylindricity values are defined by the minimum zone (MZ) criterion. If one wants to know the form tolerance value and the corresponding uncertainty according to the MZ criterion one can always recalculate form deviation values with the stored profile of the virtual features and with the stored sampled points (buffer points) of the virtual features, resulting in respectively  $^{true}f$  and  $^{meas}f$ :

$$^{err}f = ^{meas}f - ^{true}f$$

This means that for every processed measured feature not only all simulated true parameters and simulated measured parameters, but that also all  $M$  simulated true profiles and all  $M$  simulated sets of probing points need to be stored. This is a reason why the number of points representing the true profile should not be too large. Within this research, free form profile tolerances (that do not apply to circles, lines, planes or cylinders) are not considered.



Tolerances	Characteristics	Symbol	Datum needed
Form	Straightness	—	no
	Flatness	▭	no
	Roundness	○	no
	Cylindricity	⊘	no
	Profile any line	⤿	no
	Profile any surface	⤿	no
Orientation	Parallelism	//	yes
	Perpendicularity	⊥	yes
	Angularity	∠	yes
	Profile any line	⤿	yes
	Profile any surface	⤿	yes
Location	Position	⊕	yes or no
	Concentricity (for centre points)	◎	yes
	Coaxiality (for axes)	◎	yes
	Symmetry	≡	yes
	Profile any line	⤿	yes
	Profile any surface	⤿	yes
Run-out	Circular run-out	↗	yes
	Total run-out	↗	yes

Table 6.1: Geometrical tolerances defined by ISO 1101 [43].

### 6.3.2 Related geometrical tolerances

Related geometrical tolerances are tolerances that need a datum, as there are orientation, location and run-out tolerances. All of these tolerances are influenced by the form deviation of the toleranced feature. This means that just as for form tolerances, the buffer points of the simulated measurements will be needed. Buffer points are the separate feature points that are measured (sampled). The uncertainty for the related geometrical tolerances can, just as for unrelated geometrical tolerances, be obtained from the  $M$  simulated tolerance errors  $^{err}t$ . To calculate these  $^{err}t$ , the tolerance value is calculated  $M$  times based on the  $M$  stored sets of  $^{true}$  simulated data from toleranced feature and datum and  $M$  times the  $^{meas}$  simulated data:

$$^{err}t = ^{meas}t - ^{true}t$$

## 6.4 Software layout

The uncertainty calculation methods described in this thesis were implemented in object oriented Matlab®. Important advantages of object oriented programming (OOP) are understandability, maintainability and reusability:

- *Understandability*: Software objects often *model real life objects*, which makes the program structure very clear. Examples of classes in the developed software are `CMM`, `Circle`, `Line`, `Plane`, `Cylndr` that model the behaviour of their ‘real life’ counterparts.
- *Maintainability*: The *modular design* of OOP makes that the software can easily be maintained, extended and modified.
- *Re-usability*: Parts of the code can easily be reused because of the modular design and properties like *inheritance*.

Figure 6.2 shows a reduced class diagram of the developed software. Of every class one or more instances can be created. Of every class only the most important attributes and methods are shown. The different classes are shortly discussed in Appendix C.

## 6.5 Algorithm libraries

Some algorithms are not really suited to be integrated as methods in the different classes, therefore they are collected in algorithm libraries that can be called by the

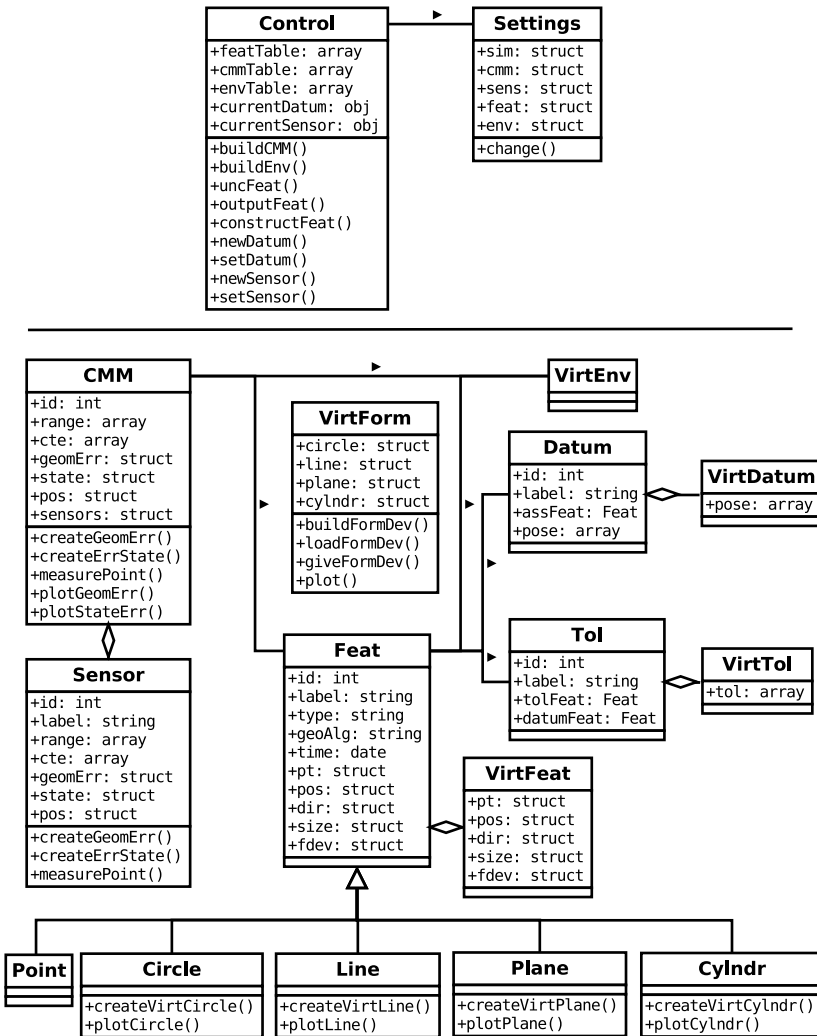


Figure 6.2: Reduced class diagram of the developed software.

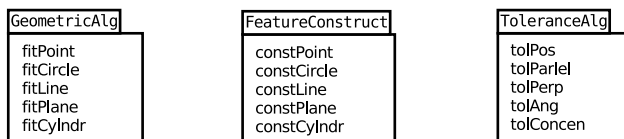


Figure 6.3: Algorithm libraries of the developed software.

different classes. The different algorithm libraries, illustrated in Figure 6.3, are the following:

- *Geometric algorithm library (GeometricAlg)*: This library contains functions to fit associated features through a set of points according to a given fitting criterion. Only the least squares fitting criterion has been implemented, using the algorithms from the Least Squares Geometric Elements (LSGE) library for Matlab. The LSGE library was developed by NPL Centre for Mathematics and Scientific Computing.
- *Feature construction algorithm library (FeatConstAlg)*: This library has been kept very limited. Only algorithms necessary to prove the validity of the developed software (Chapter 7) were implemented, like e.g. line-line intersection.
- *Tolerance algorithm library (ToleranceAlg)*: To calculate measured tolerance values, the tolerance algorithm database is used. Not all types of tolerances are implemented at this stage.

## 6.6 Interface to the CMM measurement software

In order to illustrate the practical applicability of the developed uncertainty calculation method, it is necessary to make a CMM measurement software communicate with the developed uncertainty calculation software (UES). Although the available CMM measurement software (Camio®, version 6.0) has possibilities to call external programs, these possibilities are not sufficiently extensive to realise a smooth integration between both applications.

An ad hoc solution is used to establish communication between Camio and the UES. Commands that need to be send to the UES are written to the file `iCMMinput.txt`. This file is read by the UES running in the background. The commands are executed and results are written in DMIS language to the file `iCMMoutput.dmi`, which is again read by Camio. Figure 6.4 illustrates this graphically.

If a feature needs to be added to the UES software, the buffer points of the measured feature also need to be transferred. This data will not be written to `iCMMinput.txt` but to a separate file: `camioBuffer.txt`. This latter file is deleted once the feature is added to the UES.

Within Camio, two developed subroutines are used to communicate with the UES:

- `iCMMaddFeat.dmi`: This subroutine, that accepts the label of a feature as its argument, can be called from any DMIS-program. It writes the buffer points of that feature to the file `camioBuffer.txt`, and adds the

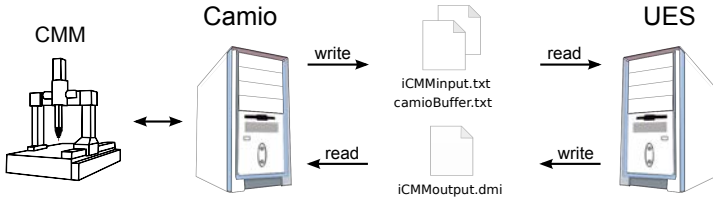


Figure 6.4: Communication between measurement software and UES by means of input and output files.

<code>iCMMaddFeat</code>	Add a measured feature to feature list of UES.
<code>iCMMaddDatum</code>	Construct a datum with given features from feature list.
<code>iCMMaddToI</code>	Define tolerance for a given feature.
<code>iCMMcalcUnc</code>	Calculate uncertainty of added feature, datum, tolerance.
<code>iCMMresults</code>	Give (uncertainty) of added feature, datum, tolerance.
<code>iCMMclear</code>	Clear all added features, datums, tolerances and the associated results. Allows to clean up without restarting.
<code>iCMMstart</code>	Start or restart UES. Creates all virtual CMMs and loads the form error databases. Feature list of UES will be empty.
<code>iCMMset</code>	Allows to change settings of the UES: e.g. Turn on/off inclusion of form deviation uncertainties / hardware uncertainties. Change confidence level from 95% to 99%.
<code>iCMMsetSensor</code>	Define sensor configuration to be used for uncertainty calculations.

Table 6.2: Overview of commands accepted by UES.

command `iCMMaddFeat` to the file `iCMMinput.txt`. When the UES receives this command it reads in the buffer points and feature information from `camioBuffer.txt`.

- `iCMMaddCommand.dmi`: Adds the command, that is passed as an argument to the file `iCMMinput.txt`. For an overview of the possible commands: see Table 6.2. Once the command is executed, the answer from the UES, stored in the file `iCMMoutput.dmi`, is imported into Camio.

## 6.7 Conclusions

Knowing the uncertainty of parameters expressed in the machine coordinate system (MCS) will usually not be sufficient to determine measurement uncertainties of actual CMM measurements. Measurement results will usually be reported relative to a given part coordinate system (PCS), also called datum. Since a PCS is

constructed based on measured features, there is also a measurement uncertainty associated with the PCS itself. This chapter explained how the uncertainty on the PCS can be calculated and taken into account when reporting feature uncertainties relative to a given datum.

Sometimes features need to be constructed based on one or more other features. Again there will also be an uncertainty associated to the constructed feature. The calculation of this uncertainty is similar to the calculation of datum uncertainty. Based on  $M$  simulated constructed true features and  $M$  simulated constructed measured features  $M$  simulated errors can be calculated for every parameter of the constructed feature. These errors can be used to calculate the measurement uncertainty.

In a similar way the uncertainty of geometrical tolerances can be calculated. Besides the parameters of the measured and true simulated feature, also the profile points and buffer points of every simulated feature will need to be stored for the calculation of uncertainties related to geometrical tolerances.

Further the object oriented software layout of the developed UES and the interfacing with the CMM measurement software are discussed.

# Chapter 7

## Verification of results

The goal of this chapter is to illustrate the validity of the developed uncertainty evaluation software (UES). A first test is worked out to see if the integrated hardware error model is valid. This is done by means of gauge blocks. Form deviations of calibrated reference artefacts like gauge blocks are sufficiently small, so that they will not influence the measurement uncertainty. In practice however, most features that need to be measured with a CMM, exhibit form deviations. Two additional tests show that calculated measurement uncertainties are only reliable when these form deviations are taken into account. For these tests own made artefacts with form deviations are used.

### 7.1 Test 1: Set of gauge blocks

An easy way to verify errors of a CMM is to measure a set of gauge blocks. A gauge block has a reference length with a very low calibration uncertainty<sup>1</sup>. The calculated errors, obtained by subtracting the reference value from the value measured with the CMM, can be compared with the calculated measurement uncertainties. The reference value should be situated within the calculated uncertainty interval for the measurement.

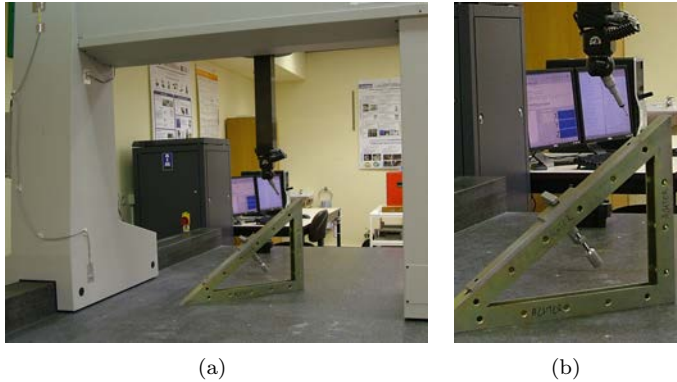


Figure 7.1: Gauge blocks measurement on the CMM.

### 7.1.1 Test set-up

One measurement is not sufficient to prove the validity of the integrated hardware error model. Multiple measurements of gauge blocks with different lengths are necessary. They also need to be measured under different orientations and on different locations in the CMM measurement volume. An adapted version of the procedure described in ISO 10360-2 is used [22]: two reference lengths, a short one (S: 100 mm) and a longer one (L: 500 mm), are measured under 7 different locations or orientations. For every measurement the error is compared with the calculated measurement uncertainty. Figure 7.2 illustrates the different measurement positions and orientations that are used:

- x1: measurement along the  $x$ -direction, very close to the  $x$ -scale.
- x2: measurement along the  $x$ -direction, with a large Abbe-offset in  $y$ -direction to the  $x$ -scale.
- y1: measurement along the  $y$ -direction, very close to the  $y$ -scale.
- y2: measurement along the  $y$ -direction, with a large Abbe-offset in  $z$ -direction to the  $y$ -scale.
- z1: measurement along the  $z$ -direction.
- d1: measurement along a diagonal parallel to the  $x$ - $y$ -plane.
- d2: measurement along a space diagonal.

<sup>1</sup>Calibration uncertainties lower than  $0.1 \mu\text{m}$  ( $k = 2$ ) can be obtained for lengths up to 300 mm (based on information from the federal public service economy, national metrology service).



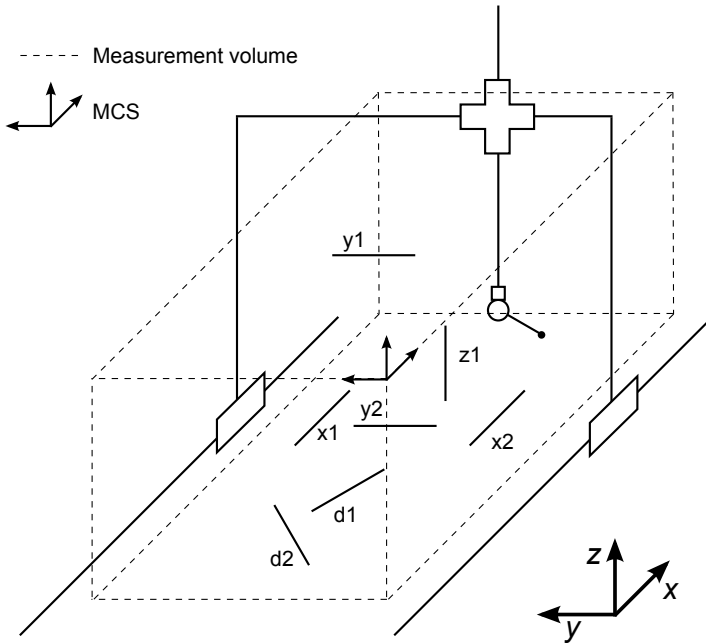


Figure 7.2: Measurement positions and orientations used for the test.

Every gauge block is aligned (i.e. a PCS is defined) before its length is measured. The  $x$ -axis is aligned with the calibrated direction of the gauge block. The length is defined as the  $x$ -distance between two points, one at each end of the gauge block. Since point features can not have a form deviation, the influence of form deviation on the measurement uncertainty will not be included in the results. Although a PCS is defined, the uncertainty of the PCS is not taken into account for the measurement uncertainty calculation. Because a gauge block has accurately finished faces, the uncertainty on the PCS will have little influence on the measurement results if the alignment is done carefully. This means that calculated measurement uncertainties will only be influenced by the simulated CMM hardware errors, which are described in Chapter 4. This test allows to check the validity of the CMM hardware error modelling (geometric errors and probe errors).

## 7.1.2 Test results

The results of the measurements and the calculated uncertainties are given in Table 7.1. The upper and lower confidence limits (UCL and LCL) are given relative to the measured values. It is clear from the results that all calculated uncertainties

		LCL	Meas.	UCL	Result
x1	S	-0.0017	100.0005	0.0017	✓
	L	-0.0040	499.9988	0.0042	✓
x2	S	-0.0028	99.9976	0.0026	✓
	L	-0.0049	499.9958	0.0051	✓
y1	S	-0.0018	99.9998	0.0019	✓
	L	-0.0044	499.9998	0.0045	✓
y2	S	-0.0027	99.9986	0.0033	✓
	L	-0.0073	500.0022	0.0081	✓
z1	S	-0.0016	99.9986	0.0017	✓
	L	-0.0034	500.0019	0.0035	✓
d1	S	-0.0023	100.0013	0.0025	✓
	L	-0.0058	500.0039	0.0059	✓
d2	S	-0.0025	99.9981	0.0024	✓
	L	-0.0063	499.9974	0.0064	✓

Table 7.1: Measurement results and calculated uncertainties (95% confidence level) for gauge block measurements.

cover the true value<sup>2</sup>. It can also be seen that the calculated uncertainties take into account the effect of size (the uncertainties for the longer gauge block are systematically higher) and the effect of Abbe-errors (the measurements with larger Abbe-offsets result in higher uncertainties). These results confirm that the methods to model hardware uncertainties, that are described in this thesis, result in reliable uncertainty statements. The settings used to model the geometric errors of the virtual CMMs are taken from Table 4.1 on page 92. A normally distributed random error was used for the probing error (with  $\sigma = 0.5 \mu\text{m}$ ). 1000 virtual CMMs were used and 1000 Monte Carlo runs were executed before calculating the 95% confidence limits.

## 7.2 Test 2: Circle with form deviation

Form deviations of a gauge block do not influence the measurement uncertainties because the magnitude of the form deviations is negligible. However, in practice form deviations will have an important influence on the measurement uncertainty.

<sup>2</sup>If the measured value and calculated uncertainty are compared to the nominal value of the gauge block, also the calibrated deviation from the nominal value and the calibration uncertainty of the gauge block should be taken into account when deciding whether or not the calculated uncertainty covers the true value. The calibrated deviation for the 100 mm gauge block equals  $-0.22 \mu\text{m}$ ,  $U = 0.12 \mu\text{m}$  ( $k = 2$ ). The calibrated deviation for the 500 mm gauge block equals  $-1.10 \mu\text{m}$ ,  $U = 1.2 \mu\text{m}$  ( $k = 2$ ). These deviations and calibration uncertainties were taken into account when evaluating the calculated uncertainties.

This test shows whether or not the developed UES reflects the influence of form deviation correctly for the measurement of a circle with a 3-lobed form deviation.

### 7.2.1 Test set-up

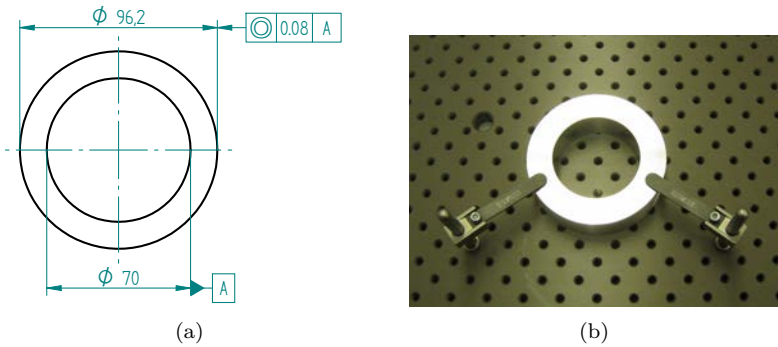


Figure 7.3: Drawing and picture of the part used in the test.

In this test the dimensions and the concentricity tolerance of the part represented in Figure 7.3 are measured. Only one measurement location is used; the part is placed in the middle of the CMM-volume with its face pointing in  $z$ -direction. The inner (C1) and outer (C2) circle of the part are measured twice: once with only four equidistant sampling points for each circle ( $N = 4$ ) and once with 10 equidistant sampling points for each circle ( $N = 10$ ). For each measurement the uncertainties are calculated twice: once taking into account only the influence of CMM hardware errors (HW) and once when taking into account also the influence of feature form deviations (HW+FD). The form deviation database used during uncertainty calculation contains simulated 3-lobed form deviations ( $a_2 = 0.2, a_3 = 0.7$ ). The part was also measured at several places on the CMM, with 50 points for each circle. The average of these measurement values is considered as an approximation of the true value.

### 7.2.2 Test results

#### Measurements with four equidistant points ( $N = 4$ )

The results of the measurements and the calculated uncertainties are given in Table 7.2. For  $N = 4$  the calculated uncertainties are much higher when besides CMM hardware errors also feature form deviations are taken into account. It can be seen that the error of  $32 \mu\text{m}$  ( $0.101 - 0.069 = 0.032$ ) on the concentricity value

				LCL	Meas.	UCL	True	Result
$N = 4$	C1	dia	HW	-0.0020	69.969	0.0022	69.969	✓
			HW+FD	-0.0122	69.969	0.0102	69.969	✓
		form	HW	-0.0022	0.009	-0.0000	0.070	✗
			HW+FD	0.0304	0.009	0.4276	0.070	✓
	C2	dia	HW	-0.0027	96.176	0.0023	96.175	✓
			HW+FD	-0.0109	96.176	0.0094	96.175	✓
		form	HW	-0.0029	0.005	-0.0000	0.017	✗
			HW+FD	0.0173	0.005	0.4264	0.017	✗
	conc	HW	-0.0022	0.101	0.0021	0.069	✗	
		HW+FD	-0.1010	0.101	0.0236	0.069	✓	
$N = 10$	C1	dia	HW	-0.0015	69.968	0.0015	69.969	✓
			HW+FD	-0.0020	69.968	0.0022	69.969	✓
		form	HW	-0.0046	0.064	-0.0013	0.070	✗
			HW+FD	0.0001	0.064	0.0160	0.070	✓
	C2	dia	HW	-0.0015	96.174	0.0018	96.175	✓
			HW+FD	-0.0017	96.174	0.0016	96.175	✓
		form	HW	-0.0049	0.014	-0.0015	0.017	✗
			HW+FD	-0.0022	0.014	0.0038	0.017	✓
	conc	HW	-0.0011	0.070	0.0012	0.069	✓	
		HW+FD	-0.0017	0.070	0.0016	0.069	✓	

Table 7.2: Measurement results and calculated uncertainties (95% confidence level) for the measurements of the circular test part (dia = LSQ diameter, form = roundness, conc = concentricity).

is not at all covered by the calculated coverage interval  $([-0.0022, 0.0021])$ , when only hardware errors are taken into account during uncertainty calculation. Based on the measurement result and the concentricity tolerance on the drawing, this part will be wrongly rejected. However, if also uncertainties due to form deviations are included, the calculated uncertainty does cover the true value. The part will also not be rejected based on this result; the result is uncertain (i.e. no accept or reject decision can be taken) and a more accurate measurement will be necessary to prove conformance or non-conformance. It might look strange that the calculated coverage interval for the concentricity value also includes zero  $(0.101 - 0.101 = 0)$ . This can be explained as follows: it is possible that the measured circles do have a significant form deviation that is not revealed by the four-points measurement (this is also reflected in the form deviation uncertainty). For a circle with a high form deviation (this can be the toleranced circle or datum circle) it is possible that perfectly concentric circles result in a measured concentricity value of 0.101. This is the reason why zero is included in the coverage interval.

The true concentricity value equals  $69 \mu\text{m}$ . Not many people, including dimensional metrology specialists, would expect a  $32 \mu\text{m}$  large error for a concentricity

measurement on such a part. This error is mainly caused by the 3-lobed form deviation of the datum circle (C1) which is represented in Figure 7.4(a). Four-points measurements of 3-lobed form deviations will always result in large position errors of the associated circle (see also Figure 1.9 on page 17). This uncertainty, related to the datum feature, is correctly taken into account by the UES. This example illustrates that form deviations need to be taken into account to obtain reliable uncertainty statements.

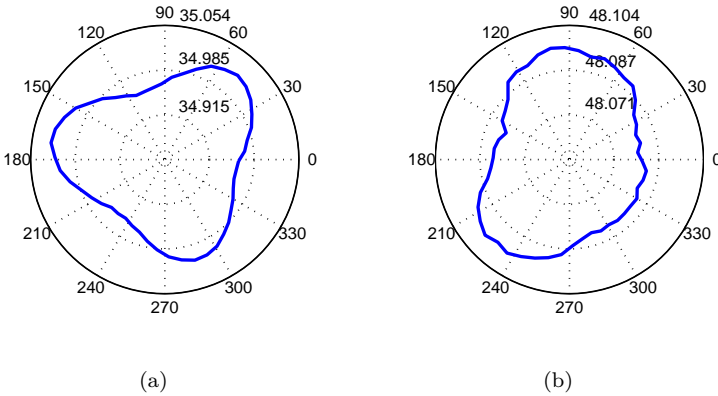


Figure 7.4: Roundness plots of the inner (C1) and outer (C2) circle.

In case of  $N = 4$ , calculated uncertainties are very high if form deviation uncertainty is taken into account. This is because the form deviation value can not be reliably assessed with four points, resulting in high form deviation uncertainties. High form deviation uncertainties will result in high uncertainties on other feature parameters. The LCL of the calculated uncertainty (HW+FD) for C2 is too high; the UES predicted an underestimation of the form deviation of at least 0.017 mm while the true underestimation was only 0.012 mm. This underestimation is related to the fact that the 3-lobed form deviation of C2 is very asymmetric (see Figure 7.4(b)) while the used form deviation database contains more ‘regular’ shaped 3-lobed form deviations.

**Measurements with ten equidistant points ( $N = 10$ )**

When more measurement points are taken it can be seen that the calculated uncertainties become much lower (for HW+FD) while still covering the true values for all feature parameters. In this case the calculated uncertainties that take only hardware errors into account (HW) also cover most of the true values, except for the form deviation value. Some readers might conclude from these results that it

is unnecessary to take into account form deviation influences as long as enough (e.g. more than 10) points are measured and form deviations are measured with dedicated equipment like roundness measuring devices since differences between the two calculated coverage intervals are not that large. However, the next section will illustrate that in case of partial circle measurements, the influence of feature form deviations will be very important for the measurement uncertainty, independent of the number of measurement points.

### Partial circle measurements

The same test part can also be used to illustrate the influence of partial circle measurements on the measurement uncertainty. In Appendix A it was already shown that partial circle measurements in combination with feature form deviations results in high measurement uncertainties.

				LCL	Meas.	UCL	True	Result
$N = 25$	C1	dia	HW	-0.0020	69.974	0.0021	69.969	✗
			HW+FD	-0.0697	69.974	0.0740	69.969	✓
		form	HW	-0.0056	0.060	-0.0027	0.070	✗
			HW+FD	-0.0051	0.060	0.0277	0.070	✓
	C2	dia	HW	-0.0023	96.165	0.0024	96.175	✗
			HW+FD	-0.0144	96.165	0.0146	96.175	✓
		form	HW	-0.0054	0.010	-0.0026	0.017	✗
			HW+FD	-0.0031	0.010	0.0040	0.017	✗
		conc	HW	-0.0017	0.091	0.0015	0.069	✗
			HW+FD	-0.0420	0.091	0.0209	0.069	✓

Table 7.3: Measurement results and calculated uncertainties (95% confidence level) for the partial measurements of the circular test part.

Table 7.3 gives the measurement results for the inner circle (C1), the outer circle (C2) and the concentricity value if this circle is measured with 25 points ( $N = 25$ ) over 180 degrees. It is clear from the results that measurement errors are significantly larger, although 25 measurement points were used. It is also clear that the calculated uncertainties do not cover the true values if only HW errors are taken into account. Based on this measurement result and the concentricity tolerance on the drawing the part will be wrongly rejected, although 25 measurement points were used. However, when also form deviation influence is taken into account, it is clear that the value of the concentricity tolerance is included in the uncertainty interval and that no accept or reject decision can be taken based on this measurement result. The true values are always covered by the calculated uncertainty except for the form deviation of C2, which is slightly underestimated. The large errors and uncertainties originate from the fact that the associated circle of half the circular

profile will be different from the associated circle of the complete profile with form deviation, even if an infinite number of probing points is used.

In practice this circle would never be measured over 180 degrees if the complete circle is accessible over 360 degrees. In case of diameter measurements of larger cylindrical parts, it often occurs that only half the circle is measured. This example is used to illustrate the influence of partial feature measurements on the measurement uncertainty.

## 7.3 Test 3: Plate with holes

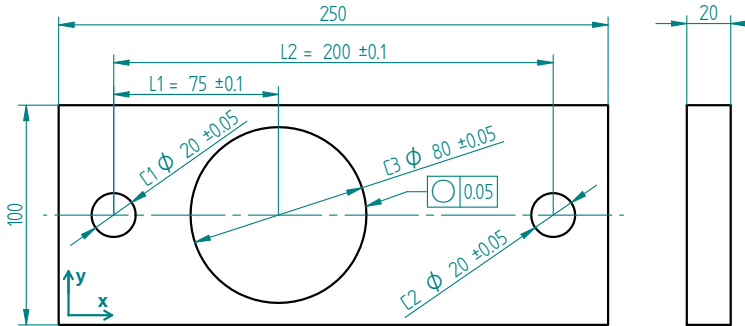
The next test part is again an actual workpiece. It is the same part as the one used in 3.1 to illustrate that form deviations can be the most important uncertainty contributor. The drawing of the part and a picture of the actual part are given in Figure 7.5.

### 7.3.1 Test set-up

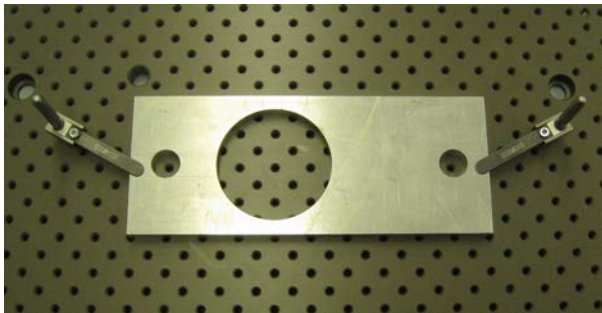
For this test the diameter of the central circle (C3) and the distances L1 (distance from left circle to central circle) and L2 (distance between left and right circle) are measured. Again the circles are measured with two different numbers of sampling points,  $N = 4$  and  $N = 10$ . Uncertainties are also reported twice: once when taking into account only the influence of CMM hardware errors (HW) and once when taking into account the influence of CMM hardware errors and feature form deviation (HW+FD). The form deviation database used during uncertainty calculation contains simulated 2-lobed, 3-lobed and 4-lobed form deviations. Again, the part was also measured at several places on the CMM, with 360 points for each circle. The average of these measurement values is considered an approximation of the true value.

### 7.3.2 Test results

The results of the measurements and the calculated uncertainties are given in Table 7.4. It is clear from the results that the true values are not always covered by the calculated coverage intervals if the influence of form deviation is not taken into account. Calculated coverage intervals that also take into account the influence of feature form deviations (HW+FD) do always cover the true value. It is interesting to have a closer look at the uncertainties for L1 and L2 (for  $N = 10$ ). Because L2 is larger than L1, a higher uncertainty for L2 is expected. The calculated uncertainty for L2 is indeed higher when only hardware influence is taken into account (HW).



(a) drawing



(b) picture

Figure 7.5: Drawing and picture of the used test part.

				LCL	Meas.	UCL	True	Result
$N = 4$	C3	dia	HW	-0.0023	79.900	0.0022	79.874	✗
			HW+FD	-0.3084	79.900	0.3383	79.874	✓
	L1		HW	-0.0025	75.032	0.0020	75.018	✗
			HW+FD	-0.1581	75.032	0.1454	75.018	✓
	L2		HW	-0.0029	199.989	0.0029	200.001	✗
			HW+FD	-0.1618	199.989	0.1782	200.001	✓
$N = 10$	C3	dia	HW	-0.0018	79.880	0.0016	79.874	✗
			HW+FD	-0.0076	79.880	0.0065	79.874	✓
	L1		HW	-0.0017	75.014	0.0015	75.018	✗
			HW+FD	-0.0044	75.014	0.0046	75.018	✓
	L2		HW	-0.0024	200.001	0.0023	200.001	✓
			HW+FD	-0.0024	200.001	0.0028	200.001	✓

Table 7.4: Measurement results and calculated uncertainties (95% confidence level) for the measurements of the test part.



However if form deviation influence is taken into account as well, the uncertainty for L1 is significantly higher, because of the large true form deviation of C3 (true value: 0.112 mm). A large form deviation results in a higher position uncertainty which results in a higher distance uncertainty. The form deviations of C1 and C2 are much smaller (true values: 0.006 mm and 0.009 mm), which results in a lower uncertainty on L2.

### Part coordinate system uncertainty

This test part can also be used to illustrate the influence of part coordinate system (PCS) uncertainty. The uncertainties on distances L1 and L2, on diameters and on form deviations are independent of the PCS. For the position of a circle in the PCS, the uncertainty of the PCS itself should be taken into account. To illustrate this, the position of circle C2 is measured in the PCS.

The PCS is defined as follows: the  $z$ -axis is defined by the orientation of the top plane. The  $x$ -axis is defined by the bottom edge, the origin is defined by the intersection of the bottom edge and the left edge. The uncertainty of the PCS will be determined by the uncertainties of the measured and constructed features (plane, line and point) that are used to construct the PCS. The PCS is defined twice: once when the complete bottom edge is measured with three points (PCS1) and once when the bottom edge is only measured over half its length with three points (PCS2). The difference between PCS1 and PCS2 is illustrated in Figure 7.6. The top plane was measured with seven points for PCS1 and PCS2.

Table 7.5 gives the position of C2, measured with 10 equidistant points, expressed in the PCS, together with the calculated uncertainties (HW+FD). It can be seen that the  $y$ -position uncertainty for C2, expressed in PCS1 is much lower than in PCS2, because the alignment strategy for PCS1 is more robust. It is also clear that  $y$ -position uncertainty deteriorates significantly for PCS2 while it has much less influence on the  $x$ -position. This is what is expected for this kind of alignment. It shows that the task-specificness of the measurement uncertainty is taken into account. It should also be noticed that  $x$ -position uncertainty for PCS1 is more than twice as high as the  $y$ -position uncertainty. This is because of the larger form deviation of the left edge which results in an orientation uncertainty that leads to a higher  $x$ -position uncertainty of the origin (defined as intersection of left and bottom edge). Since positions measured in a PCS are often used to evaluate tolerances, PCS uncertainty should definitely be taken into account.

The PCS uncertainty will also depend on the number of points that is used to measure the features that compose the PCS. The more measurement points that are used, the lower the PCS uncertainty will be. Therefore it is advisable to take enough measurement points, certainly for features that are used to construct the PCS. A good rule of thumb is to take at least five times the minimum number of

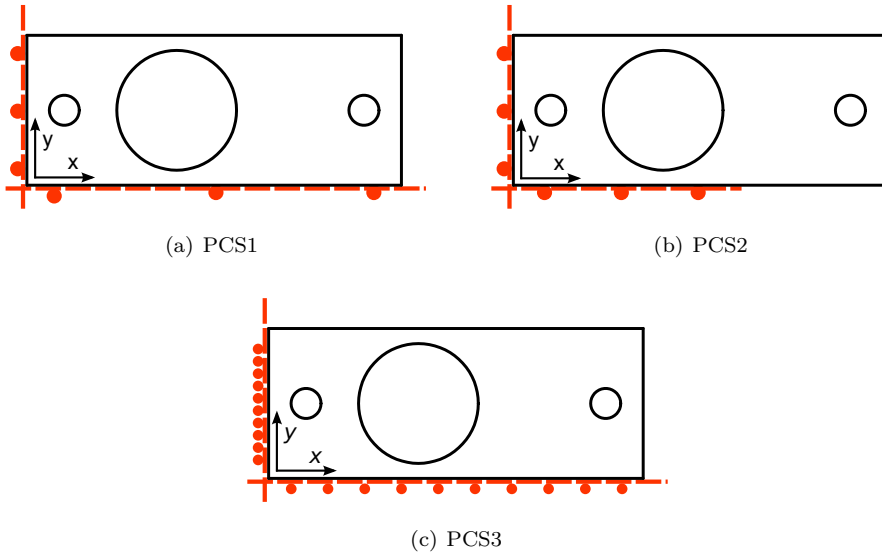


Figure 7.6: Difference in measurement strategy between PCS1, PCS2 and PCS3.

				LCL	Meas.	UCL
$N = 10$	C2	x	PCS1	-0.0115	228.864	0.0109
			PCS2	-0.0270	228.867	0.0248
			PCS3	-0.0058	228.866	0.0056
		y	PCS1	-0.0054	53.990	0.0053
			PCS2	-0.0509	53.982	0.0555
			PCS3	-0.0018	53.989	0.0022
		z	PCS1	-0.0297	-5.000	0.0300
			PCS2	-0.0297	-5.000	0.0300
			PCS3	-0.0247	-5.000	0.0252
	dia	PCS1	-0.0014	20.026	0.0013	
		PCS2	-0.0014	20.026	0.0013	
		PCS3	-0.0014	20.026	0.0013	
	form	PCS1	-0.0021	0.007	0.0026	
		PCS2	-0.0021	0.007	0.0026	
		PCS3	-0.0021	0.007	0.0026	

Table 7.5: Measurement results and calculated uncertainties (95% confidence level) for the position, diameter and form deviation of circle C2 expressed in PCS1, PCS2 and PCS3.

points needed to construct the feature (for lines  $5 \times 2 = 10$ , for planes  $5 \times 3 = 15$ )<sup>3</sup>. To illustrate the influence of the number of points on the PCS uncertainty, a third PCS (PCS3) was constructed, taking into account this rule of thumb; i.e. the plane was measured with 15 points and both lines were measured with 10 points (see Figure 7.6(c)). The results in Table 7.5 illustrate that the PCS uncertainty is reduced significantly compared to PCS1; the uncertainties on  $x$ - and  $y$ -position of circle C2 are much lower. The uncertainty on  $x$ -position is still higher than the uncertainty on  $y$ -position because of the larger form deviation of the left edge. The difference in  $z$ -position uncertainty is less significant. This is mainly because the software can not yet handle incomplete features. The software assumes that a complete plane needs to be measured, while the user can only measure points outside the holes. This can result in overestimated measurement uncertainties.

## 7.4 Conclusions

In this chapter three tests that illustrate the validity of the developed UES are described. The first test used gauge blocks to check the validity of the hardware error modelling of the UES and illustrated that different measurement positions and orientations of the part on the machine will result in different coverage intervals for the measurement uncertainty. Measurements along the diagonal of the machine and measurements far from the scales (large Abbe-distances) have the highest measurement uncertainty. All the calculated uncertainty intervals during this test covered the calibrated length of the gauge blocks.

The second test described the measurement of two concentric circles with 3-lobed form deviations and the influence of this form deviation on the uncertainty of the measured concentricity value. The results of the test showed that the measurement uncertainties are underestimated if the influence of feature form deviation is not taken into account. If the influence of feature form deviation is taken into account the calculated coverage intervals cover the true value. Additional tests also illustrated that measurement errors for partial circle measurements can be very high, also due to the form deviation of the feature. Uncertainties for these kinds of measurements were also calculated correctly by the UES.

The third test described diameter, distance and position measurements of a workpiece with circular features. One of the circles has an important form deviation. The UES showed that the uncertainty for a distance that involves the position of the circle with the large form deviation is significantly higher than the uncertainty for another distance not including this particular circle. The calculated uncertainties (that take into account the influence of form deviation) cover the true value.

---

<sup>3</sup>Thanks to W. Knapp for mentioning this rule of thumb and for the suggestion to include it in the test.

This test part was also used to illustrate the influence of PCS uncertainty on measurement results expressed in a PCS. This influence can be significant and should definitely be taken into account.

# Chapter 8

## General conclusions

This thesis describes a small part of the wonderful world of dimensional metrology. This chapter presents the conclusions on the main contributions of the conducted research. It also gives some suggestions for future research.

### 8.1 Context of the research

Dimensional quality control is an important part of the production process in the manufacturing industry. Parts are designed and produced to fulfil a certain function. To be sure that the part will eventually be able to fulfil this function, the designer assigns tolerances to the part. Particularly tolerances on the dimensions of a part are often of major importance. Dimensional quality control ensures that the dimensional properties of the product comply with the tolerances. Nowadays very accurate coordinate measuring systems are available to perform dimensional quality control. Among the broad range of coordinate measuring systems that exists today, conventional cartesian coordinate measuring machines (CMMs) with tactile probes are still the most used for accurate series measurements.

For unambiguous evaluation of conformance to tolerances, measurement results should always be provided together with an uncertainty value. The conventional GUM ‘recipe’ of analytical uncertainty propagation is the best known method for uncertainty evaluations. However, because of some drawbacks of the conventional GUM method and the complexity of CMM measurements, this conventional GUM method is not really suited for uncertainty evaluations of CMM measurements.

Uncertainty calculations for CMM measurements are extremely difficult because they do not only depend on the accuracy of the CMM, but also on many other

error sources like measurement strategy, environment, workpiece, etc. The large number of uncertainty contributors for CMM measurements implies that uncertainty statements for CMMs will be very task-specific. Almost every CMM measurement will have another measurement uncertainty. In order to obtain reliable measurement uncertainties, every important uncertainty contributor should be taken into account. The influence of feature form deviations is often neglected while it has an important influence on the measurement uncertainty. In many situations it is even the most important uncertainty contributor.

As uncertainty statement to be provided with the measurement result people often use the performance specification of the CMM. It should be emphasised that results of CMM performance specification tests can be used for benchmarking of coordinate measuring systems but not for uncertainty evaluations. Performance specifications are an indication for the instrument uncertainty (of the CMM) and not a measure for the measurement uncertainty of a specific CMM measurement. Valid methods for uncertainty evaluations of CMM measurements include *multiple measurement strategies*, the use of *calibrated workpieces*, *expert judgement* and *computer simulation*. The use of computer simulation has much potential and is already investigated by several authors. There even exists commercially available uncertainty evaluation software, but this software is not yet adopted by industry. Current software neglects some important uncertainty contributors, like the influence of feature form deviations, and can not be used online.

The goal of this research was formulated as follows:

*Determine for each CMM measurement result a measurement uncertainty in order to make unambiguous evaluation of tolerances possible and dimensional quality control more reliable.*

## 8.2 Main contributions

This section summarises the four most important contributions of the research.

### 8.2.1 Integrating feature form deviations in uncertainty determination

The influence of feature form deviations in combination with limited point sampling in coordinate measurement is often overlooked when considering uncertainties for feature measurements. However the influence of feature form deviations can be very important, in several situations even more important than all other influences. This was illustrated in the introductory section of Chapter 3. Among the few uncertainty

evaluation software (UES) that exist, there is no software that really integrates the influence of feature form deviations, although integration of feature form deviations is necessary to obtain reliable uncertainty statements.

**This thesis proposes a methodology to integrate the influence of feature form deviations in uncertainty calculations by Monte Carlo simulations.**

The developed Monte Carlo method relies on an error simulation module that simulates errors due to limited sampling of profiles with a form deviation. An important part of the error simulation method is the profile simulator which allows to generate profiles based on measured form deviations or based on simulated form deviations. This thesis demonstrates that form deviations for circles, lines, planes as well as cylinders can all be simulated based on the method to simulate linear form deviations.

The generated feature profiles are sampled according to a given sampling strategy and the sampled points are used to create a *measured associated feature*. Through comparison with the *true associated feature* of the (unsampled) profile, errors on position, orientation, size and form deviation are calculated. The process is repeated multiple times in order to obtain error distributions. Examples developed in this thesis illustrate the importance of form deviations on the measurement uncertainty in case of limited sampling and also show the usefulness of Monte Carlo simulations.

### **8.2.2 Simplified method to simulate realistic CMM hardware errors**

The measurement accuracy of the CMM does vary over the measurement volume. This is mainly due to the geometric errors of the individual axes of the CMM in combination with Abbe-offsets to the scales. In order to model this behaviour accurately, the position of the scales needs to be incorporated in the kinematic model of the CMM.

Most methods that are used in current uncertainty evaluation software try to determine the true error state of the CMM and use this information for the uncertainty calculation. However including known CMM hardware errors in the uncertainty calculation method does not make much sense because of two reasons. Firstly, if the true errors are known, the measurement results should be compensated for these errors instead of including the errors in the measurement uncertainty. Secondly, the measured errors are the errors at that specific moment. After a few days, hours or even minutes, the errors can be different due to thermal influences on the CMM. Measuring the true error state of a CMM is also very time consuming. It is impossible and unnecessary to know the true non-compensated geometric error components, but one should be able to model realistic geometric error components.

**This thesis presents a method to model geometric errors of a CMM**

**which takes into account the Abbe-offsets to the scales.** The method is based on the kinematic model of the CMM and 21 simulated geometric error components. The kinematic model and the simulated geometric error components can be used to build so-called virtual CMMs. In order to check whether a virtual CMM exhibits errors that are representative for the actual CMM, a virtual ISO 10360-2 test is performed. The only input that is needed for the developed method are the scale positions of the actual CMM and its (valid) ISO 10360-2 specification.

A test that described the measurement of two gauge blocks of different lengths at several locations and orientations on the CMM showed that uncertainties calculated based on error simulations by the developed method are very reliable.

### **8.2.3 Uncertainty determination of feature measurements based on measured form deviation and CMM hardware errors**

Based on the previous two contributions, an error simulation method has been worked out that integrates the influence of feature form deviations and CMM hardware errors. Simulated hardware errors of a virtual CMM will be added to the sampled points from simulated profiles. This allows to simulate measurement errors on feature parameters. It takes into account points sampling strategy, CMM hardware errors and the influence of feature form deviations. To determine the errors, the true parameters of the feature need to be known, but in practice only the measured parameters are known. Particularly, the true form deviation influences the measurement errors but is not known in advance.

**This thesis shows how the influence of feature form deviations and CMM hardware errors can be combined in an uncertainty determination method for feature measurements.** This method relies on a new two-step Monte Carlo approach: a first step to determine the form deviation uncertainty, a second step to determine the uncertainties of the other feature parameters. The form deviation uncertainty can be obtained by simulating errors for different possible magnitudes of form deviation. Based on these results, the likelihood of the true form deviation is determined, which provides the form deviation uncertainty (step 1). The range of possible form deviations (defined by the form deviation uncertainty) is used to determine the uncertainties on the other feature parameters (step 2).

From two case studies describing measurements of parts with significant form deviations, it became clear that calculated uncertainties are only reliable if the influence of form deviation is taken into account. For a limited set of probing points the true errors were often highly underestimated by the calculated uncertainties if only CMM hardware uncertainties were taken into account (i.e. if influence of feature form deviation was neglected). Influence of form deviation becomes even more important for partial feature measurements, as also illustrated in this thesis.



### 8.2.4 Development of an uncertainty evaluation software that integrates the influence of form deviations and CMM hardware errors

The standard input and output of the method (i.e. coordinates and uncertainties on coordinates) derived from the previous contribution is given in machine coordinates. This is necessary to correctly implement the influence of CMM hardware uncertainty. However, knowing the uncertainty of parameters expressed in the machine coordinate system (MCS) will usually not be sufficient to determine measurement uncertainties of actual CMM measurements. Measurement results will usually be reported relative to a given part coordinate system (PCS). Since a PCS is constructed based on measured features, there is also a measurement uncertainty associated with the PCS itself. Chapter 6 of this thesis explains how the uncertainty on the PCS can be calculated and taken into account when reporting feature uncertainties relative to a given datum. Sometimes features need to be constructed based on one or more other (measured) features. Again there will also be an uncertainty associated to the constructed feature. The calculation of this uncertainty is similar to the calculation of PCS uncertainty. Also the uncertainty of measured geometrical tolerances, based on multiple features (perpendicularity, parallelism, coaxiality, . . . ) can be calculated similarly.

**This research resulted in an uncertainty evaluation software that is able to perform online uncertainty calculations and that takes into account the influence of feature form deviations as well as CMM hardware errors.** Also derived uncertainties, like part coordinate system uncertainty and uncertainties on measured geometrical tolerances based on multiple features are integrated in the calculated uncertainties. The software was implemented in object oriented Matlab® code and was integrated with Camio® measurement software running on a retrofitted Coord3® CMM.

## 8.3 Suggestions for future research

The developed uncertainty evaluation software (UES) is able to calculate reliable uncertainty statements under most circumstances, as shown by the tests in Chapter 7. Nevertheless, certain uncertainty contributors are not yet modelled or can be modelled more accurately:

- *Thermal influences*

Systematic (uncompensated) temperature deviations (from 20°C) of the CMM are taken into account by the modelled positional deviations of the axis as long as the CMM still complies with its specification. However, thermal fluctuations in time are not taken into account. The UES assumes that

hardware errors are static, that they do not change in time. In practice, errors due to thermal influences on the CMM can be significant. Temperature deviations of the CMM can be due to environmental temperature deviations or to heat dissipation of the CMM components. The influence of thermal effects can be minimized by minimizing measurement time, e.g. using automated measurements. For measurements that require more time, influence of thermal effects should be integrated in the uncertainty calculations. This could be implemented by making use of ‘virtual environments’, that simulate possible temperature variations.

- *Probing errors*

Probing errors are modelled as purely random deviations. This is a simplification of reality. Actual probe errors will also have important systematic components. Better probe error modelling would be advantageous for the reliability of the calculated uncertainties.

- *Random CMM errors*

Geometric errors of the CMM are considered to be purely systematic. In reality each of the 18 geometric errors will also have a more or less random component. These random errors could be modelled relatively easily in a way analogue to the one used for the systematic errors. This approach will take into account the fact that a random geometric error (e.g. a random yaw error) will have more influence for larger Abbe-distances. Modelling reversal errors of the CMM, that can also be important, will be more difficult because the direction of motion of the axes needs to be taken into account.

- *Improvement of form deviation modelling*

The way simulated form deviations are taken from the database could be improved. Now the form deviations are taken randomly from a large set of standardised form deviations defined by the user. This can be e.g. a set of only 3-lobed deviations or a set that contains 2-lobed, 3-lobed and 4-lobed form deviations. The method could be improved further by selecting form deviations based on information from the actual measurement; if a significant amount of points (e.g. 15) is measured it could be detected whether the shape is rather 2-lobed, 3-lobed, 4-lobed or a combination of those [73]. Based on this information, the method could automatically select the form deviations from a specific database.

- *Extension to incomplete features*

Currently the UES implicitly assumes that the user always wants to measure complete features, i.e. if the user measured a circle segment over  $90^\circ$ , the software assumes that the user is interested in the parameters of the complete circle, and that he was only able to measure over  $90^\circ$ . If form deviation uncertainty is included, this will result in very high uncertainties. However,

it could be that the user measured the radius of a  $90^\circ$  rounding. In that case there is no complete circle available, and only the radius of that circle segment needs to be known. The same problem holds for plane measurements. If a plane with an opening (due to e.g. a hole or a pocket) is measured, no measurement points can be taken in the region of the opening, although the software assumes that a complete plane (without opening) was measured. This can result in overestimated uncertainty values.

This research focusses on conventional CMMs, but many methods could also be transferred to *other coordinate measurement systems*. E.g. the way to model hardware errors of the CMM could, mutatis mutandis, also be applied to articulating arms and other non-conventional coordinate measuring systems [74]. Detailed uncertainty modelling for optical coordinate measuring systems (such as fringe projection systems or laser line scanners [75]) will be more difficult.

The uncertainty evaluation software developed during this research is implemented as a stand-alone software package. It is recommendable that the error simulation and uncertainty calculation algorithms of the developed UES are *integrated in currently available CMM software*. These software have all algorithms for feature fitting, feature construction and geometrical tolerance evaluation available. In this way exactly the same algorithms can be used to calculate the measurement results and measurement uncertainties.

Most facilitators are available for an adoption of developed uncertainty evaluation software by the CMM industry. The methods have been worked out and tested and computing power (for Monte Carlo simulations) is no longer a constraint. The usage of uncertainty evaluation software could prevent many false acceptances and rejections of parts and could save a significant amount of money. To encourage industry to adopt uncertainty evaluation methods, well defined *standards and regulations* about this topic are still necessary.



## Appendix A

# Measurement errors expressed relatively to the measured form deviation

Section 3.10 showed that the developed error simulation method allows to calculate the confidence limits of the measurement errors for a given (assumed) value of true roundness and a given measurement strategy (number of equidistant sampling points). Such simulations can then be used to define the confidence limits for other values of true roundness, because the errors are directly proportional to the true roundness value. For a true roundness value of 0.2 mm, all errors (and as a consequence also the confidence limits) of Figure 3.17(a) and Figure 3.17(b) will be two times larger, as the latter are based on a roundness value 0.1 mm. For a true roundness value of 0.01 mm, they will be ten times smaller. As long as CMM hardware and environmental uncertainty contributors are neglected, the diameter and the position of the circle will not influence the errors. This means that one can also express all uncertainties relative to the true roundness [45, 76].

Even if results are expressed relative to the true roundness, their practical use is limited. When measuring a circle with a limited set of points, only the measured roundness value is known, which is often a significant underestimation of the true roundness value. To solve this issue one could try to express the uncertainties relative to the measured roundness value instead of relative to the true roundness value. Since we are using computer simulations, the solution to this is quite straightforward. Instead of just calculating the errors with the error calculation module (step 4 in Figure 3.5), the calculated errors can be divided by the (simulated) “measured” roundness as described by Eq. 3.10. This is done for every Monte Carlo run. Errors

will then be expressed relatively to the “measured” roundness value. This concept was proposed by the author at the CAT2007 conference [76].

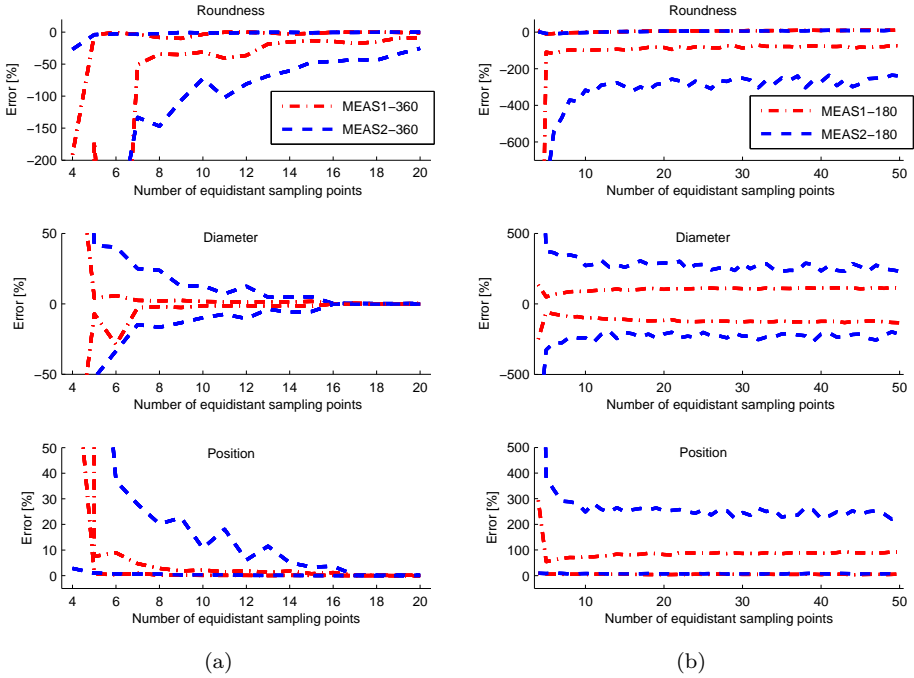


Figure A.1: Confidence limits (95%) of errors on the parameters of the LSQ circle, expressed relative to the measured roundness. Evaluated for two types of measured form databases. Equidistant sampling over 360° (a) and 180° (b) of the profile.

Figure A.1(a) shows the results of Figure 3.17(a), which are now expressed relatively to the measured roundness values. For very small numbers of sampling points, the measured roundness values are often very close to zero. As a consequence the relative uncertainties will be very high and are out of the scales of the figure. These results can be used in practice for CMM measurements as follows. Suppose a circle is measured with eight points and the type of manufacturing signature is unknown (MEAS2): the maximum possible error (95% confidence level) on diameter and position (Euclidean distance) will then be about 20% of the measured roundness value. Again, the errors for diameter and position are zero once the number of points exceeds the used filtering frequency (15 UPR).

In practice points are not always taken over the complete profile. Due to accessibility restrictions, circular profiles are sometimes only measured over 180°, although one would like to know the exact parameters of the full circle. Measuring arc segments

instead of complete circles will always increase the measurement uncertainty. The influence of feature form deviations will in these situations be very important as illustrated in Figure A.1(b).

This figure shows the confidence limits for the errors, expressed relative to the measured roundness. The errors are calculated by comparing *measured* values (sampled over  $180^\circ$ ) with the *true* value of the complete  $360^\circ$  circular profile. The relative errors are of course much larger than in case of  $360^\circ$  sampling. Not only will the errors (numerator) be larger, also the measured roundness (denominator) will be much smaller. The errors are plotted for  $n = 4$  to  $n = 50$  to show that the errors are not converging to zero. This is because only half the circular profile is sampled, even if this is done with an infinite number of sampling points. Because results are expressed relatively to the measured form deviation, they can also be used in practice. The relative uncertainties on diameter and position will be about 100% for MEAS1 and about 300% for MEAS2, even for a large number of sampling points. E.g. if a circle is sampled over  $180^\circ$  with 30 points and the measured roundness value equals  $10\ \mu\text{m}$ , one can expect errors on position and roundness up to  $30\ \mu\text{m}$ .

This example illustrates very well the power of Monte Carlo simulations for uncertainty calculations. Estimating the diameter and position uncertainty for a circle that is only sampled over  $180^\circ$  is very difficult / impossible based on expert knowledge. Every CMM expert will know that sampling circle segments is unfavourable for measurement uncertainty but they will not be able to define accurately the uncertainty related to the measurement. Even estimating the order of magnitude of the uncertainty will be difficult. Monte Carlo simulations are very useful under these circumstances, as shown by the latter example.

Because this method expresses the confidence limits relative to the measured roundness, it has the important advantage that the confidence limits are not dependent on true roundness, diameter or position, *as long as CMM hardware uncertainties can be neglected*. This is the major drawback of this approach, it can not account for hardware uncertainties. Once hardware uncertainties are taken into account uncertainties expressed relative to the measured roundness will no longer be independent of true size and form deviation. In practice CMM hardware will also have an influence on the measurement uncertainty. The results described in this section can then be considered as a lower limit of the measurement uncertainty. In order to model the influence of CMM hardware uncertainties, the error simulation method described in Chapter 3 must be adapted.

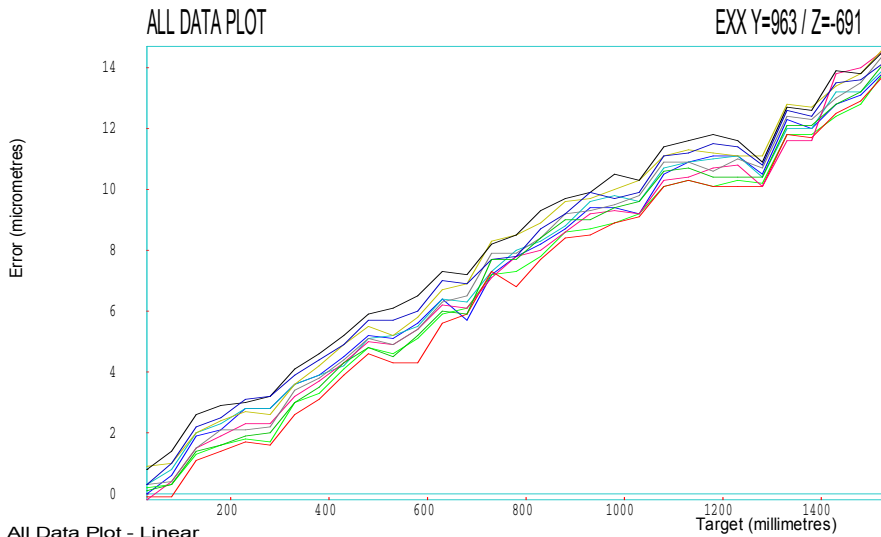




## Appendix B

# Measured geometric errors of Coord3 MC 16

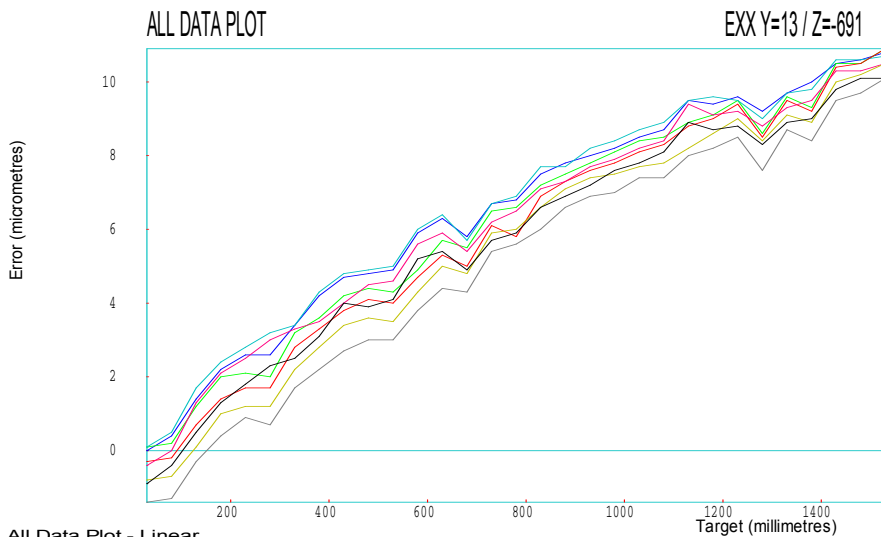
This appendix shows the results of the geometric error measurements performed on the  $x$ -axis of the Coord3 MC 16 CMM (cf. Section 1.9). The positioning error  $exx$ , the straightness errors  $eyx$ , straightness error  $ezx$ , pitch error  $ebx$  and yaw error  $ecx$  were measured. A calibrated Renishaw ML10 laser interferometer, equipped with a EC10 compensation unit, was used to perform the measurements. The specification of the laser interferometer for linear measurements is  $0.025 \mu\text{m} \pm 1.1 \mu\text{m}/\text{m}$  ( $k = 2$ ).



All Data Plot - Linear

Machine:Coord3 MC 16  
 Serial No:219 0.0 632  
 Date:13:20 Jan 30 2009  
 By:JVK & NVG

Axis:X  
 Location:Labo PMA  
 Filename: track1\_exx.rtl  
 Bidirectional



All Data Plot - Linear

Machine:Coord3 MC 16  
 Serial No:219 0.0 632  
 Date:12:30 Jan 29 2009  
 By:JVK & NVG

Axis:X  
 Location:Labo PMA  
 Filename: track2\_exx.rtl  
 Bidirectional

Figure B.1: Measurement of positioning error ( $exx$ ) along  $x$ -axis.

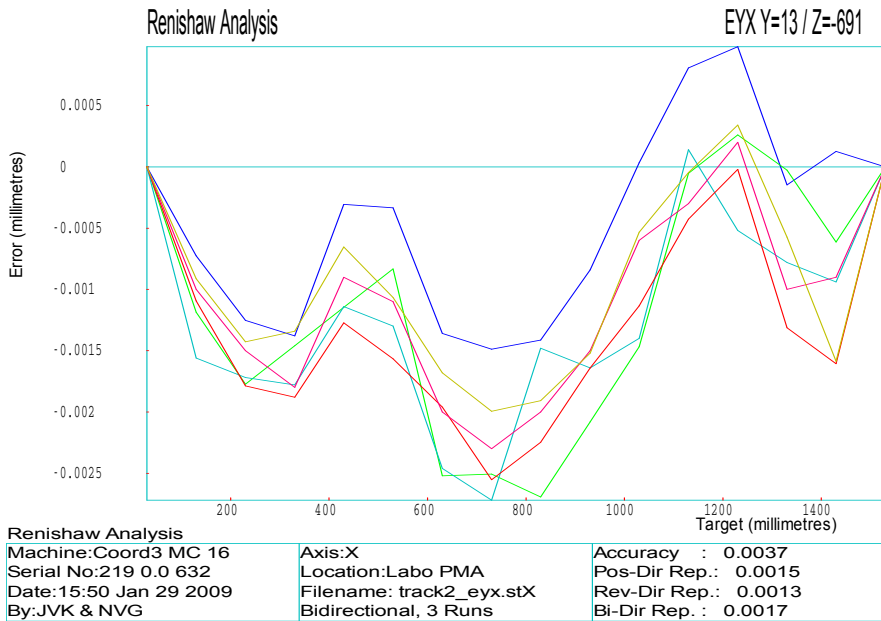
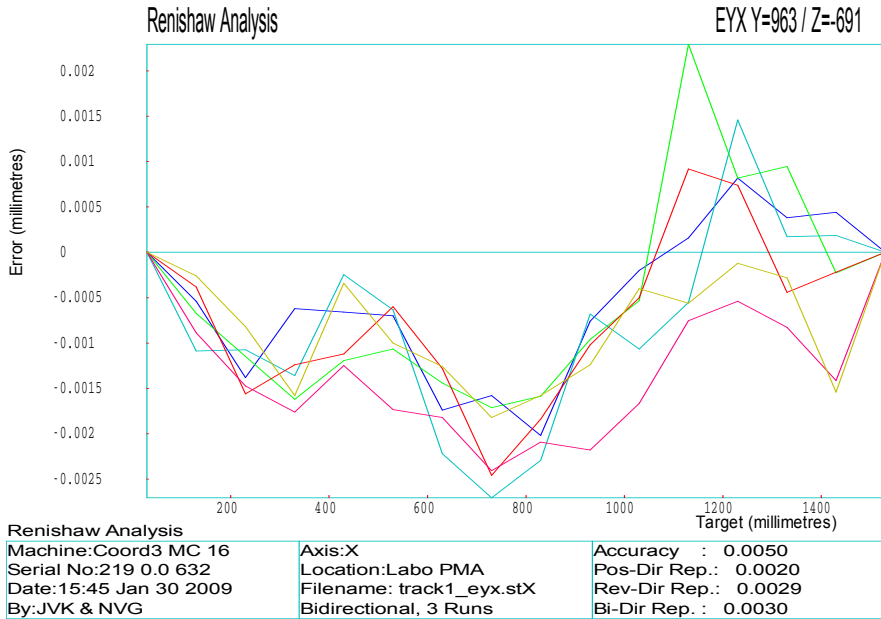


Figure B.2: Measurement of straightness error (*eyx*) along *x*-axis.

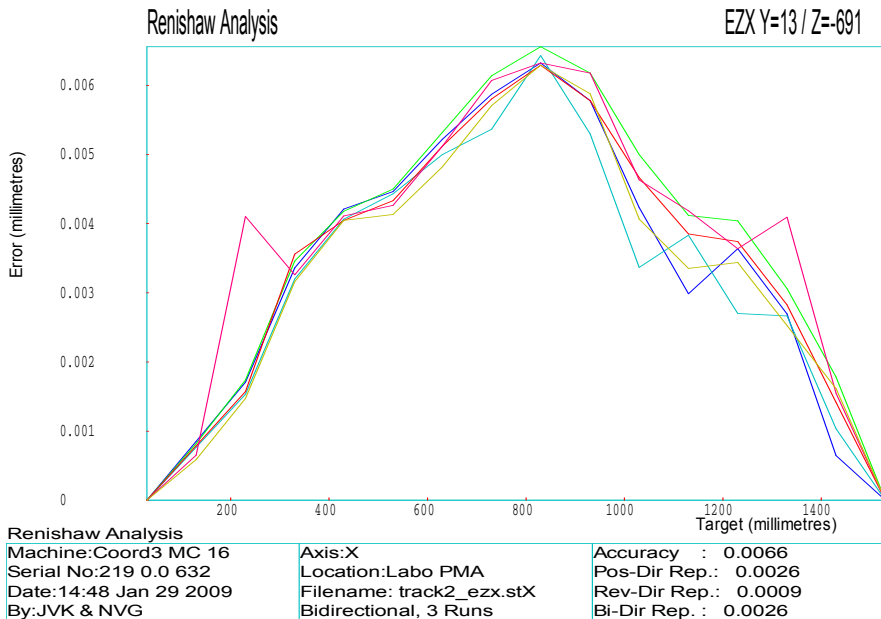
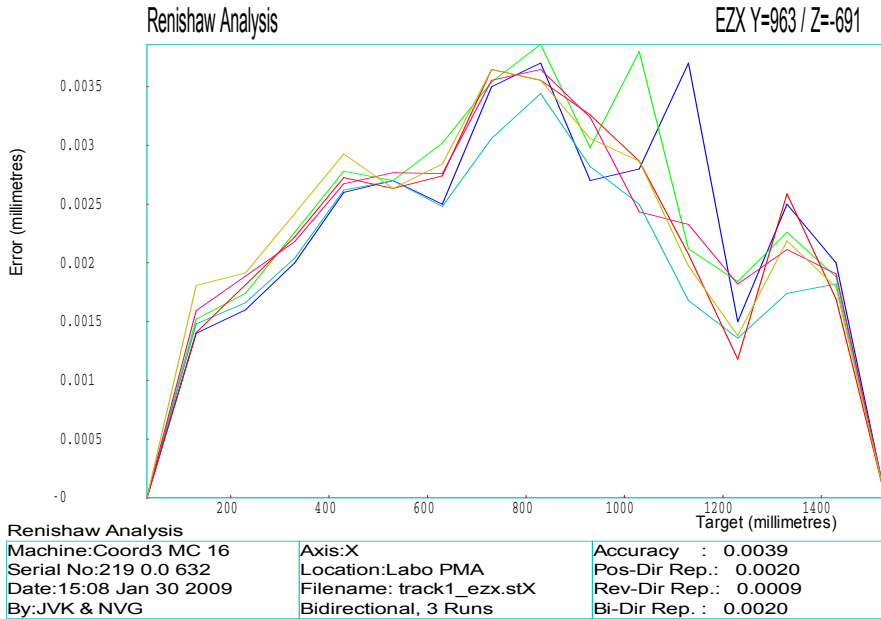


Figure B.3: Measurement of straightness error (*ezx*) along *x*-axis.

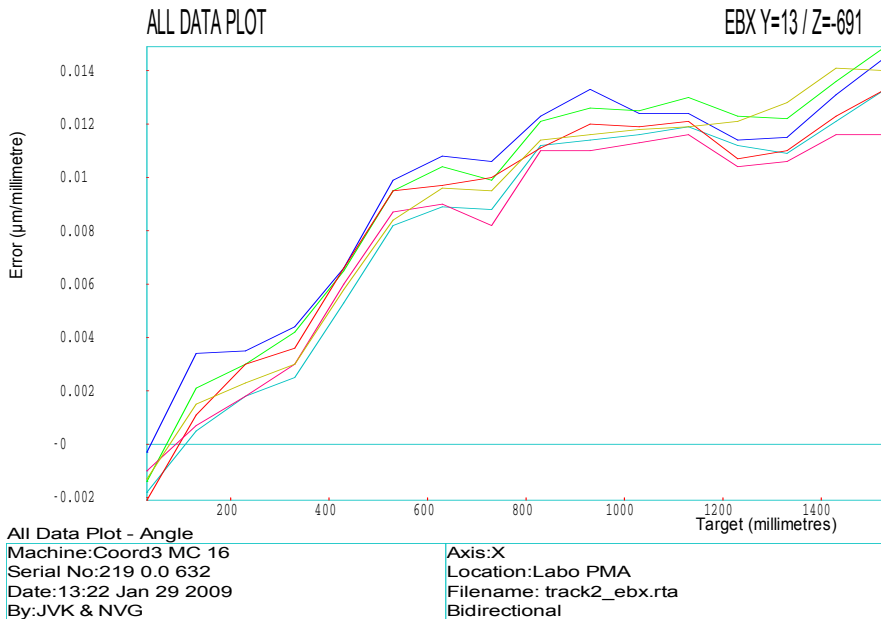
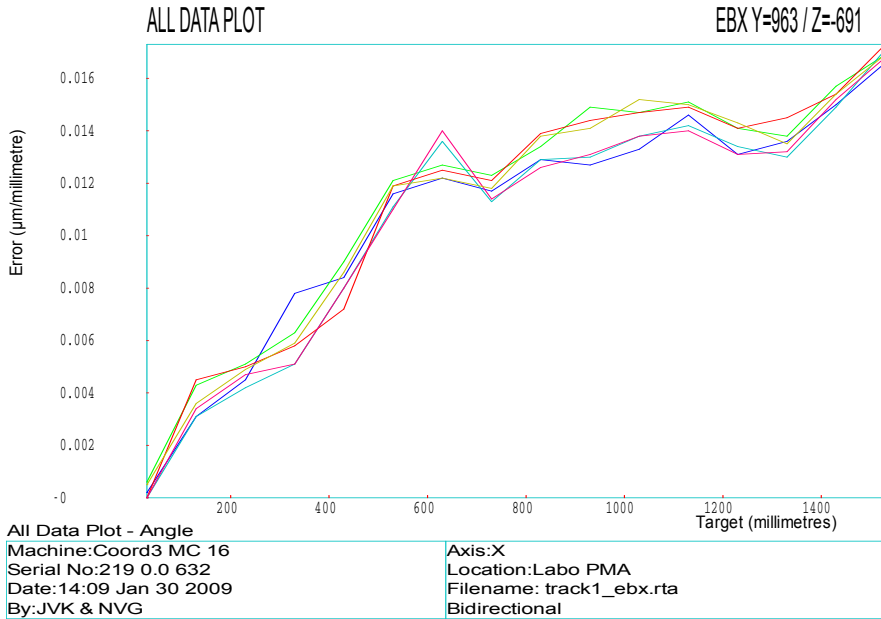
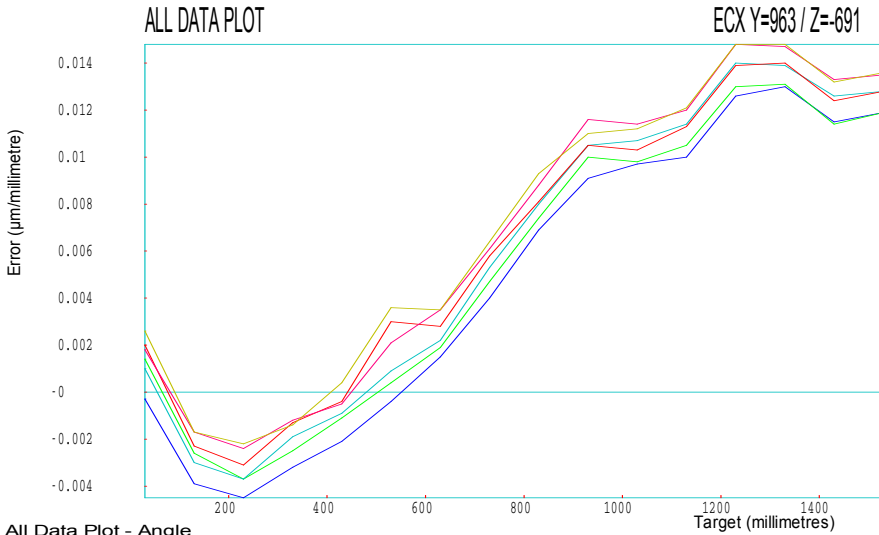


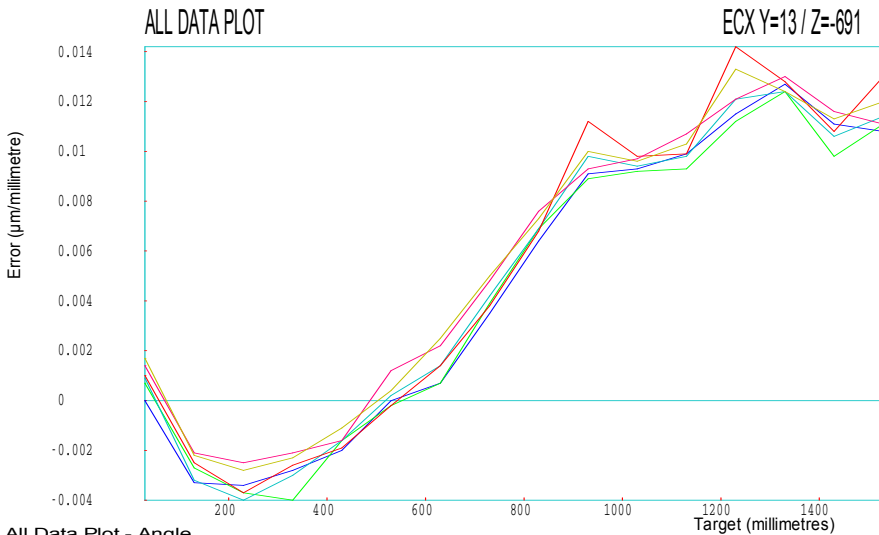
Figure B.4: Measurement of pitch error (*ebx*) along *x*-axis.



All Data Plot - Angle

Machine:Coord3 MC 16  
 Serial No:219 0.0 632  
 Date:14:35 Jan 30 2009  
 By:JVK & NVG

Axis:X  
 Location:Labo PMA  
 Filename: track1\_ecx.rta  
 Bidirectional



All Data Plot - Angle

Machine:Coord3 MC 16  
 Serial No:219 0.0 632  
 Date:13:57 Jan 29 2009  
 By:JVK & NVG

Axis:X  
 Location:Labo PMA  
 Filename: track2\_ecx.rta  
 Bidirectional

Figure B.5: Measurement of yaw error (*ecx*) along *x*-axis.

# Appendix C

## Class descriptions

**Control class (Control)** This is the main class. All input of data and output of results is done by calling methods of this class. Instances of the CMM class, the different feature classes, the datum class and the tolerance class are created by methods of the control class and are stored in attributes of this class. This class also contains the methods that initiate the error simulation and uncertainty calculation procedures.

**Settings class (Settings)** The settings class has a set of structure attributes that contain parameter settings necessary for the UES: number of Monte Carlo runs, measurement volume of the CMM, performance specification of the CMM, ...

**Feature class (Feat)** Since all kinds of features have similar parameters (like position, orientation, size and form deviation) the feature class is used as a *parent class* that only contains attributes, no methods. These attributes are inherited by the classes of the different features.

**Circle class (Circle)** The circle class is a child of the feature class. Its attributes are inherited from the feature class. The methods of the circle class are used to create and measure virtual circles.

**Line class (Line)** The line class is a child of the feature class. Its attributes are inherited from the feature class. The methods of the line class are used to create and measure virtual lines.

**Plane class (Plane)** The plane class is a child of the feature class. Its attributes are inherited from the feature class. The methods of the plane class are used to create and measure virtual planes.

**Cylinder class (Cylindr)** The cylinder a class is child of the feature class. Its attributes are inherited from the feature class. The methods of the feature class are used to create and measure virtual cylinders.

**Point class (Point)** The point class is a child of the feature class. Its attributes are inherited from the feature class. The point class can be used when an intersection point of two features needs to be calculated.

**Virtual feature class (VirtFeat)** The virtual feature class has some structure attributes that contain all information of the created virtual profiles: points of the true virtual profiles, virtual sampled points, true and measured virtual position, orientation, size and form deviation. The feature class contains information about the actual measured feature. The virtual feature class contains information about the associated virtual features. The virtual feature class is a composition with the feature class.

**Virtual form deviation class (VirtForm)** The structure attributes of the virtual form deviation class contain virtual form deviation profiles for the different kind of features (form databases discussed in Section 3.5).

**Virtual CMM class (CMM)** Every created instance of the CMM class represents one virtual CMM. It contains several methods to construct the virtual geometric errors and the error state of the CMM. Once the virtual CMM is built, it can be called to return the probe tip position error at a given position in the measurement volume of the virtual CMM. This can be used to simulate the sampling of a feature.

**Virtual sensor class (Sensor)** The virtual sensor class is a composition with the CMM class. More than one virtual sensor can be associated with a virtual CMM. The virtual sensor class models the hardware errors of the articulating probe head and the used sensor.

**Datum class (Datum)** An instance of the datum class is created for every used reference datum frame during the measurement. It contains methods to calculate the datum matrix from the composing datum features and to create the virtual datums for the corresponding virtual features.

**Virtual datum class (VirtDatum)** The virtual datum class has a structure attribute that contains all information of the created virtual datum.

**Tolerance class (Tol)** An instance of the tolerance class is created for every defined tolerance. It contains all relevant information for the tolerance: type of tolerance, toleranced feature, datum feature, tolerance limits, measured tolerance value, ... It uses the algorithms from the tolerance algorithm database to calculate the tolerance values for the actual features and all associated virtual features.



**Virtual tolerance class (VirtTol)** The virtual datum class has a structure attribute that contains all information of the created virtual tolerance.

**Virtual environment class** The virtual environment class has never been integrated. Although it is still shown in the class diagram because it illustrates that it could be used to integrate the influence of temperature deviations / fluctuations on the calculated measurement uncertainty.



# Bibliography

- [1] P. Bleys, N. Van Gestel, F. Welkenhuyzen, and J.P. Kruth. Probing systems for 3D coordinate measuring machines. Poster, April 2008.
- [2] A. Weckenmann, T. Estler, G. Peggs, and D. McMurtry. Probing systems in dimensional metrology. *CIRP Annals-Manufacturing Technology*, 53(2):657–684, 2004.
- [3] W. Knapp and A. Wirtz. Accuracy of length measurement and positioning: statical measurement and contouring mode. *CIRP Annals-Manufacturing Technology*, 37(1):511–514, 1988.
- [4] P.H. Pereira and R.J. Hocken. Characterization and compensation of dynamic errors of a scanning coordinate measuring machine. *Precision Engineering*, 31(1):22–32, 2007.
- [5] E. Bos, R. Heldens, F. Delbressine, P. Schellekens, and A. Dietzel. Compensation of the anisotropic behavior of single crystalline silicon in a 3D tactile sensor. *Sensors and Actuators A: Physical*, 134(2):374–381, 2007.
- [6] N. Van Gestel, S. Cuypers, P. Bleys, and J.P. Kruth. A performance evaluation test for laser line scanners on CMMs. *Opt. Lasers Eng.*, 47(3-4):336–342, 2009.
- [7] W. Cuypers and N. Van Gestel. *Gids voor mobiele Coördinatenmeettechniek*. Katholieke Universiteit Leuven, Department of Mechanical Engineering, 2008.
- [8] N. Van Gestel, W. Cuypers, P. Bleys, A. Voet, and J.P. Kruth. Mobile and Large Scale Dimensional Metrology. Poster, April 2008.
- [9] W. Cuypers, N. Van Gestel, A. Voet, J.P. Kruth, J. Mingneau, and P. Bleys. Optical measurement techniques for mobile and large-scale dimensional metrology. *Opt. Lasers Eng.*, 47(3-4):292–300, 2009.
- [10] J.P. Kruth, M. Bartscher, S. Carmignato, R. Schmitt, L. De Chiffre, and A. Weckenmann. Computed tomography for dimensional metrology. *CIRP Ann.*, 60(2):821 – 842, 2011.

- [11] K. Kiekens, F. Welkenhuyzen, Y. Tan, P. Bleys, A. Voet, W. Dewulf, and J.P. Kruth. A test object for calibration and accuracy assessment in X-ray CT metrology. In *Proceedings of the 10th International Symposium on Measurement and Quality Control 2010*, 5th-9th September 2010.
- [12] ISO/IEC Guide 99:2007. *International vocabulary of metrology – Basic and general concepts and associated terms (VIM)*. ISO/IEC, 2007.
- [13] ISO/IEC Guide 98-3:2008. *Uncertainty of measurement – Part 3: Guide to the expression of uncertainty in measurement (GUM:1995)*. ISO/IEC, 2008.
- [14] ISO 14253-1:1998. *Geometrical Product Specifications (GPS) – Inspection by measurement of workpieces and measuring equipment – Part 1: Decision rules for proving conformance or non-conformance with specifications*. ISO, 1998.
- [15] J.P. Kruth, P. Vanherck, and C. Van den Bergh. Compensation of static and transient thermal errors on CMMs. *CIRP Ann.*, 50(1):377–380, 2001.
- [16] D. Croimans and N. Van Gestel. Vergelijking van nauwkeurigheid en inzetbaarheid van optische en mechanische coördinatenmeetmachines. Master’s thesis, Katholieke Universiteit Leuven, Department of Mechanical Engineering, 2005.
- [17] S. De Ron and J. Vander Wilt. 3D opmeten van Rapid Manufacturing producten en terugkoppeling naar het proces. Master’s thesis, Hogeschool De Nayer, Mechelen, 2008.
- [18] W. Lotze. Unsicherheit des Ausgleichskreises aus Koordinatenmessungen. *Feingerätetechnik*, 32(2):72–75, 1983.
- [19] ISO 22093:2003. *Industrial automation systems and integration – Physical device control – Dimensional Measuring Interface Standard (DMIS)*. ISO, 2003.
- [20] ISO/TR 16015:2003. *Geometrical product specifications (GPS) – Systematic errors and contributions to measurement uncertainty of length measurement due to thermal influences*. ISO, 2003.
- [21] ISO/IEC Guide 98-3:2008/Suppl 1:2008. *Propagation of distributions using a Monte Carlo method*. ISO/IEC, 2008.
- [22] ISO 10360-2:2001. *Geometrical Product Specifications (GPS) – Acceptance and reverification tests for coordinate measuring machines (CMM) – Part 2: CMMs used for measuring size*. ISO, 2001.
- [23] A. Contri, P. Bourdet, and C. Lartigue. Quality of 3D digitised points obtained with non-contact optical sensors. *CIRP Annals-Manufacturing Technology*, 51(1):443–446, 2002.

- [24] S. Martinez, E. Cuesta, J. Barreiro, and B. Alvarez. Analysis of laser scanning and strategies for dimensional and geometrical control. *The International Journal of Advanced Manufacturing Technology*, 46(5):621–629, 2010.
- [25] ISO/TS 15530-3:2004. *Geometrical Product Specifications (GPS) – Coordinate measuring machines (CMM): Technique for determining the uncertainty of measurement – Part 3: Use of calibrated workpieces or standards*. ISO, 2004.
- [26] J.M. Baldwin, K.D. Summerhays, D.A. Campbell, and R.P. Henke. Application of simulation software to coordinate measurement uncertainty evaluations. In *Proceedings of the NCSL International Workshop and Symposium*, 2004.
- [27] ISO/TS 15530-4:2008. *Geometrical Product Specifications (GPS) – Coordinate measuring machines (CMM): Technique for determining the uncertainty of measurement – Part 4: Evaluating task-specific measurement uncertainty using simulation*. ISO, 2008.
- [28] H. Schwenke, M. Franke, J. Hannaford, and H. Kunzmann. Error mapping of CMMs and machine tools by a single tracking interferometer. *CIRP Annals-Manufacturing Technology*, 54(1):475–478, 2005.
- [29] B. Bringmann and W. Knapp. Machine tool calibration: Geometric test uncertainty depends on machine tool performance. *Precision Engineering*, 33(4):524–529, 2009.
- [30] T. Liebrich, B. Bringmann, and W. Knapp. Calibration of a 3D-ball plate. *Precision Engineering*, 33(1):1–6, 2009.
- [31] E. Trapet and F. Wäldele. The virtual CMM concept. *Series on Advances in Mathematics for Applied Sciences*, 40:238–247, 1996.
- [32] J. Beaman and E. Morse. Experimental evaluation of software estimates of task specific measurement uncertainty for CMMs. *Precision Engineering*, 34(1):28–33, 2010.
- [33] S. Phillips, B. Borchardt, D. Sawyer, W. Estler, K. Eberhardt, MS Levenson, and M. McClain. A constrained Monte Carlo simulation method for the calculation of CMM measurement uncertainty. unpublished, 1999.
- [34] R.G. Wilhelm, R. Hocken, and H. Schwenke. Task specific uncertainty in coordinate measurement. *CIRP Annals-Manufacturing Technology*, 50(2):553–563, 2001.
- [35] A. Balsamo, M. Di Ciommo, R. Mugno, BI Rebaglia, E. Ricci, and R. Grella. Evaluation of CMM uncertainty through Monte Carlo simulations. *CIRP Annals-Manufacturing Technology*, 48(1):425–428, 1999.

- [36] D. Sola, E. Ricci, A. Balsamo, M. Di Ciommo, and B.I. Rebaglia. *Method of determining the measuring uncertainty of a coordinate measuring device*. US Patent No. US6178389B1, 2001.
- [37] G. Henzold. *Geometrical dimensioning and tolerancing for design, manufacturing and inspection: a handbook for geometrical product specification using ISO and ASME standards*. Butterworth-Heinemann, 2006.
- [38] ISO 4287:1997. *Geometrical Product Specifications (GPS) – Surface texture: Profile method – Terms, definitions and surface texture parameters*. ISO, 1997.
- [39] R. Leach. *NPL Good Practice Guide 37: The Measurement of Surface Texture using Stylus Instruments*. National Physical Laboratory, UK, 2001.
- [40] ISO 3274:1996. *Geometrical Product Specifications (GPS) – Surface texture: Profile method – Nominal characteristics of contact (stylus) instruments*. ISO, 1996.
- [41] ISO 4288:1996. *Geometrical Product Specifications (GPS) – Surface texture: Profile method – Rules and procedures for the assessment of surface texture*. ISO, 1996.
- [42] VDI/VDE 2601. *Requirements on the surface structure to cover function capability of surfaces manufactured by cutting; list of parameters*. VDI/VDE, 1991.
- [43] ISO 1101:2004. *Geometrical Product Specifications (GPS) – Geometrical tolerancing – Tolerances of form, orientation, location and run-out*. ISO, 2004.
- [44] A. Wirtz. Einfluss von Formfehlern auf Mass- und Lagebestimmung. *CIRP Annals-Manufacturing Technology*, 23(1):141–142, 1974.
- [45] A. Weckenmann, H. Eitzert, M. Garmer, and H. Weber. Functionality-oriented evaluation and sampling strategy in coordinate metrology. *Precision Engineering*, 17(4):244–252, 1995.
- [46] A. Weckenmann, M. Knauer, and H. Kunzmann. The influence of measurement strategy on the uncertainty of CMM-measurements. *CIRP Annals-Manufacturing Technology*, 47(1):451–454, 1998.
- [47] W. Choi, T.R. Kurfess, and J. Cagans. Sampling uncertainty in coordinate measurement data analysis. *Precision Engineering*, 22(3):153–163, 1998.
- [48] K.D. Summerhays, R.P. Henke, J.M. Baldwin, R.M. Cassou, and C.W. Brown. Optimizing discrete point sample patterns and measurement data analysis on internal cylindrical surfaces with systematic form deviations. *Precision Engineering*, 26(1):105–121, 2002.

- [49] A. Rossi. A form of deviation-based method for coordinate measuring machine sampling optimization in an assessment of roundness. *Proceedings of the Institution of Mechanical Engineers, Part B: Journal of Engineering Manufacture*, 215(11):1505–1518, 2001.
- [50] ISO 11562:1996. *Geometrical Product Specifications (GPS) – Surface texture: Profile method – Metrological characteristics of phase correct filters*. ISO, 1996.
- [51] ISO/TS 12181-2:2003. *Geometrical Product Specifications (GPS) – Roundness – Part 2: Specification operators*. ISO, 2003.
- [52] K. Lingadurai and MS Shunmugam. Analysis of 3D-reference surfaces established by Gaussian filter for engineering surfaces. *Institution of Engineers India Part PE Production Engineering Division*, 86:8–14, 2005.
- [53] H. Hanada, T. Saito, M. Hasegawa, and K. Yanagi. Sophisticated filtration technique for 3D surface topography data of rectangular area. *Wear*, 264:422–427, 2008.
- [54] R.P. Henke, K.D. Summerhays, J.M. Baldwin, R.M. Cassou, and C.W. Brown. Methods for evaluation of systematic geometric deviations in machined parts and their relationships to process variables. *Precision Engineering*, 23(4):273–292, 1999.
- [55] D. Verstraeten. Vormfoutensimulator voor het bepalen van meetonzekerheden bij CMMs. Master’s thesis, Katholieke Universiteit Leuven, Department of Mechanical Engineering, 2010.
- [56] L.N. Thibos, R.A. Applegate, J.T. Schwiegerling, R. Webb, et al. Standards for reporting the optical aberrations of eyes. *Journal of Refractive Surgery*, 18(5):652–660, 2002.
- [57] D.C. Montgomery. *Introduction to statistical quality control*. Wiley, 2007.
- [58] P.D. Moore, F. Hoppe, D.S. Moore, G.P. McCabe, W.M. Duckworth, and S.L. Sclove. *The Practice of Business Statistics Excel Manual*. WH Freeman & Co, 2003.
- [59] B. Efron. Bootstrap methods: another look at the jackknife. *The annals of Statistics*, 7(1):1–26, 1979.
- [60] C. Van Den Bergh. *Reducing thermal errors of CMM located on the shop-floor*. PhD thesis, Katholieke Universiteit Leuven, Department of Mechanical Engineering, 2001.
- [61] ISO 230-1:1996. *Test code for machine tools – Part 1: Geometric accuracy of machines operating under no-load or finishing conditions*. ISO, 1996.

- [62] J.A. Bosch. *Coordinate measuring machines and systems*. CRC, 1995.
- [63] W. Knapp and E. Matthias. Test of the three-dimensional uncertainty of machine tools and measuring machines and its relation to the machine errors. *CIRP Annals-Manufacturing Technology*, 32(1):459–464, 1983.
- [64] G. Zhang, R. Veale, T. Charlton, B. Borchardt, and R. Hocken. Error compensation of coordinate measuring machines. *CIRP Annals-Manufacturing Technology*, 34(1):445–448, 1985.
- [65] P.S. Huang and J. Ni. On-line error compensation of coordinate measuring machines. *International Journal of Machine Tools and Manufacture*, 35(5):725–738, 1995.
- [66] J.P. Kruth, P. Vanherck, and L. De Jonge. Self-calibration method and software error correction for three-dimensional coordinate measuring machines using artefact measurements. *Measurement*, 14(2):157–167, 1994.
- [67] GX Zhang. A study on the Abbe principle and Abbe error. *CIRP Annals-Manufacturing Technology*, 38(1):525–528, 1989.
- [68] H. Schwenke, W. Knapp, H. Haitjema, A. Weckenmann, R. Schmitt, and F. Delbressine. Geometric error measurement and compensation of machines—An update. *CIRP Annals-Manufacturing Technology*, 57(2):660–675, 2008.
- [69] Renishaw. *PH10 motorised heads and controllers - Installation guide*, 2006.
- [70] N. Van Gestel, F. Welkenhuyzen, P. Bleys, and J.P. Kruth. Evaluation of measurement uncertainty contributors for vision CMMs. In *Proceedings of the OPTIMESS 2009 conference*, Antwerp, Belgium, 25th-26th May 2009.
- [71] D. Jiang and Zhao Y. Combination of laser line scanning and tactile probing on coordinate measuring machines. Master’s thesis, GROUP T, Leuven Engineering College, 2009.
- [72] ISO 5459:1981. *Technical drawings – Geometrical tolerancing – Datums and datum-systems for geometrical tolerances*. ISO, 1981.
- [73] S. Bens and F. Justin. Optimalisatie van meetstrategieën voor 3D-coördinatenmeetmachines. Master’s thesis, Katholieke Universiteit Leuven, Department of Mechanical Engineering, 2008.
- [74] F. Welkenhuyzen, N. Van Gestel, P. Bleys, and J.P. Kruth. Accuracy enhancement of the measuring probe for a camera based mobile CMM. In *Proceedings of the LAMDAMAP 2009 conference*, Teddington, UK, 30th June - 2nd July 2009.



- [75] P. Boogmans and J. Hoefkens. Combinatie van laserlijnscannen en tactiel meten op een 3D CMM. Master's thesis, Katholieke Universiteit Leuven, Department of Mechanical Engineering, 2010.
- [76] P. Bleys, N. Van Gestel, S. Cuypers, and J.P. Kruth. Uncertainty due to limited sampling of circular features on coordinate measuring machines. In *Proceedings of the CAT2007 conference*, Erlangen, Germany, 21th-23th March 2007.



# Curriculum vitae

## Personal Data

Nick Van Gestel

° June 30th 1982, Turnhout

Address: Klinkersbos 47, 2470 Retie

E-mail: nick.vangestel@gmail.com

## Education

- **2007-2011: PhD in Mechanical Engineering**, Katholieke Universiteit Leuven.
- **2002-2005: Master of Science in Mechanical Engineering** option Manufacturing & Management, Katholieke Universiteit Leuven.  
Master thesis: *Comparison of optical and tactile coordinate measuring machines*
- **2003-2005: Bachelor of Business Economics: Business Engineering**, Katholieke Universiteit Leuven.
- **2000-2002: Bachelor in Engineering**, Katholieke Universiteit Leuven.
- **1994-2000: Secondary school**: Latin-Mathematics, Sint-Pietersinstituut, Turnhout.



# List of publications

## Articles in internationally reviewed scientific journals

- Van Gestel, N., Bleys, P., Welkenhuyzen, F., Kruth, J. (2011). Influence of feature form deviations on CMM measurement uncertainties. *International Journal of Precision Technology*, 2(2/3), 192-210.
- Van Gestel, N., Cuypers, S., Bleys, P., Kruth, J. (2009). A performance evaluation test for laser line scanners on CMMs. *Optics and Lasers in Engineering*, 47, 336-342.
- Cuypers, W., Van Gestel, N., Voet, A., Kruth, J., Bleys, P. (2009). Optical measurement techniques for mobile and large scale dimensional metrology. *Optics and Lasers in Engineering*, 47, 292-300.
- Kruth, J., Van Gestel, N., Bleys, P., Welkenhuyzen, F. (2009). Uncertainty determination for CMMs by Monte Carlo simulation integrating feature form deviations. *CIRP Annals*, 58(1), 463-466.

## Papers at international conferences and symposia, published in full in proceedings

- Lauwers, B., Kruth, J., Bleys, P., Ten Haaf, P., Saelen, S., Van Gestel, N., Welkenhuyzen, F., Mielnik, K. (2010). Evaluation and Implementation of an Integrated Measuring System within a Multi-tasking Machining Centre. In: *Proceedings of 4th CIRP International Conference on High Performance Cutting*, 2010, 2. CIRP International Conference on High Performance Cutting, Gifu, Japan, 24-26 October 2010 (pp. 233-238).
- Lauwers, B., Van Gestel, N., Vanparys, M., Plakhotnik, D. (2009). Machining of ceramics and ecological steels using a mill turn centre equipped with an

- ultrasonic assisted tooling system. In: *Proceedings of MTTRF 2009 Meeting*, (Yamazaki, K. (Eds.)). MTTRF 2009 Annual meeting. Shanghai (China), 8-9 July 2009 (pp. 183-200). MTTRF (Machine Tools Technologies Research Foundation).
- Welkenhuyzen, F., Van Gestel, N., Bleys, P., Kruth, J. (2009). Accuracy enhancement of the measuring probe for a camera based mobile CMM. In: *Proceedings of the LAMDAMAP 2009 conference*. LAMDAMAP 2009. Teddington, UK, 29 June-2 July 2009.
  - Van Gestel, N., Welkenhuyzen, F., Bleys, P., Kruth, J. (2009). Evaluation of Measurement Uncertainty Contributors for Vision CMMs. In: *Proceedings of the 4th International Conference on Optical Measurement Techniques for Structures and Systems*. International Conference on Optical Measurement Techniques for Structures and Systems. Antwerp, Belgium, 25-26 May 2009.
  - Cuypers, W., Van Gestel, N., Voet, A., Kruth, J., Bleys, P. (2007). Optical measurement techniques for mobile and large scale dimensional metrology. In: *Proceedings of the 3rd Workshop on Optical Measurements Techniques for Structures and Systems*. 3rd Workshop on Optical Measurements Techniques for Structures and Systems. Leuven, Belgium, 28-30 May 2007 (pp. 346-357).
  - Van Gestel, N., Cuypers, S., Bleys, P., Kruth, J. (2007). A performance evaluation test for laser line scanners on CMMs. In: *Proceedings of the 3rd Workshop on Optical Measurements Techniques for Structures and Systems*. 3rd Workshop on Optical Measurements Techniques for Structures and Systems. Leuven, Belgium, 28-30 May 2007 (pp. 147-154).
  - Van Gestel, N., Cuypers, S., Kruth, J., Bleys, P. (2007). Uncertainty due to limited sampling of circular features on coordinate measuring machines. In: *Proceedings of the 10th CIRP Computer Aided Tolerancing 2007*. 10th CIRP Computer Aided Tolerancing 2007. Erlangen, Germany, 21-23 March 2007.

## **Papers at local conferences and symposia, published in full in proceedings**

- Corthouts, P., Van Gestel, N., Bleys, P., Kruth, J. (2005). Study of the disturbance influences on optical coordinate measuring machines. In: *Proceedings of the 2nd OPTIMESS Workshop*. 2nd OPTIMESS Workshop. Gent, Brussel, 27 October 2005.

## Meeting abstracts, presented at international conferences and symposia, published or not published in proceedings or journals

- Bleys, P., Van Gestel, N. (2010). Uncertainty determination for CMMs - Don't forget the influence of feature form deviations. Metromeet 2010 - 6th International Conference on Industrial Dimensional Metrology, Bilbao, 25-26 February 2010.
- Bleys, P., Van Gestel, N. (2009). Mobile measurement of large objects - industrial case studies. CIRP STC-P meeting, Boston, USA, 28 August 2009.

## Meeting abstracts, presented at local conferences and symposia, published or not published in proceedings or journals

- Van Gestel, N. (2009). Meetonzekerheid voor CMMs: Hoe onzeker bent u van uw meting?. *Themadag Precisiemeten*, Leuven, 10 december 2009.
- Van Gestel, N. (2009). Meetonzekerheid voor CMMs. *Technologiedag Meten - Innovaties in de geometrische meettechniek*, Delft, Nederland, 5 februari 2009.
- Van Gestel, N. (2008). Mobiele 3D-Coördinatenmeetmachines: Overzicht en toepassingen. *VVGT-studieavond Contactloze 3D-metingen en hun toepassingen in de gieterij*, Gent, 21 april 2008.

## Other journal publications / miscellaneous

- Van Gestel, N., Bleys, P. (2009). Hoe onzeker bent u van uw meting?. In: *Industrie Technisch Management*, April 2009, 74-79: Roularta Media Group.
- Paulus, P., Bleys, P., Van Gestel, N. (2008). Het meten van microstructuren vergt uiterste van huidige systemen. In: *Metallerie*, 118, 45-47: Professional Media Group.
- Van Parys, D., Bleys, P., Van Gestel, N., Cuypers, W. (2008). Selectieprocedure en praktijkvoorbeelden van mobiele CMMs. In: *Metallerie*, 117, 31-34: Professional Media Group.

- Van Parys, D., Van Gestel, N., Cuypers, W., Bleys, P. (2008). Belang van mobiele coördinatenmeettechniek neemt toe. In: *Metallerie*, 116, 11-13: Professional Media Group.

## **Other published books: as author**

- Cuypers, W., Van Gestel, N., Voet, A. (as contributor) Kruth, J. (as contributor) Mingneau, J. (as contributor) Bleys, P. (as contributor) (2008). *Gids voor Mobiele Coördinatenmeettechniek*.





Arenberg Doctoraatsschool Wetenschap & Technologie

Faculteit Ingenieurswetenschappen

Departement Werktuigkunde

Afdeling Productietechnieken, Machinebouw en Automatisering

Celestijnenlaan 300b - bus 2420, B-3001 Heverlee